Electrocaloric Effect in Electron Irradiated GNPs/P(VDF-HFP) Composites

Ardian Agus Permana

Electrocaloric Effect in Electron Irradiated GNPs/P(VDF-HFP) Composites

Ardian Agus Permana

**A Thesis Submitted in Fulfillment of the Requirements for the Degree of
Master of Science in Physics (International Program)
Prince of Songkla University
2020**

Thesis Title   Electrocaloric Effect in Electron Irradiated GNPs/P(VDF-HFP) Composites
Author   Mr. Ardian Agus Permana
Major Program   Physics (International Program)

_____

Major Advisor

....
(Assoc. Prof. Dr. Chatchai Putson)

Examining Committee:

....Chairperson
(Asst. Prof. Dr. Nawal Binhayeeniyi)

....Committee
(Asst. Prof. Dr. Chalongrat Daengngam)

....Committee
(Assoc. Prof. Dr. Chatchai Putson)

The Graduate School, Prince of Songkla University, has approved this thesis as fulfillment of the requirements for the Master of Science Degree in Physics (International Program).

....
(Prof. Dr. Damrongsak Faroongsarng)
Dean of Graduate School

This is to certify that the work here submitted is the result of the candidate's own investigations. Due acknowledgement has been made of any assistance received.

....Signature
(Assoc. Prof. Dr. Chatchai Putson)
Major Advisor

....Signature
(Mr. Ardian Agus Permana)
Candidate

I hereby certify that this work has not been accepted in substance for any degree, and is not being currently submitted in candidature for any degree.

....Signature
(Mr. Ardian Agus Permana)
Candidate

Thesis Title   Electrocaloric Effect in Electron Irradiated GNPs/P(VDF-HFP) Composites

Author   Ardian Agus Permana

Major   Physics

Acadenic Year   2019

ABSTRACT

Nowadays, environmental issues lead the scientists to find and discover new materials and methods for advanced technology that eco-friendly, easy to process and low-cost. One of the sexiest issues that rapidly grows is eco-friendly cooling system with high energy efficiency. Not only for common cooling devices such as air conditioner and refrigerator, this cooling system is also proposed to be applied in thinny devices such as microchips with huge amounts of micro-components. The demand of this technology finally desire not only strong power and high storage energy density but also should be flexible, lightweight, durable and achievable. Among other ferroelectric materials, PVDF-based polymer shows the outstanding properties. Nevertheless, some approaches have been being investigated to improve the properties of the polymer. In this work, poly(vinylidene fluoride-hexafluoropropylene) was modified by incoorporating graphene nanoplatelets conducting nanofillers to boost up dielectric properties and electrocaloric effect behavior. Further, combining this method with electron beam irradiation could bring the benefit for energy properties improvement. The neat polymer and composites thin films were kindly fabricated by solution casting technique. Crystalline phase modification affected by graphene nanoplatelets filler and electron irradiation towards its surface, microstructure, electrical, ferroelectric, electrocaloric effect and energy properties have been elaborated. As the result, reduction of pores size lead to improve film homogeneity and its hydrophobicity that als brought benefit for dielectric and energy properties. The percentage crystallinity and high polarity β-phase fraction improvement then drastically give an impact on electrical properties and

electrocaloric effect by gaining polarization and permittivity. The elctrocaloric effect of the composites were bigger compared to pure P(VDF-HFP) indicated by the ΔT and T_c. Considering those two electrocaloric parameters, the $|\Delta T_{max}/T_c|$ ratio for HFP/GN composites was improved to almost two times of the neat P(VDF-HFP). On the other hands, electron beam irradiation dramatically reduced the crystals size into two times smaller. Hence, bigger storage energy density can be generated along with dropping energy loss. As final result, energy efficiency of neat polymer was improved to 74.66% after irradiation, much higher that unirradiated samples of 68.11. this number was alsi bigger than previously reported by another study of 58%. For the composites, enery efficiency improvement was almost doubled for all condition filler concentration.

ACKNOWLEDGEMENTS

Puji syukur ka Hyang Agung, neda jembar hampura-Na

Puji tur puja kagungan pangeran, Maha Raja, Maha Welas tur Heman

Gusti mangka muka pura bagja, Alloh ya Robbi, Mantenna Maha Uninga

Salam sinareng solawat, muga netes ka kanjeng Nabi Muhammad

Natrat ka para Karabat, para ahli jeung sohabat

Foremost, the deepest appreciation belong to Assoc. Prof. Dr. Chatchai Putson as my Advisor. Like an emerald of the Equator, and the Jewel of this Golden Land, you never give up on me. Your lessons and wisdom will be last forever.

My sincere gratitude will always be expressed to my research committees, Asst. Prof. Dr. Nawal Binhayeeniyi from Princess of Naradhiwas University and Asst. Prof. Dr. Chalongrat Daengngam from Prince of Songkla University. Your critical comments and suggestions are very useful for this research improvement.

My calm buddy, Ahamad Salea (Pee Pang), I can say nothing but thank for your pure sincerity to take care of me. For my Thai family, the members of Material Physics laboratory, Kunthisa Jehlaeh (Fah), Suphita Chaipo (Nong Beam), Jakkapat Kho-Iam (Nong Jame) and Ratchaneewan Siri (Pee Mai), I love the way how you guys making the lab's atmosphere as warm as home *literally home.

From my deepest heart, big hugs will always belong to my Indonesian family, Overseas Indonesian Student Association in Thailand (PERMITHA). We fight, we argue, we even stop talking to each other at times. But in the end, family is family. The love will always be there.

I also would like to deliver my respect and appreciation to my international friends, all members of International Student Association (ISA) in PSU as well as Science International Student Association (SISA) who make my day like a rainbow, filled with amazing color and diversity.

My gratitude for the Consulate of the Republic of Indonesia in Songkhla, Thailand. Thank for the opportunity to involve me as the President of Overseas Indonesian Student Association in Thailand (PERMITHA), chapter PSU.

The special acknowledgement to the scholarship funding provider, Thailand's Education Hub for ASEAN Countries (TEH-AC) scholarship awards, Graduate School Research Funding, Center of Excellent in Nanotechnology for Energy (CENE) PSU, Thailand Center of Excellence in Physics (ThEP-61-PHY-PSU3), Institute of Biomedical Engineering, Faculty of Medicine, PSU and Department of Physics, Faculty of Science, PSU.

The last, My beloved Mom and Dad, Juherman and Popon Karmila. I have gone this far only for you, for our family. No matter how thousands pains that I got, you always hear me, see me, and stand with me. To my dearest younger sister and brother, Winda Kamilasari and Aldy Nugraha, I am so sorry that I can not be your side like other elder brothers.

Ardian Agus Permana

The Relevance of the research Work to Thailand

The objectives of the research are to improve the dielectric, energy efficiency and electrocaloric properties of P(VDF-HFP) ferroelectric polymer. Those parameters are useful to discover the materials for cooling system as well as energy-based electronic devices. In Thailand, the electronic industry grows as one of the most promising sectors. The results of this work can be a guidance for the further researches as well as for industry application. The modified P(VDF-HFP) copolymers can take an important role on energy based devices and technology. These following devices can be more developed based on P(VDF-HFP) copolymers:

- Electrocaloric cooling system
- Microcapacitor
- Self-cleaning materials
- Actuators
- Energy-based electronics

TABLE OF CONTENTS

TABLE OF CONTENTS (CONT.)

LIST OF FIGURES

LIST OF FIGURES (Cont.)

LIST OF FIGURES (Cont.)

LIST OF TABLES

LIST OF ABBREVITIONS AND SYMBOLS

ΔS	Entropy change
ΔT	Temperature change
GNPs	Graphene Nanoplathelets
C	Heat capacity
P	Polarization
E	Electric Field
ECE	Electrocaloric effect
P(VDF-HFP)	Poly (vinylidene fluoride hexafluoroprophylene)
η	Energy efficiency
U_e	Storage energy denstity
E_b	Breakdown strength
ε_r	Relative permittivity of dielectric
ε_o	Vacuum permittivity
U_l	Energy loss
D	Displacement
X_c	Crystallinity
AFM	Atomic force microscopy
Sq	Surface roughness
WCA	Water Contact Angle
SEM	Scanning Electron Microscopy
XRD	X-Ray Powder Diffraction
FTIR	Fourier-Transform Infrared Spectroscopy
$F(\beta)$	β-phase fraction
A_α	Absorbance at wavenumber of 764 cm^{-1}
A_β	Absorbance at wavenumber of 840 cm^{-1}
K_α	α-phase absorption coefficients (6.1 x 10^4 cm^2 mol^{-1})
K_β	β-phase absorption coefficients (7.7 x 10^4 cm^2 mol^{-1})
D	Crystal sheets/crystal size

LIST OF ABBREVITIONS AND SYMBOLS (CONT.)

K	The constant of Scherrer ($K = 0.89$)
λ	The wavelength of X-ray ($\lambda = 0.154$ nm)
B	The width of the half-maximum
θ	The location of the diffraction peak.
ΔH_m	Melting enthalpy
T_m	Melting temperature
ϕ	The mass fraction comparison of the fillers and matrix
C	Capacitance
d	Thickness
A	Area of the electrode
G	Conductance
σ_{ac}	AC conductivity
T_c	Curie temperature
ΔT_{max}	Maximum ΔT

LIST OF PUBLICATIONS AND PROCEEDINGS

Salea, A., Chaipo, S., **Permana, A. A.**, Jehlaeh, K., and Putson, C. (2020). The microstructure of negative electrocaloric Polyvinylidene fluoride-hexafluoropropylene copolymer on graphene loading for eco-friendly cooling technology. *Journal of Cleaner Production*. (Published)

Permana, A. A., Chirasatitsin, S., and Putson, C. (2020). Electron beam irradiation for boosting storage energy density of tuned poly(vinylidene fluoride-hexafluoropropylene)/graphene nanoplatelet polymer composites. *Crystals*. (Published)

Permana, A. A., Ngamdee, W., and Putson, C. (2019). Improvement of electrocaloric properties of P(VDF-HFP)/GNPs composites for refrigerator cooling. *Journal of Physics: Conference Series (JPCS)*. (Published)

Permana, A. A., and Putson, C. (2020). Discharge Energy Efficiency Improvement of P(VDF-HFP) Copolymers Thin Films by Stretching and Electron Beam Irradiation. *IOP Conference Series: Materials Science and Engineering*. (Published)

Chapter 1 Introduction

1.1 Motivation and scientific background of the research

Until now, the design of air conditioning and refrigerators are still dominated by vapour compression technique. In that technique, chlorofluorocarbons (CFCs) or freon gases and hydrochlorofluorocarbons (HCFCs) have ever become the most efficient refrigerants (Correia and Zhang, 2014). Unfortunately, they can produce the emission gases which can deplete the ozone and make holes of it. Ozone is the natural barrier that can against the radiation from ultraviolet (UV). If there is no concern on it, it can be a big problem for public health especially causing skin cancer (Vienneau et al., 2017). The awareness of environmental issue, make the researchers try to find new refrigerants to reflace CFCs and HCFCs. R407, one of the eco-friendly hydrofluorocarbon (HFC) refrigerants, has been proposed as one of the potential candidates (Sachdeva and Jain, 2016). So that, nowaday some industries try to produce eco-friendly cooling system. Nevertheless, the energy conversion efficiency of vapour compression system only reach 40-50 % Carnot and it has already saturated (Correia and Zhang, 2014).

At the same time, microelectronics industries rapidly grow. Some industries try to create a new leading innovation on it. Wide demands of the lightweight, flexible and minute devices make this industry rapidly expand (Correia and Zhang, 2014). Microelectronics industries focus on how to integrate a lot of electronic components in one thin device. Integrated circuits (ICs) is one of the examples. The growth of this technology make it possible to compose hundreds or even thousands electronic components in a chip. As the consequences, the heat production in each spot or throughout the chip area can not be denied. This is a challenge to find and develop a new cooling system that can be applied to chip refrigerator. Beside of its eco-friendly, the new innovative cooling system has to possess efficient energy as well as thin, lightweight and flexible characteristic.

Due to those reasons, in recent decades, the researchers propose new idea to change vapor compression system by solid-state cooling system. The most interesting candidate is electrocaloric cooling system. Beside of its eco-friendly, due to its solid-

state materials, which will not produce emission gases to the atmosphere, electrocaloric cooling system possess some advantages compared with the other systems.

The first electrocaloric effect was observed in Rochelle salt. Before Kobeko and Kurchatov discovered it in 1930, the magnetocaloric effect had already well known. The vary magnetisation of the magnetic materials is the main principle of magnetocaloric energy conversion system (Vuarnoz et al., 2012). Based on magnetocaloric effect, in this system, the heat is driven by magnetic field. It causes magnetic domains have the same direction with the magnetic field that was applied in the system. So, it is lowering entropy and as the consequence, raising the temperature of the materials. Furthermore, the magnetic dipoles will be able to relax if the magnetic field is withdrawn. As the consequence, the magnetic dipoles can absorb some heat from the material (especially from crystal lattice) thereby lowering temperature.

"Due to its higher energy conversion efficiency and more enviromental friendly", magnetocaloric cooling system, which based on magnetocaloric effect, "emerges as a visible alternative new technology to traditional gas compression refrigerant" (Jia, Namiki, Kasai, Li, and Nishimura, 2018). The efficiency of energy conversion in magnetocaloric cooling system is 60-70 % Carnot (Correia and Zhang, 2014). Unfortunately, magnetocaloric cooling system does not show its suitability to be widely fabricated. To run the devices, the magnetocaloric cooling system needs heavy permanent magnetic field which can be provided by expensive and large superconducting magnets.

Those limitations motivated the scientists to find the other alternatives. The most promising way is to find the electrical analog of magnetocaloric cooling system. From the beginning of discovery, the studies of electrocaloric effect focused on bulk material. Unfortunately, the result did not satisfy them. The measurement of electrocaloric effect on bulk material was quite small compared with magnetocaloric effect. The electrocaloric temperature changes in bulk material only reach around 2 K. A good electrocaloric material has to possess high entropy variation (ΔS) as well as temperature change (ΔT). This situation had decreased the scientist interest to dedicate their research on developing electrocaloric refrigeration. It is also known from the

academic paper publications at that era. From 1961 to 2000, only 416 academic papers of electrocaloric effect that have been published. This number is quite different with the number of publications of vapour compression system that reach 24.321 papers.

The study about electrocaloric effect has rapidly grown start from 2006. At that time, giant electrocaloric effect was observed in $PbZr_{0.95}Ti_{0.05}O_3$ ceramics thin film at 225 ^{o}C for the first time (Mischenko, 2006). Although the electrocaloric effect observed in very high temperature (225 ^{o}C), but this study has already changed the direction of the electrocaloric research. That study showed that electrocaloric effect in thin films is bigger than the electrocaloric effect in bulk materials. The electrocaloric temperature change (ΔT) in $PbZr_{0.95}Ti_{0.05}O_3$ ceramics thin film is close to 12 K. Unfortunately, beside its high electrocaloric property, we also need flexible materials. Ceramics are brittle and easy do be damaged by external forces. To improve the ceramic's ability, the scientists found ferroelectric polymers especially poly (vinylidene fluoride)/P(VDF)-based poymers. With lightweight and flexible structure, P(VDF)-based polymers can be used to heavy and rigid the ceramics or the other inorganic materials (He et al., 2016). In 2008, another giant electrocaloric effect was also observed in P(VDF-TrFE) thin films at 70 ^{o}C with the electrocaloric temperature change (ΔT) of 12 ^{o}C (Neese et al., 2018). These two studies led to a promising era of electrocaloric cooling system. From 2008 until now, the electrocaloric study is increasing significantly.

The scientists's dedication on finding the analog of magnetocaloric cooling system obtained good result. The efficiency of energy conversion in electrocaloric solid-state cooling system is 60 % Carnot, exceeds the efficiency of vapour compression system (Pakhomov, Karmanenko, Semenov, and Starkov, 2010). This number shows that the electrocaloric cooling system has almost equal effectiveness with magnetic cooling. But different with magnetocaloric cooling system, electrocaloric cooling system possess additional advantages such as less weight, compact size and economic sustainability (Kitanovski, Tu, and Poredo, 2014).

The trends of the recent studies focus on how to observe and develop new electrocaloric thin films as well as to enhanced the electrocaloric effect near to room temperature (Correia and Zhang, 2014). This study will focus on how to get high

electrocaloric effect by using P(VDF-HFP) copolymers as the matrix. P(VDF)-based polymers have at least 5 crystalline phases. To be used in real application, the β-phase (all trans TTTT zigzag conformation) content is the most electrically active phase due to its highest polarization (Martins, Lopes, and Lanceros-Mendez, 2014). To get higher β-phase, Graphene Nanoplathelets (GNPs) has been used as filler. GNPs is carbon-based material that contain positive ions. If this material are mixed with P(VDF)-based materials that contain negative ions from fluorine atoms, the β-phase should be constructed so that the higher polarization will be obtained. So that, high electrocaloric effect can be obatained. An additional approach that used in this study is electron beam irradiation. High energy electron irradiation can break the big domain size into smaller. As the result, the lower energy loss can be obtained.

In simple term, the main advantages of this study are to produce high electrocaloric effect on electron irradiated GNPs/P(VDF-HFP) composites and understand its mechanism. Moreover, the value of temperature and entropy change of the samples have been investigated as well as their characterization. So, the best solutions for electrocaloric cooling system on these composites will be obtained. Until now, it is rare to find the study that combining two approaches; adding nanofillers and electron beam irradiation to increase the electrocaloric effect of the composites.

1.2   Objectives of the research

The objectives of the research are to improve the dielectric, energy efficiency and electrocaloric properties of P(VDF-HFP) ferroelectric polymer. Two following strategies have been conducted to reach the objectives.

Strategy I: the P(VDF-HFP) matrix was filled by GNPs conducting nanofillers to enhance the dielectric and electrocaloric properties.

Strategy II: the composite thin films were emitted by the electron beam to improve the energy efficiency properties.

1.3   Thesis Organization

The thesis was divided into six chapters. Each chapter describes the different topic but is still related to each other.

The first chapter presents the importance of the research, related to the motivation as well as its scientific background.

Chapter 2 explains the preparation steps of the GNPs/P(VDF-HFP) composite thin films and the electron beam irradiation process.

Chapter 3 shows the characterization of the electron beam irradiated GNPs/P(VDF-HFP) related to their morphology, microstructure and thermal behavior.

Chapter 4 plots the dielectric properties and AC conductivity measurements of the composite thin films.

Chapter 5 merges the measurement results of the ferroelectricity P-E loops, energy efficiency properties and electrocaloric effect of the P(VDF-HFP) copolymers before and after treated by GNPs nanofiller and electron beam irradiation.

The last, chapter 6 summarizes the general conclusions of the thesis as well as proposes the suggestions of the future work.

1.4 Concept of electrocaloric

1.4.1 Electrocaloric Effect

The electrocaloric effect can not be separated from pyroelectric effect. Both of them originally come from the cross-coupling between temperature and polarization of a dielectric materials (Li et al., 2013). The electrocaloric effect can be defined as the change in entropy (ΔS) and temperature (ΔT) of materials under adiabatic conditions when an external electric field is applied or removed. In simple terms, electrocaloric effect refers to the temperature change caused by polarization change, while the reversed process defined as pyroelectric effect (Abdessalem, Kriaa, Aydi, and Abdelmoula, 2018; Correia and Zhang, 2014; Li et al., 2013).

For dielectric materials, the Gibbs free energy (G) is expressed as an entropy (S) temperature (T), strain (x), stress (X), electric field (E) and electric displacement (D) function as follows (Correia and Zhang, 2014; X. Li et al., 2013):

$$G = U - TS - X_{ij}x_{ij} - E_iD_i \qquad (1)$$

where U is the system's internal energy. The field term and the stress are expressed by Einstein notation with i (1 to 6) and j (1 to 3). The equation (1) can be written as differential form:

$$dG = -SdT - x_{ij}dX_{ij} - D_i dE_i \tag{2}$$

and thus,

$$-\left(\frac{\partial G}{\partial T}\right)_{E,X} = S, \quad -\left(\frac{\partial G}{\partial X_{ij}}\right)_{E,T} = x_{ij}, \quad -\left(\frac{\partial G}{\partial E_i}\right)_{X,T} = D_i \tag{3}$$

These equations above represent heat capacity, elasticity and dielectric permittivity, respectively. The differential forms of the equation (3) are the Maxwell relations:

$$-\left(\frac{\partial^2 G}{\partial T \partial E_i}\right)_X = \left(\frac{\partial D_i}{\partial T}\right)_{X,E} = \left(\frac{\partial S}{\partial E_i}\right)_{X,T} = p_i \tag{4}$$

$$-\left(\frac{\partial^2 G}{\partial X_{ij}\partial E_k}\right)_T = \left(\frac{\partial X_{ij}}{\partial E_k}\right)_{X,T} = \left(\frac{\partial D_k}{\partial X_{ij}}\right)_{E,T} = d_{ijk} \tag{5}$$

$$-\left(\frac{\partial^2 G}{\partial X_{ij}\partial T}\right)_E = \left(\frac{\partial X_{ij}}{\partial T}\right)_{X,E} = \left(\frac{\partial S}{\partial X_{ij}}\right)_{E,T} = \alpha_{ij} \tag{6}$$

These equations above show the equalisation between pyroelectric coefficient and electrocaloric effect, piezoelectric effect and direct effect, also thermal expansion coefficient and piezocaloric effect, respectively.

The equation (6) indicates that at isothermal and constant X condition, the entropy variation of electrocaloric is:

$$dS = \left(\frac{\partial D_i}{\partial T}\right)_{X,E} dE_j \tag{7}$$

and thus,

$$\Delta S = \int_{E_1}^{E_2} \left(\frac{\partial D_i}{\partial T}\right)_{X,E} dE_j \qquad (8)$$

where E_1 is the starting electric field and E_2 is the final electric field. According to the heat capacity definition, C:

$$C = T \left(\frac{\partial S}{\partial T}\right)_E \qquad (9)$$

The temperature change at adiabatic condition can be used to describe the electrocaloric effect

$$dT = -\frac{T}{C}\left(\frac{\partial D_i}{\partial T}\right)_{X,E} dE_j \qquad (10)$$

and,

$$\Delta T = -\frac{T}{C} \int_{E_1}^{E_2} \left(\frac{\partial D_i}{\partial T}\right)_{X,E} dE_j \qquad (11)$$

where C independent of E.

In most pyroelectric materials, the displacement (D) is almost equal with polarization (P). So that, the equation (8) and (11) can be expressed as:

$$\Delta S = \int_{E_1}^{E_2} \left(\frac{\partial P_i}{\partial T}\right)_{X,E} dE_j \qquad (12)$$

$$\Delta T = -\frac{T}{C} \int_{E_1}^{E_2} \left(\frac{\partial P_i}{\partial T}\right)_{X,E} dE_j \qquad (13)$$

respectively.

1.4.2   Electrocaloric cooling

Electrocaloric cooling is based on electrocaloric effect. It means that when there is no applied electric field to the electroclaoric material, the electric dipoles are randomly oriented (disorder orientation state). When the external electric fields are applied to the electrocaloric material, the direction of electrical dipoles will change to the same direction with the applied electric field. This can influence the inner structure of the material. Decreasing the disorder of the thermodinamycal system will decrease the entropy as well as heat capacity of the electrocaloric material. Since in adiabatic condition, where there is no heat loss because the material is isolated from its surroundings, the temperature of the electrocaloric material will increase (Correia and Zhang, 2014).
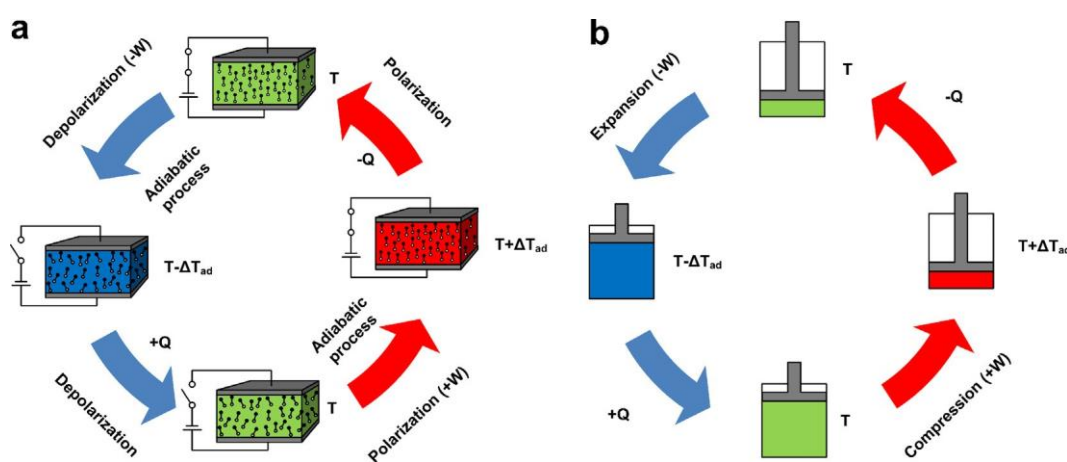
Figure 1.1. (a) Electrocaloric refrigeration, **(b)** vapour compression refrigeration (Kitanovski et al., 2013).

Due to its reversible process, when the external electric field is removed from the material, so the opposite result will be obtained. Removing external electric field will change the electrical dipole's directions from order to disorder orientation. The material's entropy will increase and at the same time decreasing the material's temperature as long as in adiabatic condition. If these two phenomena are merged with the states that enable heat transfer

from or to the material into a cycle, the cooling or heating system will be obtained (Correia and Zhang, 2014; Kitanovski, Tu, and Poredo, 2014). Figure 1.1 shows the comparation between electrocaloric refrigeration and vapour compression refrigeration.

1.4.3   Electrocaloric effect measurement method

There are two types of electrocaloric effect measurements (Asbani et al., 2015; Li et al., 2013):

a) Indirect method: ΔS (entropy change) and ΔT (temperature change) are deduced using Maxwell relation.

b) Direct method: ΔS (entropy change) and ΔT (temperature change) are obtained from calorimeters with the special design.

Due to the difficulties, there were not many electrocaloric effect studies that present the direct measurement method (Asbani et al., 2015). To measure the electrocaloric effect specially in thin films, the scientists often generate it from the measurement of pyroelectric coefficient rather than the measurement of electrocaloric directly (Correia and Zhang, 2014). It cause many studies focus on how to increase the the pyroelectric coefficient, because high pyroelectric coefficient means high electrocaloric effect. But, since a rapid growth of the study in electrocaloric, the accuracy of the electrocaloric measurement, especially in thin film, get a big concern. There is any possibility to get unpredictable and significant errors when relating two different effects by using Maxwell relation.

Even so, direct techniques only can be used to probe bulk ceramics/large samples or large-area capasitors, but does not work well for measuring small volume samples (Pandya et al., 2017). The small and nonuniform heat capacity and heat transfer are the reson why the electrocaloric measurement in thin films is lack of precision (Lubomirsky and Stafsudd, 2012). In 2010, a study reported the direct measurement in bulk materials and thin films. That study indicates a good agreement between the direct and indirect measurement method for most of the electrocaloric materials (Maiwa, 2015). For relaxor, which are non-equilibrium (in

mechanical, thermal/chemical aspects), using equilibrium statistical, like Maxwell relations, to measure the electrocaloric effect is technically unjustified (Lu, Zhang, and Kutnjak, 2010).

Table 1.1. Electrocaloric behaviour of PZT-based materials, PMN–PT, and BZT (Maiwa, 2015).

Sample	dP/dT $(\mu Cm^{-2}K^{-1})$	ΔT Estimation (K)	ΔT from experiment (K)
Soft PZT, T_c of 190 °C	-0.022	0.33	0.27
Hard PZT, T_c of 145 °C	-0.033	0.50	0.30
BZT	-0.024	0.31	0.19
Hard PZT, T_c of 325 °C	-0.013	0.20	0.14
Soft PZT, T_c of 330 °C	-0.016	0.24	0.31
PMN-PT	-0.058	0.66	0.36
PLZT (9.1/65/35)	-0.042	0.48	0.39

1.4.4   Electrocaloric materials

Generally, electrocaloric materials as well as pyroelectric materials can be devided into two main groups (He et al., 2016; Kitanovski et al., 2014; Li et al., 2013):

a) Inorganic materials (including ceramics, monocrystal and semi-conductors).

b) Organic materials (including side-chain liquid crystal and P(VDF-based) polymers).

In simple term, organic materials defined as living organism or non-living materials that containing carbon and the opposite is defined as inorganic materials ("IUPAC Provision Recomendation," 2004).

The good electrocaloric materials have to possess high entropy variation as well as high temperature change. It means that the electrocaloric materials should have high dielectric strength (the critical electric field value). This is important to minimize the electromechanical breakdown that can be caused by long-term high electric field expose (Review, War and States, 1988; Kitanovski, Tu and Poredo, 2014).

In the early of electrocaloric studies, the material that used were ceramis and crystals. Monocrystals and bulk samples do not possess high dielectric strength, so that they can not withstand under the stresses of high electric fields. Hence, they showed small electrocaloric effects observed. Many studies show that ceramics provide high coefficient both in piezoelectric and pyroelectric. Unluckily, they are brittle so that the continuous external forces can damage the materials easily (He et al., 2016).

1.5   Conclusion

Environmental change and rapid microelectronics industries growth that focus on how to integrate a lot of electronic components in one thin device required the scientist to find and create a new leading innovation, including in cooling system. The challenge is not only about the strong electrical ability but also efficient for the energy issue as well as lightweight, flexible and low cost for mass production. Since discovered in 1930 and rehits in 2006 when giant electrocaloric effect has been observed in ceramic thin film, the massive researches are still continuing to understand its unclear mechanism as well as to find the outstanding materials and optimum methods to improve the properties.

Chapter 2 Preparation of electron irradiated GNPs/P(VDF-HFP)

2.1   Introduction

Since the electrocaloric cooling system that mainly based on electrocaloric effect is a new trend, a plenty of works have to be conducted to understand. Many ways that can attacked to discover and optimize it. Finding and manipulating the materials as well as variating the methods and approaches are some of the promising techniques. With outstanding properties among other ferroelectric polymers, P(VDF-HFP) organic copolymers was choosen as the main material. Further, among some well known techniques, this work combined two approaches, adding GNPs conducting nanofillers and electron beam irradiation that is not really well explored.

2.2   Literature reviews of P(VDF-HFP) and GNPs

2.2.1   P(VDF-HFP)

To improve the ceramic's ability, the scientist found ferroelectric polymers especially poly (vinylidene fluoride)/P(VDF)-based polymers. With lightweight and flexible structure, P(VDF)-based polymers can be used to heavy and rigid the ceramics or the other inorganic materials (Malmonge, Malmonge, and Sakamoto, 2003). "Being a fluoropolymer with the molecular formula $(CH_2{=}CF_2)_n$, P(VDF) is readily prepared through free radical polymerization of gaseous monomers 1,1 difluoroethylene" (Li and Wang, 2016). P(VDF) polymer and its copolymers such as poly (vinylidene fluoride hexafluoroprophylene)/P(VDF-HFP) and poly (vinylidene fluoride trifluoroethylene)/P(VDF-TrFE) become some of the most important electroactive polymers, especially after the discovery of huge electrocaloric effect on them. Compared with another materials that possess pyro, piezo and ferroelectricity, P(VDF) and its copolymers are the best one that possess all electroactive properties (Martins, Lopes, and Lanceros-Mendez, 2014).

To be used in commercial cooling devices, P(VDF)-based polymers can be fabricated into thin film as well as can be used for large size devices. The previous study shows that due to their capability to withstand under high

electric fields, the polymer thin films possess the biggest temperature and entropy change over the other electrocaloric materials (Kitanovski et al., 2014). Because of those advantages, P(VDF)-based polymers become the target to be developed and to be applied in commercial applications.

P(VDF) and its copolymers are classified as semi-crystalline polymer. It means that the responses to external electric field are from the contribution of crystalline and amorphous phase. P(VDF)-based materials have three molecular conformation modes, TGTG´, TTTT, and $T_3GT_3G´$ (Tiwari et al., 2013). P(VDF)-based materials have also five kind of crystalline phases. These phases are α, β, γ, δ, and ε. The most stable crystalline phase is the α-phase (non-polar) while the β-phase is the crystalline phase with the strongest pyroelectricity as well as piezoelectricity. It is caused by disimetris structure of the β-phase that creates highest dipole density compared with another phases. High density of dipoles provides high charge storage/surface charge because the charge is trapped at interfaces of the materials. So that, it causes high polarization as well as pyroelectricity (He et al., 2016). High dielectric constant that is possessed by the β-phase can increase the breakdown strength of the materials under high electric field. It leads to high energy density So that, to enhance the pyroelectric coefficient of P(VDF)-based materials, the researchers try to change the α-phase to the β-phase. Some approaches are used to gain the goal such as mechanical stretching and by using nanofillers. The other ways are using electrospining and high voltage polarization to enhance the pyroelectric coefficient of P(VDF)-based materials.

A study about P(VDF-HFP) was conducted by Sousa, et al in 2014. The result show that increasing the percentage of P(VDF-HFP) into P(VDF-HFP)/DMF solutions, in this case using the varying concentration from 5-20 wt%, effectively decrease the gap or hole size of the materials from ~7.5 µm in 5 (**figure 2.1. (a)**) until ~2 µm (**figure 2.1. (d)**) (Sousa et al., 2014). On the other hands, **figure 2.1. (e)** and **figure 2.1. (f)** show the effect of increasing evaporation temperature on the morphology of 20 wt% P(VDF)/DMF solution. It is clear that by increasing the evaporation temperature beyond 40

^{o}C, in this case 50 ^{o}C and 100 ^{o}C, the mobility of the chains are also increase. So, the particles are able to cover the exsisting holes. That is why there are not any holes are observed (Sousa et al., 2014).
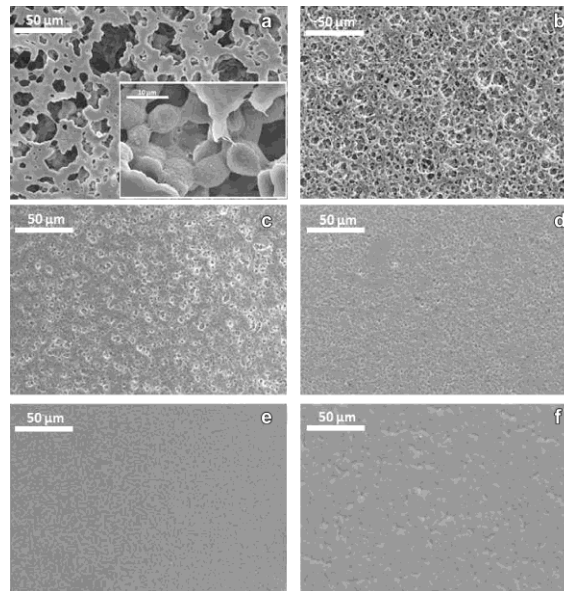
Figure 2.1. The microstructures of the P(VDF-HFP) thin films: at room temperature of evaporation with (a) 5, (b) 10, (c) and (d) 20 wt.% of P(VDF-HFP). The microstructures of P(VDF-HFP) with 20 wt.% concentration by varying solvent evaporation of (e) 50 and (f) 100 °C (Sousa et al., 2014).

Table 2.1 shows that at high temperature (in this case 100 ^{o}C), the improvement of P(VDF-HFP) concentration on the solution can decrease the exsistence of β-phase content. That is because at high temperature, the diffusivity of the solvent is lower than grow of evaporation rate (Chinaglia et al., 2010). Besides that, the influence of different temperature on the same concentration is also observed. High vaporation temperature will increase the rate of evaporation of materials. So that, the stability of the material is high, leading to α-phase crystallization. In the opposite, the low evaporation temperature will lead to the β-phase crystallization due to its low evaporation state (Martins et al., 2014).

Table 2.1. The percentage of β-phase fraction of P(VDF) materials dependent on concentrations and vaporation temperatures (Sousa et al., 2014).

Samples	β-phase (% ± 2%)
5/95, at 100 ^{o}C	75
10/90, at 100 ^{o}C	66
15/85, at 100 ^{o}C	22
20/80, at 100 ^{o}C	16
20/80, at 25 ^{o}C	79
20/80, at 50 ^{o}C	24

Compare with P(VDF) polymers, the P(VDF-HFP) copolymers possess higher piezoelectric coefficient, chemical resistance and mechanical properties (Roy, Dutta, and Bhattacharya, 2016). This copolymers become promising materials for ferro- and piezoelectric application. The improvement on those properties are caused by additional hexafluoropropylene (HFP) monomer unit to the backbone or main chain of P(VDF).
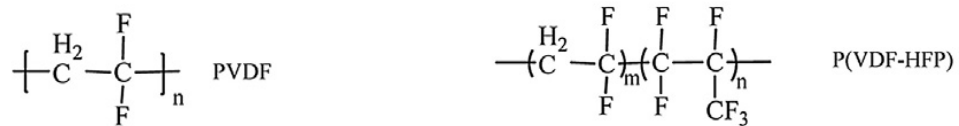
Figure 2.2. The structural formula of PVDF and P(VDF-HFP) (Zhu, Jiang, Zhang, and Huang, 2017).

According to Roy et al. (2016), "… P(VDF-HFP) turn out to be unique prospects with similar crystalline structures to that of P(VDF) but enriched flexibility and chemical resistence" as well as possess another characteristic like "nontoxicity, high stability, shape and size tailor ability and recycling aptitude" (Roy et al., 2016). In P(VDF) electroactive polymers and its copolymers, "each chain possesses a dipole moment perpendicular to the polymer chain" (Martins, Lopes, and Lanceros-Mendez, 2014).
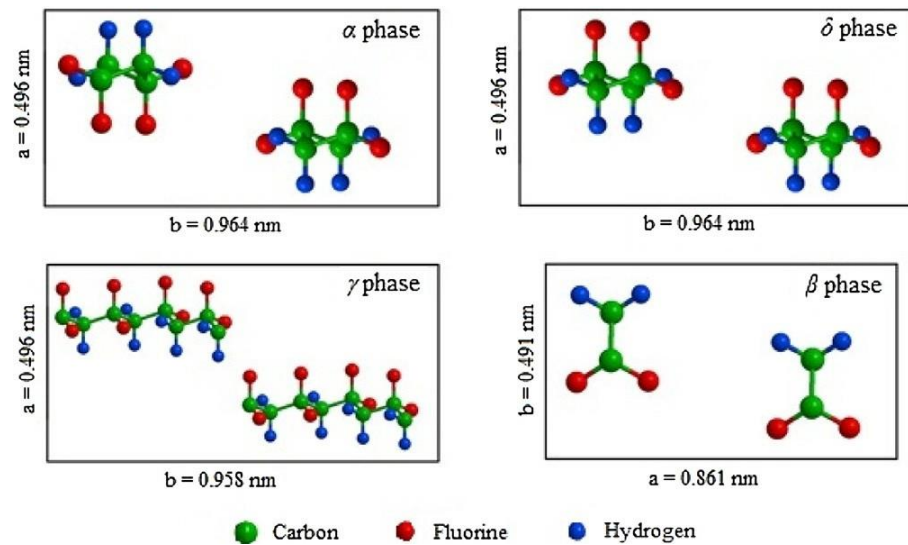
Figure 2.3. The schema of four phases of PVDF unit cells (Zhu et al., 2017).

The electronegative behavior of fluorine atoms affects the electrical dipole moments per unit cell to be high (5-8 x 10^{-30} C.m) (Martins, Lopes, and Lanceros-Mendez, 2014). To be used in real application, the β-phase (all trans TTTT zigzag conformation) content is the most electrically active phase due to its highest polarization per unit sel (8 x 10^{-30} C.m) compared with the other polar phases like γ-phase (T_3GT_3G') and δ-phase (TGTG').
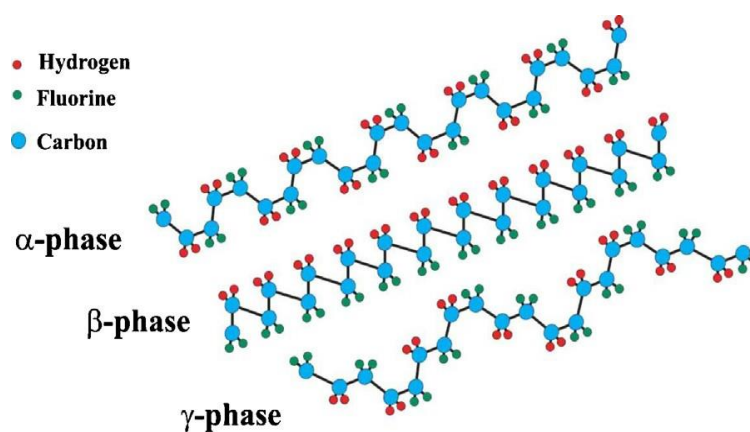
Figure 2.4. The schema of α, β and γ-phase chain conformation of PVDF (Martins et al., 2014).

The α- and ε–phases (TGTG´) are non-polar because the dipole moment packed within the unit cell in antiparallel term. (Martins, Lopes, and Lanceros-Mendez, 2014; Roy, Dutta and Bhattacharya, 2016; Roy et al., 2016). Each phase shows different morphology representing the contribution of dipolar moments per unit cell.

2.2.2   GNPs

The demand of dielectric materials that possess light weight as well as high dielectric constant but low dielectric loss is increase time by time. Many studies focus on how to obtain new materials with some specific characteristics to be applied in electrical devices (Lu, Hu, Xie, Zhuo, and Yang, 2017). Not only used for transducer, actuators or energy storage devices, dielectric materials are proposed to take a part on thermal management (Yang, Xu, Yu, Wang, and Gong, 2017). During the usage, the electrical devices can produce the heat. No doubt that the thermal management ability of the material should be improved. Graphite is one of the common fillers that usually used to reinforce the mechanical and dielectric properties as well as thermal properties (Su and Zhang, 2017). It means that beside its high thermal and electrical conductivity, graphene has already got an attention from the scientist due to another advantages like light weight, flexibility and easy to process.

There are a lot of kinds of graphene. To be suitable in wide fabrication, the efficient cost has to be considered. Graphene nanoplatelets (GNPs) or multi-sheet graphene are well known as low cost materials, because of its nanosize, and possess higher electrical conductivity compared to graphite itself or other polymer nanocomposites like carbon nanotubes (CNTs) or single-sheet graphene. That nanomaterial, by simple exfoliation, can be obtained from graphite (Kuvardina, Novokshonova, Lomakin, Timan, and Tchmutin, 2013).
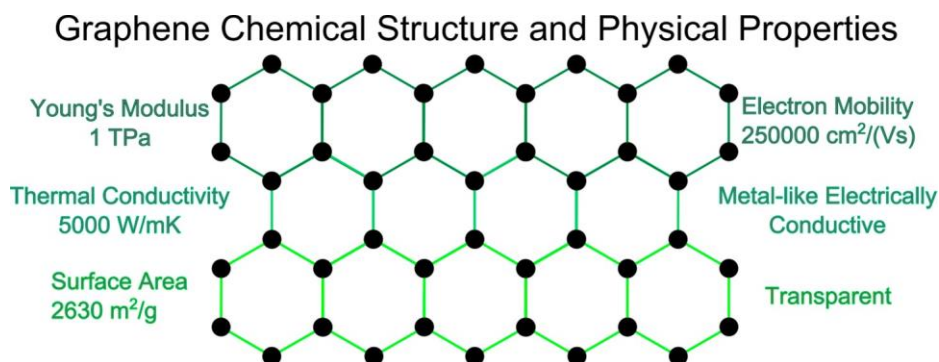
Figure 2.5. The hexagonal chemical structure of Graphene and its properties (Cataldi, 2018).

Adding some polymers with high specific area can improve the flexibility of the composites. It is because the complex viscosity of the composites is changed to become non-sensitive. To increase the thermal conductivity, mechanical properties and dielectric constant, the volume resistivity should be decreased. Filling the compatible fillers into the gap between each particles of the composites/materials can increase the crosslink density (Su and Zhang, 2017). Although some studies described that the density, hardness and modulus of the materials can be declined due to the decreasing of crystallinity as well as the damage of segment uniform, cross-linking still has an important affect to thermal and mechanical properties (Fan and Xiao, 2008). Crosslink density is the density of a small area that some parts of the polymer are arranged/connected become chains (Jenkins, Kratochvíl, Stepto, and Suter, 1996). As the consequence of doping the fillers to the materials, the composites are more rigid and its compatibility will increase. That kind of molecular structures can affect the tear and the tensile strength to be higher. So that, the huge disruption like strain or stress can be prevented (Fan and Xiao, 2008). The tensile strength is a property that determines the material's ability to be stretched without any fracture. While tear strength can be defined as the material strength to withstand under the static or kinetic force (Witkowska and Frydrych, 2004). Nevertheless, adding fillers to the main material matrix should be below percolation threshold. To

get high dielectric constant, the percolation between nanofillers is undesired. High percolation between each nanofillers will connect nanofillers particles. As the consequence, the conduction way can be formed and it leads to high dielectric loss and lowering breakdown strength (Zhu, 2014).

In 2017, a study of Graphene nanoplatelets was conducted. **Figure 2.6. (a)** shows that the graphenene nanoplatelets (GNPs) particles possess a non-uniform shape with few microns diameter. If compared with **figure 2.6. (b)**, it is so clear that the graphenene nanoplatelets (GNPs) possess a good adhesion with the PVDF/PMMA matrix since there are no gaps or holes at the interface of GNPs and PVDF/PMMA matrix. Besides that, graphenene nanoplatelets (GNPs) exhibit a well dispersion with no observed agglomerates domination as shown by SEM analysis. "The GNPs are entrapped into polymer matrix and arranged parallel to each other" (Yang et al., 2017).
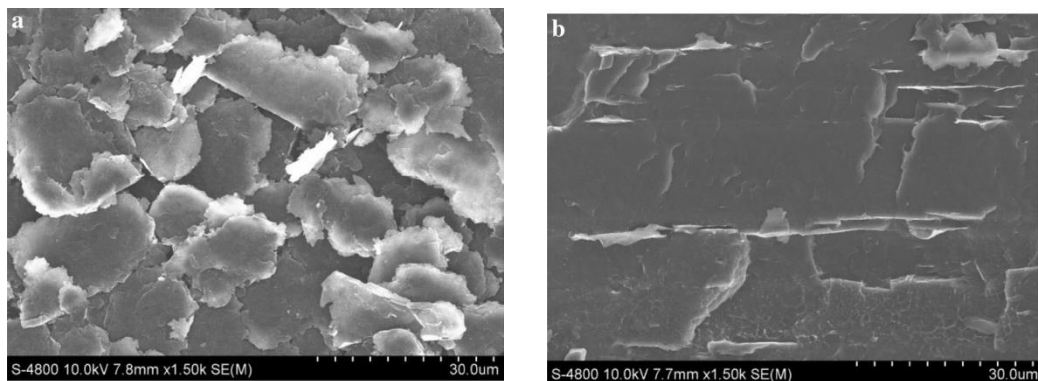
Figure 2.6. SEM image of (a) GNPs particles; (b) 4 wt% GNPs in PVDF/PMMA/GNP composites (Yang et al., 2017).

FTIR spectroscopy show that the α-phase of the PVDF/PMMA/GNP with 1 and 2 wt% GNP (in vibration peak 795, 855 and 978 cm^{-1}) almost disappear as the that in PVDF/PMMA/GNP with 3 wt% GNP, the β- and γ-phase are dominant (**Figure 2.7**). The same conclusion is also obtained from the XRD analysis.

In neat PVDF spectrum, there are three peaks that appears at 18.4°, 20.0° and 26.7°. All of them are α-phase. When the 3 wt% GNP was doped to the PVDF/PMMA, the α-phase diffraction peaks almost disappear. At the same time, the β-phase peaks at 20.1° get sharper than the β-phase peaks of neat PVDF (**Figure 2.8**) (Yang et al., 2017).
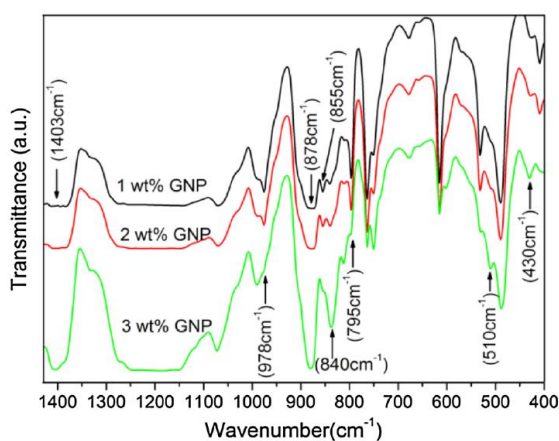
Figure 2.7. FTIR spectra of PVDF/PMMA/GNP by filler of 1, 2, and 3 wt% GNP (Yang et al., 2017).
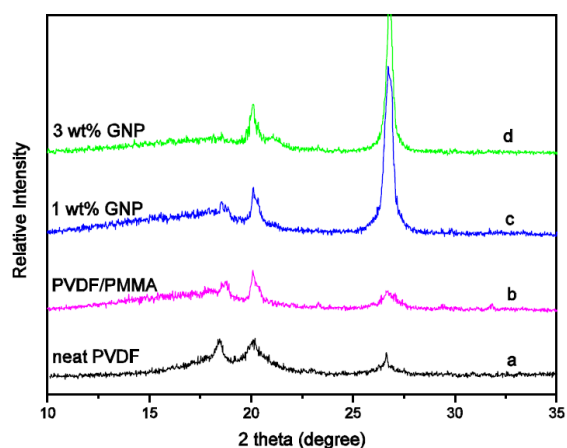
Figure 2.8. XRD spectra ofa neat PVDF, PVDF/PMMA and PVDF/PMMA/GNP composites with 1, and 3 wt% GNP (Yang et al., 2017).
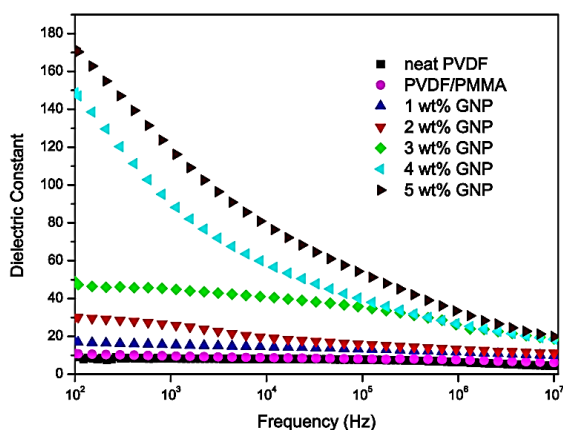
Figure 2.9. Dielectric Constant of various samples (Yang et al., 2017).
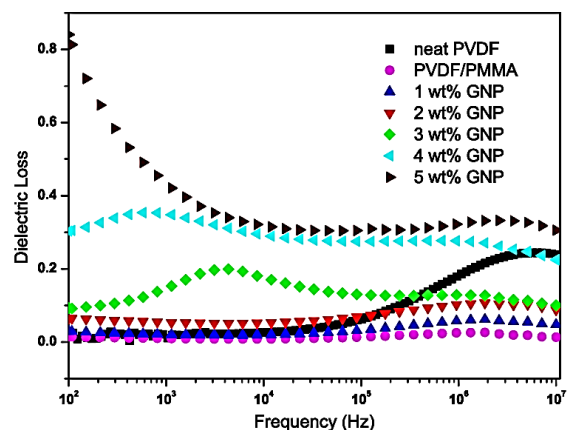
Figure 2.10. Dielectric Loss of various samples (Yang et al., 2017).

The dielectric constant and dielectric loss are presented below. **Figure 2.9** shows that there is no significant improvement of dielectric constant of the PVDF/PMMA/GNP composites with 1, 2 and 3 wt% GNP compared with the neat PVDF or PVDF/PMMA. At that condition, GNPs take a role as capacitor electrodes. The different improvement is showed by PVDF/PMMA/GNP composites with 4 wt% GNP. At that condition, GNPs is very close each other and arrange serial or parallel microcapasitors even though still in isolated system. As the consequence, the dielectric constant will significantly increase. This condition occurs at percolation threshold content. The increasing of GNP filler after that state will increase the number of microcapacitor. At the concequences, it can increase the electrical conductivity (Yang et al., 2017). This condition happens to composites with 5 wt% GNP.

Figure 2.10 shows that the significant improvement of dielectric loss occurs beyond the percolation threshold. Generally the dielectric loss is the representative of material's conductivity. It means that adding GNP fillers to the blend PVDF/PMMA will automatically increase the conductivity as well as the dielectric loss of the composites (Yang et al., 2017).

2.3   Literature reviews of electron beam irradiation and energy properties

2.3.1   Electron beam irradiation

Due to its uniqueness, the polymer composites get a lot of attention from the scientist. To obtain specific properties that required for different particular applications, a chemical approach like doping with some suitable dopants or irradiation technique could be good choices (Verma, 2018). In some cases, irradiation technique provides an advantage over chemical process. In irradiation technique, the release of harmful fumes will not occur like in chemical method.

In 2011, a study using irradiation technique was published. A giant electrocaloric effect was observed in stretched P(VDF-TrFE) copolymers with high-energy electron irradiation. The temperature change (ΔT) and

entropy change (ΔS) that has been obtained from that study are over 20 ^{o}C and over 95 J/(kgK) at 33 ^{o}C and 160 MV/m (Lu et al., 2011). That values are quite higher than P(VDF-TrFE) terpolymer blends and P(VDF-TrFE) pure copolymers which possess temperature change (ΔT) of 9 ^{o}C and 12 ^{o}C, and entropy change (ΔS) of 46 J/(kgK) and 55 J/(kgK), respectively. Those both studies were procured at room temperature and 80 ^{o}C, respectively.

The big number of temperature change (ΔT) and entropy change (ΔS) indicates a big electrocaloric effect as well as polarization of the materials. That is because of the higher randomness that occur when high energy electron irradiation change the state of the material from the normal ferroelectric into the relaxor ferroelectric state (Lu et al., 2011). Relaxor material is the material that changes their shape under applied external electric fields. That property is called electrostriction.

The high-energy of electrons when exposing the materials can damage the long all-trans chains of the material's structure. As the consequence, the short all-trans chains were easier to be oriented by the external electric field and make a big effect to the thermally stimulated depolarization current (TSDC), volume strain and of course permittivity (Lu et al., 2011; Verma, 2018). Besides that, the electron ability to cut material segments become shorter can drop the energy barrier that prohibited β-phase releasement before thechains of the polymer could switch freely. As the consequence, electron irradiation can decrease the Curie temperature (Zhu et al., 2017).

The temperature change was measured by direct method. **Figure 2.11** shows the electrocaloric temperature change (ΔT) as a function of applied electric field. If the value of electrocaloric temperature change (ΔT) has already known, the specific heat capacity and the entropy change (ΔS) can be generated. Even though, the relation between chemical structure of the relaxor materials and their electromechanical properties is still unclear (Soulestin et al., 2017).
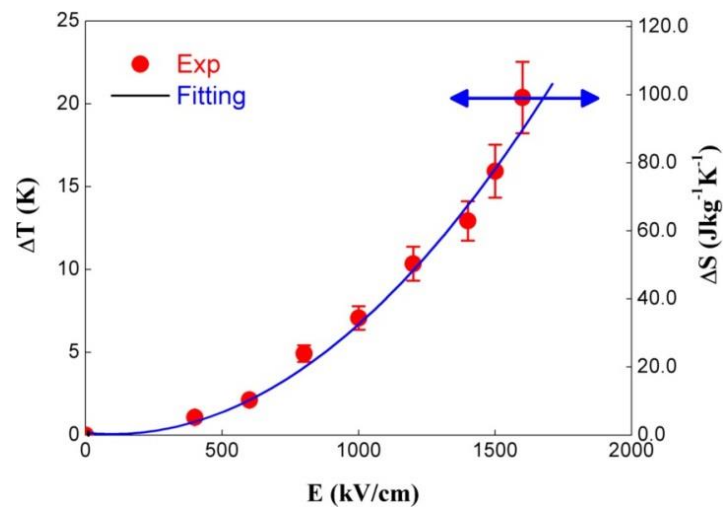
Figure 2.11. Electrocaloric temperature change as dependent on electric field (Verma, 2018).
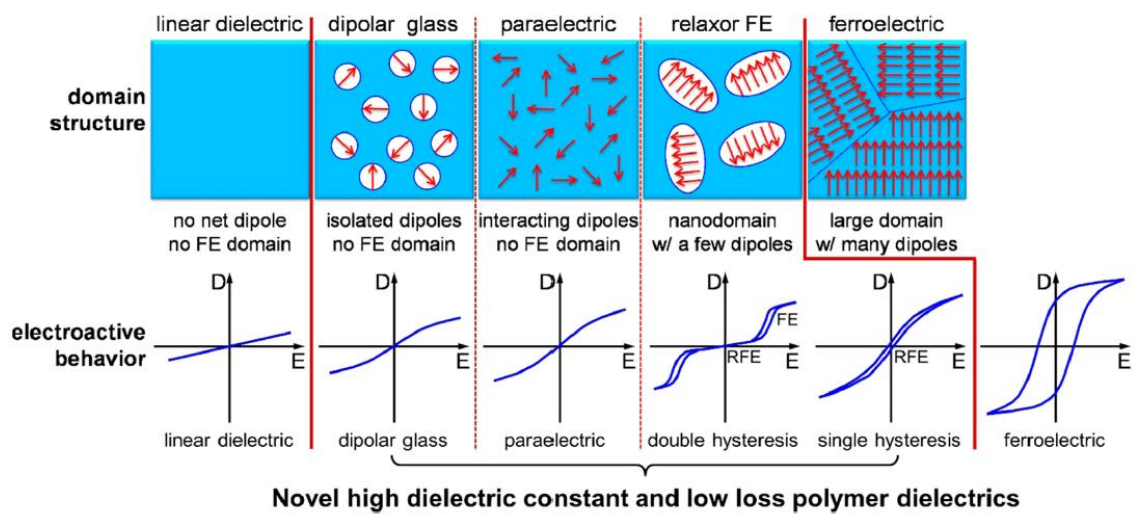
Figure 2.12. Different structures of dipole and ferroelectric domains and their *D-E* loops (Zhu, 2014)

There are several types of electroactive polymers. It depends on the D-E loops shape (Soulestin et al., 2017).

a) The first one is linear dielectrics. The response of the dipoles is linear with the electric field. It means that there is no hysteresis loop. The response of dipoles when the electric field is applied

and removed is showed in the same linear curve. The example of this material is polyethylene terephthalate.

b) The second one is dipolar glasses. These materials contain uninteraction independent dipoles. So that, there is on interaction among them or with the matrix. There is no Hysteresis D-E loops even the response to the electric field is not linear. The example of this material is PMMA.

c) The third one is paraelectric. There is still no hysteresis loops that shown. but in this state, the dipoles can interact each other and with the matrix even though they are not strongly enough to create the ferroelectric domains. The example of this material is amorphous/α-phase of P(VDF).

d) The fourth one is relaxor ferroelectric. This state occurs when the nanodomains that contain small number of aligned dipoles are formed. The slim hysteresis loops will be formed. It shows that the materials possess small remanent polarization (polarization under zero electric field). They do not show permanent spontaneous polarization when the electric field is removed. It means that nanodomains can easily relax without external electric field. The example of this material is high energy electron irradiated P(VDF-TrFE).

e) The last one is ferroelectric. This material shows high remanent polarization so that the hysteresis loops is larger than anothers. It means that the large domains can not easily relax when the external elecrric field is removed. The example of this material is crystalline P(VDF).

2.3.2   Energy properties

The other thing that should be considered is the energy efficiency. The energy efficiency is influenced by energy density and energy loss. Energy density defined as the energy per unit volume while energy loss is

energy that loss during transformation from one place/system/condition to another one. Mathematically, the energy efficiency can be expressed:

$$\eta = \frac{U_e}{U_e + U_l} \tag{14}$$

and,

$$U_e = \int_{D_1}^{D_2} E_b \ dD$$

$$U_e = \frac{1}{2} D \ E_b$$

$$U_e = \frac{1}{2} (\varepsilon \ E_b) \ E_b$$

$$U_e = \frac{1}{2} (\varepsilon_r \ \varepsilon_o \ E_b) \ E_b$$

$$U_e = \frac{1}{2} \varepsilon_r \ \varepsilon_o \ E_b{}^2 \tag{15}$$

where η is energy efficiency, U_e is energy denstity, U_l is energy loss, D is displacement, E_b is breakdown strength of dielectric, ε_o is vacum permittivity and ε_r is relative permittivity of dielectric (Zhu et al., 2017).

Although P(VDF) possess high permittivity and high breakdown strength, on the other hands, the remanent polarization cause the higher energy loss too. For normal ferroelectric, the D-E loops are large compared with other electroactive polymers. It caused by huge coupling forces among aligned domains. So that the oriented dipole can not reverse easily (Zhu et al., 2017).

In relaxor ferroelectric, the D-E hysteresis loop is slim. It means that the energy loss is lower than the normal ferroelectric. It is because high electron irradiation cuts the crystal into small domains. So that, after removing electric field, the dipoles is more reversible compared with normal ferroelectric (Yang et al., 2013). Besides its ability to reduce the dielectric loss, on the other hands, high energy electron irradiation can damage the structure especially mechanical structure of the materials. As the consequence, it can lowering breakdown strength of the material and can decrease the energy density (Zhu et al., 2017).

According to Tan et al. (2013) ''The stretched films exhibit a significantly enhanced dielectric constant, breakdown field, and energy density but depressed energy loss'' (Tan et al., 2013). That study shows that mechanical stretching can improve the quality of the film by improving the uniformity of crystal domain orientation that leads to high dielectric constant/energy density and accelerating the ferroelectric relaxation that leads to lowering dielectric/energy loss.

2.4 Preparation of electron irradiated P(VDF-HFP) thin films and its composites

2.4.1 Materials and equipment

Materials:

a) Poly (vinylidene fluoride hexafluoroprophylene)/P(VDF-HFP) powder, Solef 11010/1001, purchased from Solvay Solexis, Belgium.

b) Graphene Nanoplatelets conducting fillers (GNPs) 306633-25G, from Sigma Aldrich, USA

c) The solvent, N,N-dimethylformamide (DMF) with purity $\geq 99\%$, from RCI Labscan, Thailand.

Equipment:

a) Beaker, 250 and 500 ml

b) Analytical balance Sartorius BSA224S-CW, Scientific Promotion Co., LTD

c) Hotplate magnetic stirrer (Heidolph model MR hei-Standard and MTOPO model MS300HS)

d) Magnetic bar

e) Fume hood (Canupy Hood, FLEXLAB the laboratory makers model CNP120)

f) Ultrasonic Homogenizer Sonicator Model 150V/T

g) Adjustable film applicator, sheen S/N 102503/2 (*incl*, Shims)

h) Smooth glass plate, 25x24 cm

    i)   Incubators (Asset positively identifiable T410353 Binder)

    j)   Thickness Gauge Handing, Peacock model G-7C, resolution 0.001 mm.

2.4.2   Preparation method of the thin films

P(VDF-HFP) copolymers are used as the main matrix. In addition, Graphene Nanoplathelets (GNPs) are used as fillers. Neat P(VDF-HFP) and its composites, named as HFP/GN, were the main object of this study. Fabricated by the solution casting, neat P(VDF-HFP) was prepared by mixing P(VDF-HFP) powder containing HFP monomer of 10% and DMF solvent for 16 h by a stirrer magnetic at room temperature. The concentration of the copolymer was controlled at 20 wt% with copolymer and solven ratio was 1:4.

After rested for 1 h to eliminate undesired bubbles, the solution was cast on clean glass plates using a blade at specific thickness. The cast solution then was dried in the oven temperature of 80 ^{o}C for 12 h. The final thickness of all samples was controlled to a tolerance of 30 ± 5 μm. In the preparation of HFP/GN composite films, GNP powder was first dispersed in DMF using a sonicator for 20 min before being mixed with P(VDF-HFP) powder and stirred for 16 h. HFP/GN films were then prepared as described above. The GNP nanofiller powder loading was varied at 1, 2, 3, 4, and 5% by weight. These films were denoted HFP/GN1, HFP/GN2, HFP/GN3, HFP/GN4, and HFP/GN5, respectively.
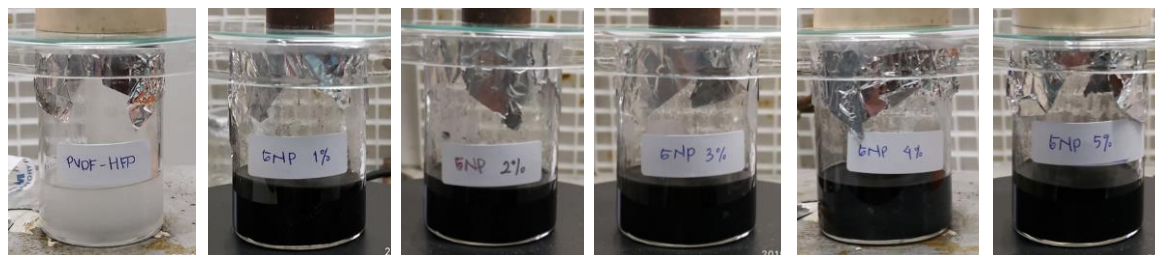
Figure 2.13. Solution of neat P(VDF-HFP) and its composites

Table 2.2. The samples preparation

Sample name	Condition	Amount of P(VDF-HFP) (g)	Percentage of fillers (%wt)	Amount of fillers (g)
P(VDF-HFP)	P(VDF-HFP)	5	0	0
HFP/GN1	1% GNPs/P(VDF-HFP)	5	1	0.05
HFP/GN2	2% GNPs/P(VDF-HFP)	5	2	0.10
HFP/GN3	3% GNPs/P(VDF-HFP)	5	3	0.15
HFP/GN4	4% GNPs/P(VDF-HFP)	5	4	0.20
HFP/GN5	5% GNPs/P(VDF-HFP)	5	5	0.25

2.4.3   Electron beam irradiation

When the samples are ready, they were divided into two groups, with and without electron irradiation. The second group were irradiated by an electron beam using an SEM model HITACHI TM3030Plus from Germany at an AV of 15 kV. Areas measuring 3 mm x 4 mm of samples were irradiated for 5 min emission time. Irradiation was conducted in a vacuum with beam current of 42.5 µA that generate the electron charge dose of 106.25×10^3 µC/cm^2.

2.5   Conclusion

Compared to other materials that show pyro, piezo and ferroelectricity behavior, P(VDF) polymer and its copolymers including poly (vinylidene fluoride hexafluoroprophylene)/P(VDF-HFP) are denoted as the most important electroactive polymers. These promising materials has been being an attention especially after the discovery of huge electrocaloric effect on them. Over the other electrocaloric materials, they can withstand even under high electric fields that make them possible

to generate biggest temperature and entropy change, with other additional advantages such as lightweight, flexible and low cost.

To improve the polymers ability especially on dielectric and electrocaloric properties, Graphene nanoplatelets (GNPs) or multi-sheet graphene were carried out as filler. This material is well known as low cost materials with higher electrical conductivity compared to graphite itself or other polymer nanocomposites like carbon nanotubes (CNTs) or single-sheet graphene due to its nanosize. Further, electron beam irradiation was also choosen to optimize the polymers properties especially for storage energy density and recoverable energy efficiency improvement.

Chapter 3 Microstructure characterization

3.1   Introduction

In one side, discovering some materials to be produced in big scale applications, especially for an integrated and miniaturized electronic device, it does not only require high power, high energy density, high efficiency as well as low energy loss but also should be low cost, compact, durable and lightweight. Moreover, additional properties such as self-cleaning abilities that relate to the surface characteristics are also important for smart materials applications (Moradi et al., 2015).

Hence, this study also observed microdomains change that is supposed to affect other parameters such as surface roughness, microstructure, and hydrophobicity of the materials. Moreover, observing the microstructural properties could help to understand the mechanism that occurs and affect to other parameters. Additionally, it is also important to explore some specific surface parameters such as hydrophobicity that show some benefits on a wide area of applications as smart materials due to its anti-sticking and self-cleaning abilities (Moradi et al., 2015). Even it does not directly relate with energy efficiency properties, this additional surface property will lead to the more outstanding characteristic for application in electronic devices.

3.2   AFM, water contact angle and SEM characterization

Atomic force microscopy (AFM) was employed to characterize the the surface area topography and interfacial morphology of the samples using an Easyscan 2 (Nanosurf AG, Switzerland) that operated in mode of dynamic force.

This measurement provides the formation of the spherulites structure information. **Figure 3.1. (a)** shows the result of neat P(VDF-HFP) before irradiated by electron. Relatively big spherulites were observed separated by relatively big holes between each spherulite. They were adressed to the most stable α-phase that could be affected by the technique of the film preparation. As reported by Ribeiro et al., the different methods of te film preparation could affect to the specific crystalline phase formation and nucleation (Ribeiro et al., 2018). In this work, evaporation process that

conducted in high temperature, more than 70 $^{\circ}$C lead to improve the evaporation rate of the materials. It is resulting on higher material's stability and forming α-phase crystal (Martins, Lopes, and Lanceros-Mendez, 2014).

Fortunately, the observed huge gaps of the polymer was reduced after adding GNPs. The smaller spherulites in the composites were formed paralelly. It caused by the reduction of the interface contact between each chain (Chenyang and Zhao, 2013). So that, the microstructures of the composite's spherulites were smaller than those of the pure polymer (**Fig. 3.1. (b)** and **(c)**). It confirms the result of the previous work that reported cross-link density improvement of the matrix that filled by suitable fillers (Jenkins et al., 1996).
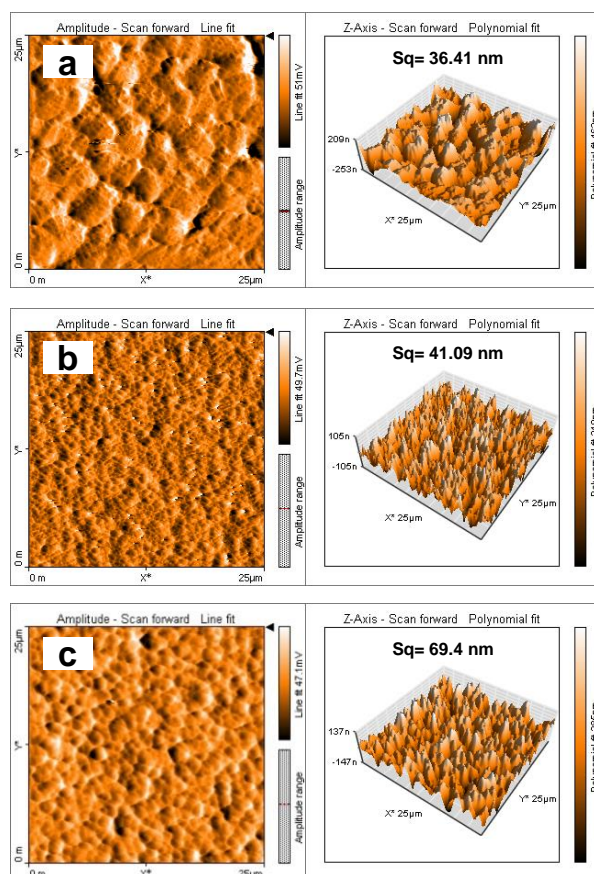
Figure 3.1. AFM images of **(a)** neat P(VDF-HFP) and its composites by **(b)** 1 wt% and **(c)** 5 wt% filler before irradiated by electron
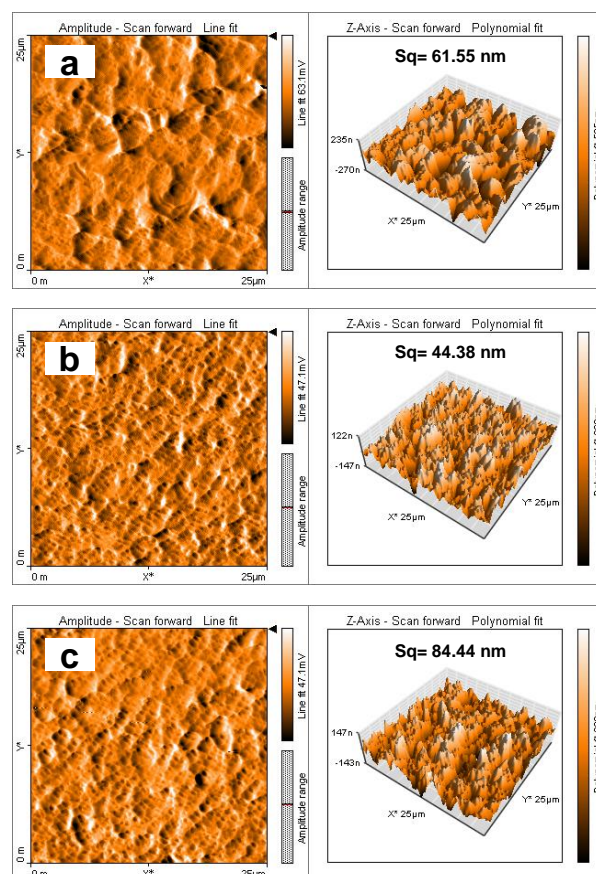
Figure 3.2. AFM images of **(a)** neat P(VDF-HFP) and its composites by **(b)** 1 wt% and **(c)** 5 wt% filler after irradiated by electron

No significant holes observed at the interface of filler and polymer matrix indicates a good adhesion of GNPs filler with P(VDF-HFP). Introducing a light amount of GNPs filler also could improve electrostatic interaction that preventing undesired agglomeration (Gérard, 2018). Moreover its strong electrostatic interaction that occurs between polymer chains and filler will improve dipole moment density and decrease the spherulites domain (Gérard, 2018). This microstructural modification finally will affect on other parameters as discussed in next chapter such as dielectric properties, etc.

Along with modifying the spherulite size, adding conducting filler also change the topography properties of the composites surface, especifically their surface roughness (Sq). P(VDF-HFP) thin film shows the lowest Sq value compared to the composites due to its comprised dense skin (Moradi et al., 2015). The improvement of Sq number of the composites was related to the full filler's exfoliation in the matrix that leads to well dispersion. Hence, it strengthen the interfacial interaction between polymer matrix and GNPs nanofillers and increase surface roughness due to micro- to nano-structure change in the structure (Moradi et al., 2015).

Interestingly, there is no significant changes of the spherulites after electron irradiation (**Fig. 3.2. (a)** to **(c)**). Further, the surface roughness of neat copolymer and composites were boosted up after irradiated by electron. The structures arrangement of the radial lamellar of spherulites is could be the main reason that causing rougher topography (Gérard, 2018). Besides that, it may be related also with the ability of electron on cuttting and breaking the polymer chains (Yang et al., 2013) as confirmed by Gregor et al. (2014) that reporting surface roughness improvement of the samples that irradiated by electron due to micro-domains formation (Gregor et al., 2014).

Since categorized as hydrophobic fluorinated polymers, PVDF and its copolymers are environmentally and chemically stable (Moradi et al., 2015). Simply, the hydrophobicity itself is normally determined by its water contact angle. Two main approaches are wll known to increase hydrophobicity either by decreasing the surface energy of high surface roughness sample, or gaining the surface roughness of low surface energy sample.
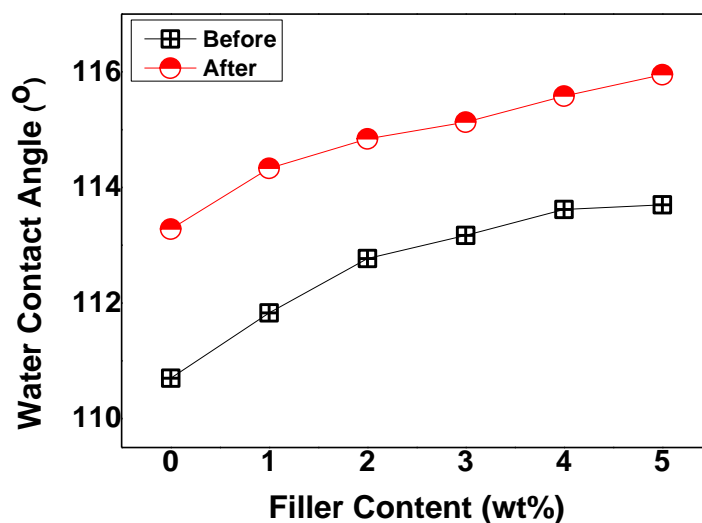
Figure 3.3. Water contact angle measurements of neat P(VDF-HFP) and its composites for both before and after irradiated by electron.

OCA 15EC (Dataphysics, Germany) was carried out to observed the water contact angle. Conducted using 55 W of an input power, a 6.3 AT fuse, and 12 V DC voltage controlled liquid volume of 2 μl. The water contact angle of P(VDF-HFP) was around 110° before irradiation. This number is higher than that of PVDF (around 90°) (Kitabata, Taddese, and Okazaki, 2018). It indicates that HFP monomer emulsion polymerization not only gain the mechanical strength of the poloymer but also boosted the hydrophobicity (Wang et al., 2018). Hence, water contact angle of the composites were higher than the pure poolymer (**Fig. 3.3**).

As mechanism, a hydrophobic material including P(VDF-HFP) possess weak hydrocarbon bonds. Therefore, high carbon density of GNPs can improve the roughness and significantly modify its hydrophobicity presented by its water contact angle and (Moradi et al., 2015). Rougher materials could improve the surface area of the surface and trap more air when the water drips drop on that kind of surface reslting on contact angle improvement. (Moradi et al., 2015).

After irradiation (**Fig. 3.3) t**he water contact angle was increased too as also reported by other works (Aronov and Rosenman, 2007; Gregor et al., 2014). By cutting chemical bonds, electron is effective on modifying hydrophobicity (Aronov

and Rosenman, 2007). The charge was induced during irradiation and the electron-holes pair will be formed in the dielectric materials. So that, the electrons that generate a negative charge will be trapped on the bulk level. Meanwhile, localized holes that exist around the surface will produce positive charge. Moreover, the creation of microdomains bby the electron will improve hydrophobicity without changing its morphology (Gregor et al., 2014).

To confirm AFM results, SEM (TM3030Plus, Hitachi, Germany) was used to observe morphological arrangements of the thin films. As shown by (**Fig. 3.4. (a)**), neat P(VDF-HFP) containing 20 wt% of concentration have a relative compact morphology but separated by holes/pores along the matrix film that represented by black zones. Possibly, the pores appear as the result of DMF solvent evaporation. (Sousa et al., 2014). Agreed with with this study, a previous work also mentioned that both increasing P(VDF-HFP) concentration and evaporation temperature (80 $^{\circ}$C) could resulting the pore size reduction (Magalhaes, Duraes, and Silva, 2011). As consequence, more homogeneous thin film with smaller pores could be obtained. This result is in an agreement with the AFM characterization that observing spherulitics arrangement as shown by **Figure 3.1**.
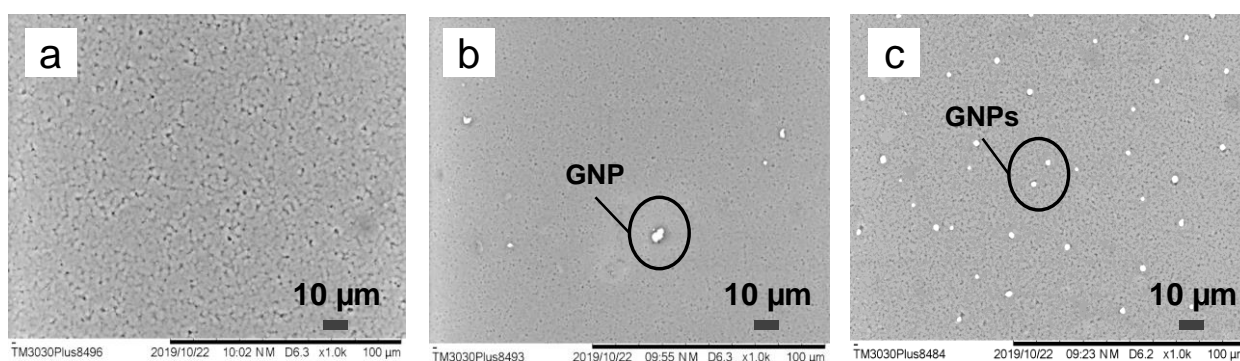
Figure 3.4. SEM characterization of: **(a)** neat P(VDF-HFP) and its composites by **(b)** 1 wt% and **(c)** 5 wt% filler before irradiated by electron

As GNPs filler was introduced to the matrix, the spreading of the filler could be observed too (**Fig. 3.4. (b)** and **(c)**). By 1 wt%, not many GNPs ciller that detected as shown by **Figure 3.4. (b).** However, more concentration of filler leads to more appearance of the filler spreding too in (**Figure 3.4. (c)**). This filler spreading finally

will form the microcapacitor inside the matrix. As the result, another parameter such as dielectric properties will be modified. More specifically, the more homogeneous matrix film were observed after adding GNPs filler. The relatively big pores in P(VDF-HFP) thin film (**Fig. 3.4. (a)**), were no longer exist after adding GNPs filler (**Figures 3.4. (b)** and **3.4. (c)**)**.** It could be manipulated by the nano-sized GNPs (0.34-100 nm) that dispersed effectively in the polymer matrix (Cataldi, 2018) so that the holes can be filled easily resulting in higher flexibility and homogeneous thin films. Thus, SEM images presented similar results to those of reported by AFM characterization.

3.3 X-Ray Powder Diffraction (XRD) pattern

X-ray diffractometry (XRD) from Empyrean, PANalytical, Netherlands was brought to determine crystalline phase. Sscanned at the (2θ) range of 5 to 90° by using a (CuKα) wavelength of 0.154 nm and a speed of 0.04^{o} sec^{-1}, the sample was put in the Cu tube at 30 mA and 40 kV. For casting method, a dominant α-phase was dominated the crystalline phase formation of P(VDF-HFP) (Daneshkhah et al., 2017). Hence, some methods have been explored to create β-phase formation.

The specific α-phase diffraction peak exist at 17.7^{o} (**Fig. 3.5.**) with no any possibilities to overlap with other phases. The intensity at that peak was drastically dropped from 4755 to 4530 after adding GNPs filler indicating the reduction of α-phase content. Moreover, α-phase diffraction peaks were also observed at 18.5^{o} (020) and 39.0^{o} (211) planes. Meanwhile, the peak at 18.5^{o} (020) and 36.2^{o} (200) correspond to γ-phase (Khalifa, Mahendran, and Anandhan, 2016).

As assumed, the intensity of β-phase peak that exist at 36.6^{o} (101) crystal plane was improved from 1151 to 1225, as well as at at 20.2^{o} (200) plane (Gérard, 2018; D. Yang et al., 2017). Identified as the specific characteristic of GNPs, a peak at 26.5^{o} (002) crystal plane wa increased drastically too (Yang et al., 2017). Over other pic, the most outstanding change was appearance at 39.0^{o} (211) that belong to α-phase. The intensity was dropped dramatically showing significant electron irradiation effect on manipulating crystalline phase. To deeply understand, FTIR analysis was also carried out.
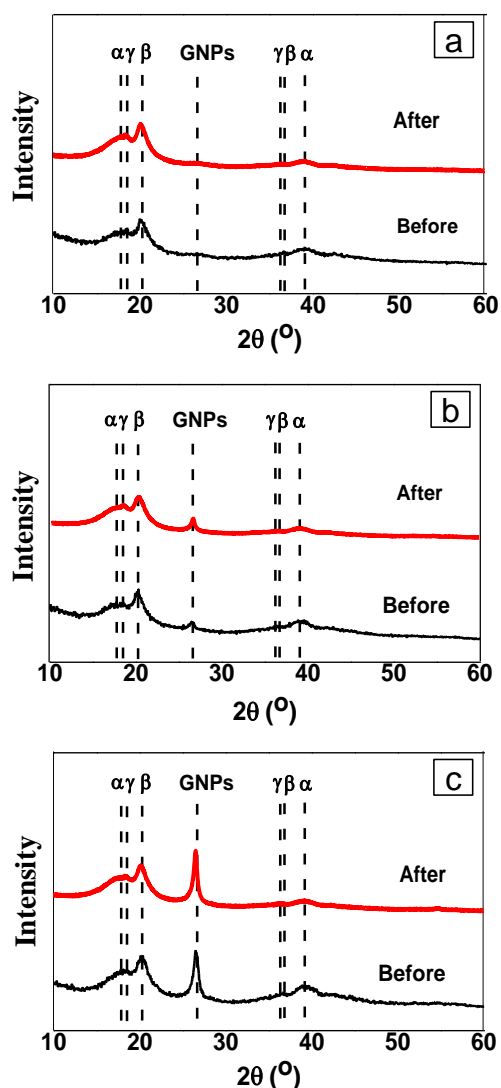
Figure 3.5. XRD results of: **(a)** neat P(VDF-HFP) and its composites by **(b)** 1 wt% and **(c)** 5 wt% filler both before and after irradiated by electron

3.4   Fourier-Transform Infrared Spectroscopy (FTIR) spectra

The spectra were observed with the range of 4000 to 400 cm^{-1} attenuated total reflectance mode (ATR) using FTIR VERTEX 70 from Bruker, Germany. **Figure 3.6. (a)** presented FTIR spectra of pure polymer and its composites before irradiation. The absorption peaks at 532, 613, 764, and 978 cm^{-1} of α-phase were affiliated to CH$_2$ and CF$_2$ vibration (Gérard, 2018; Yang et al., 2017) while peaks at 875, 1069 and 1402 cm^{-1} caused by CF$_2$ stretching in P(VDF-HFP) matrix (Daneshkhah et al., 2017). Moreover, peak at 875 cm^{-1} is existed by α-phase C-C group. However, the peak for γ- and α-phases can be appear at 1170 cm^{-1}.

Absorption peak of α-phases were dropped slightly after adding GNPs as occur at 875, 1069 and 1402 cm^{-1} that drop from 0.71, 0.34 and 0.30 to 0.63, 0.32 and 0.27, respectively, in HFP/GN5. In the opposite, peaks at 811 and 1031 cm^{-1} refers to CF$_2$ bending of γ- and β-phases (Khalifa et al., 2016) were improved from 0.19 and 0.16 to 0.21 and 0.17, respectively.

(a) **(b)**
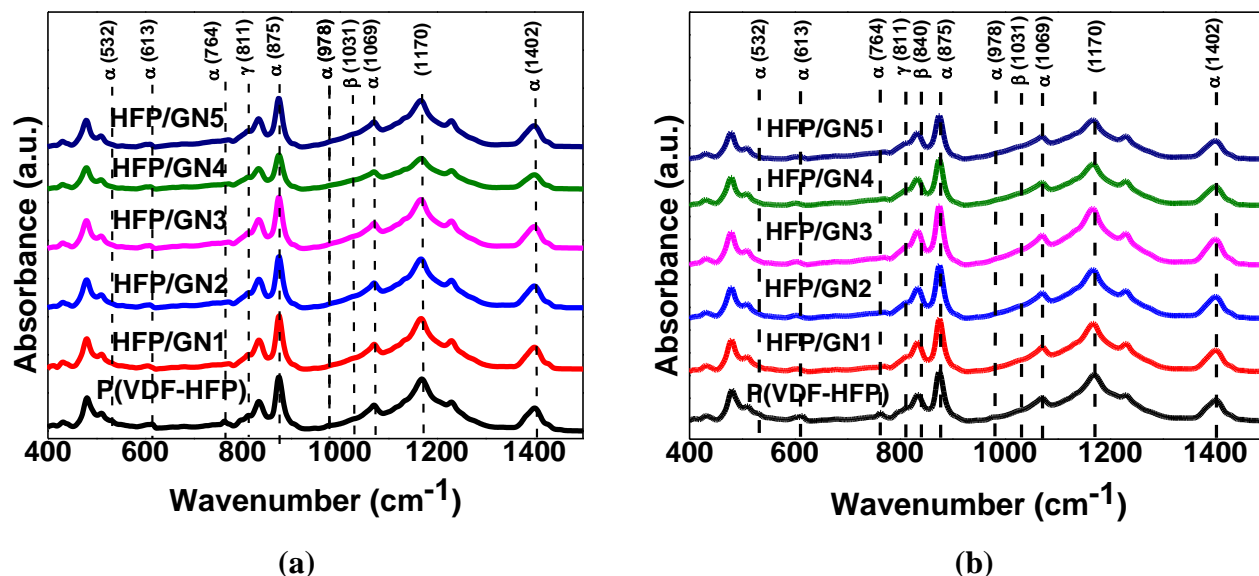
Figure 3.6. FTIR characteristic sof neat P(VDF-HFP) and its composites for both **(a)** before and **(b)** after irradiated by electron
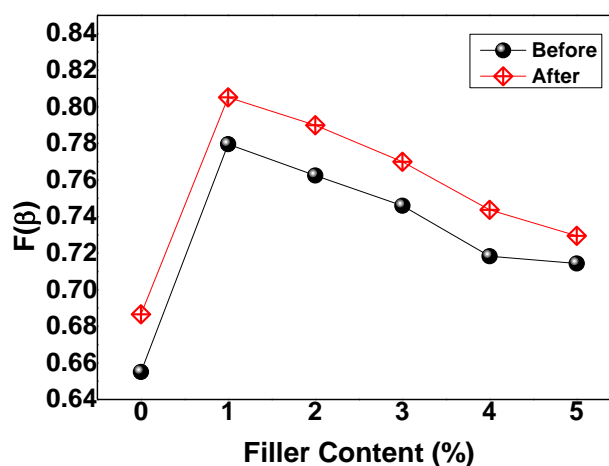
Figure 3.7. The fraction of β-phase content of neat P(VDF-HFP) and its composites both before and after irradiated by electron.

The peak of α-phase at 875, 1069 and 1402 cm^{-1} (**Fig. 3.6. (a)**) were dropped from 0.71, 0.34 and 0.30 to 0.54, 0.25 and 0.23, respectively, after irradiation (**Fig. 3.6. (b)**) as also occurred to the all composites. Further, these data could be used to get the number of β-phase ($F(\beta)$) fraction in all condition by Lambert-Beer equation:

$$F(\beta) = \frac{A_\beta}{\frac{K_\beta}{K_\alpha}A_\alpha + A_\beta} \tag{16}$$

where A_α, A_β are the absorbance at 764 cm^{-1} and 840 cm^{-1}, and their absorption coefficients are K_α of 6.1 x 10^4 cm^2 mol^{-1} and K_β of 7.7 x 10^4 cm^2 mol^{-1} (Thakur et al., 2015).

The result of β-phase fractions before and after electron irradiation were presented in **Figure 3.7**. The graph clearly show β-phase improvement after GNPs addition. Then, irradiation optimized the β-phase content.

Strong interactions of positive charge of carbon in GNPs and negative charge of fluorine in P(VDF-HFP) lead to improve dipole moment and higher β-phase content (He et al., 2016). As the same mechanism, negatively electron attracted the positively hydrogen in P(VDF-HFP) that will generate more electroactive crystalline phase (George, 2017).

XRD characterization data is very usefull to determine the crystal size of the samples. To prove electron ability on cutting the domains/crystal to be smaller (Yang et al., 2013; Zhu et al., 2017), the half-maximum width of the peaks of all condition were observed. As result, the crystal size of the crystal sheets (D) can be generated by Scherrer equation (Tan et al., 2013):

$$D = \frac{K\lambda}{B\cos\theta} \tag{17}$$

where K ($K = 0.89$) is constant, λ ($\lambda = 0.154$ nm), B and θ are the X-ray wavelength, width of the peak at half-maximum and the peak location, respectively.

Table 3.1. The width at half-maximum (*B*), crystal size (*D*) and crystallinity (X_c) at location of 20.2^o of neat P(VDF-HFP) and its composites before and after irradiated by electron.

Filler content (wt%)	*B* (rad)		*D* (nm)		X_c (%)	
	Before	*After*	*Before*	*After*	*Before*	*After*
0	0.58	1.02	0.60	0.48	26.52	26.06
1	0.71	0.92	1.46	0.68	35.56	32.24
2	0.39	0.82	2.60	0.81	38.34	30.57
3	0.87	1.07	1.91	0.58	31.47	35.20
4	0.47	0.82	1.07	0.82	27.25	28.07
5	0.55	1.10	1.38	0.54	31.67	32.25

The width of the peak at half-maximum of neat polymer after irradiation was increased from 0.58 rad to 1.02 rad but reduced the crystal size from 0.60 nm to 0.48 nm. The crystal size reduction weas shown also by the composites all condition to be almost two times smaller.

As well known, the crystal size and the dielectric loss is related one each other. They are representing the domain relaxation ehen the electric field was applied or removed. Bigger crystal size possess bigger domain crosscoupling force too. Electron ability to break the domains into smaller will help the domain to reverse and dropp the interaction force among each domain (Guan et al., 2013).

3.5   Thermal Behavior

Measurements of thermal behavior were conducted using DSC 7, from Perkin Elmer, USA in a nitrogen atmosphere using 1-3 mg of samples at temperature range of 20 to 200 ^{o}C and controlled heating rate of 10 ^{o}C min^{-1}. By knowing the melting temperature (T_m) and the melting enthalpy (ΔH_m) that generated from the peak area, the crystallinity (X_c) of the samples can be obtained using this equation:

$$X_c = \Delta H_m / ((1\text{-}\phi)\, \Delta H_{100\%}) \text{ x } 100, \tag{18}$$

where ΔH_m and $\Delta H_{100\%}$ affiliated to melting enthalpy and enthalpy of fusion of 100% P(VDF-HFP) crystals, 104.6 J g^{-1}. While ϕ is filler mass fraction in the matrix (Thakur et al., 2015).
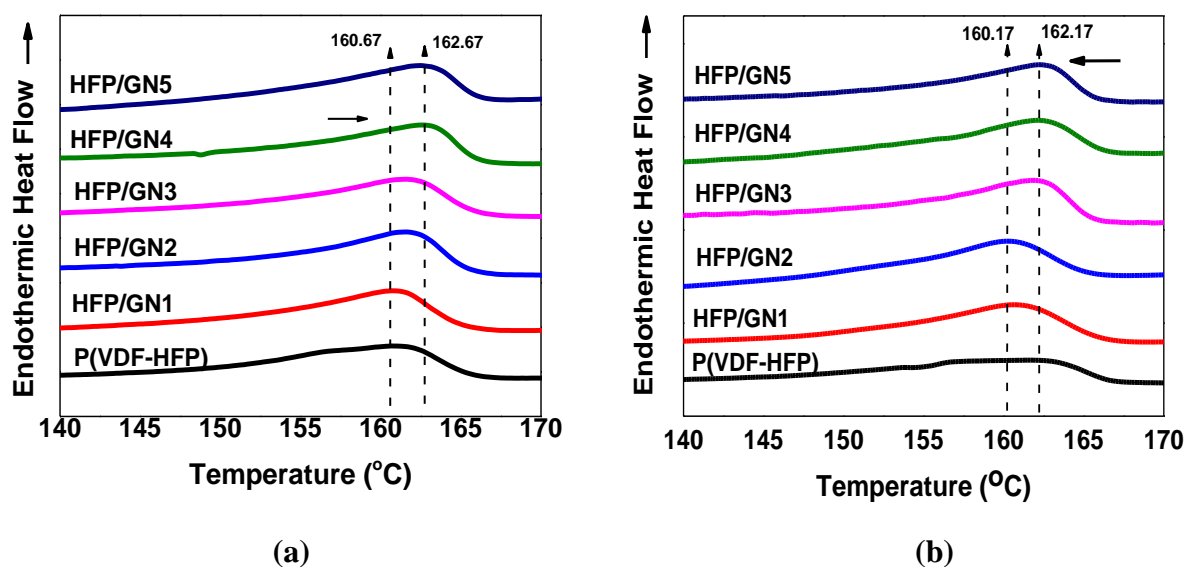
Figure 3.8. DSC analysis with T_m of neat P(VDF-HFP) and its composites for both **(a)** before and **(b)** after irradiated by electron.
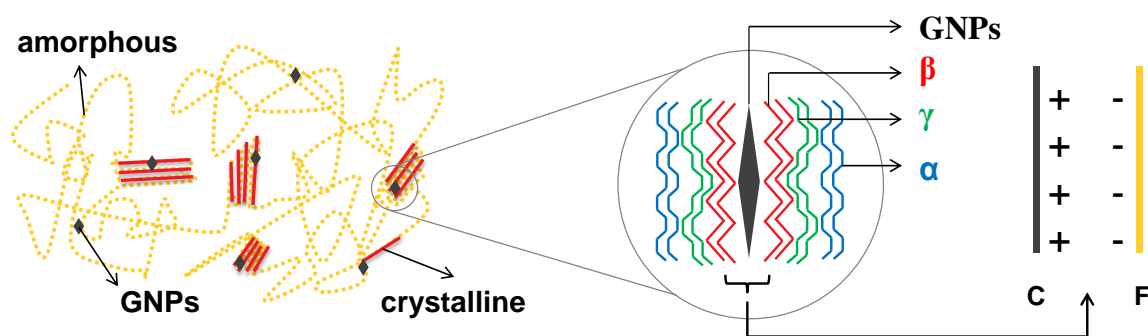
Figure 3.9. The proposed schematic of GNPs nucleation in polymer.

The T_m of all composites were higher than the pure polymer, before and after electron irradiation (**Fig. 3.8. (a)** and **(b)**). They are related to the specific crystalline phase form. Normally, higher β-phase content will lead to higher melting temperature too (Thakur et al., 2014) and crystallinity improvement will lead to greater ΔH_m.

The neat polymer matrix contain both amorphous and crystalline region that posses five types of crystalline phase (Ruan et al., 2018). When the matrix added b the

GNPs filler, the filler will be spreaded out along the matrix as shown by the schematic **Figure 3.9.** At low concentration, 1 wt%, the crystalline part will attract the GNPs particle more than the amorphous part due to the negatively fluorine in polymer that attract positively carbon in GNP.

This interaction finally could transform non polar α-phases to the mos electroactive β-phases, especially in the area that interact directly with GNPs particle. The chain of the the polymer will be reoriented to be planar zig-zag resulting on CF bond that arranged parallel oppositely with the CH bond (Roy et al., 2016). Moreover, in the area that near to the the β-phase, the γ-phase can be formed too. Nevertheless, α-phase will be still exist in the region that really far from GNPs.

Increasing the filler concentration to be more than 1 wt% lead to the spreading in the bigger area of the matrix. So that, the filler could interact not only with the crystalline region but also the amorphous part of the polymer. As the result, new crystal will be form resulting on improving overall crystallinity. Hence, this GNPs-amorphous interaction will form not only β-phases but also all other crystalline phase. As the final result, the content of β-phase in thee matrix seems slightly drop by the increasing of filler content.

3.6   Conclusion

Generally, both adding GNPs conducting nanofillers and electron beam irradiation caused a significant effect on microstructure and surface properties. Since neat P(VDF-HFP) shows a relatively bigger spherulites and porous matrix, adding GNPs could fill the gaps and increase the film homogeneity. As the consequence, it increase the crosslink density and improve the electrostatic interaction. Moreover, its full exfoliation ability make the GNPs could be dispersed in the polymer matrix and leads to increase the surface roughness. On the other hands, although there is no significant change on spherulites, electron beam irradiation is also effective on improving surface roughness of the film due to its role on pinning the polymer chains. As the consequence, both adding GNPs nanofillers and electron beam irradiation can boost the polymers hydrophobicity that represented by its water contact angle.

Further, the aforementioned strong electrostatical interaction caused by GNPs could improve overall crystallinity and facilitate the transformation of the

crystalline phase from most stable α- to the most electroactive β-phase. Along with GNPs, electron beam irradiation also made the significant change on this β-phase nucleation. Nevertheless, the outstanding ability was showed by electron beam irradiation by decreasing the crystal/domain size to be almost a half. These parameters will affect to the energy properties that will be discussed on the next chapter.

Chapter 4 Dielectric properties and AC conductivity of electron irradiated GNPs/P(VDF-HFP) composites

4.1   Introduction

Techniques or meethods are well known to gain permittivity of materials such as poling, or high voltage polarization (Hartono, Satira, and Djamal, 2016), adding nanofillers (Roy et al., 2016), electrospinning (Mansouri, Sheikholeslami, and Behzadmehr, 2019) and mechanical stretching (Ruan et al., 2018). As key factor, all of those stated techniques are focus on changing microstructural properties such as crystallinity and electroactive phase transformation from non polar α-phase to the most useful β-phase. The α- and ε–phase are denoted as the most stable crystalline phase among others. PVDF and its copolymers have at least three molecular conformation modes named TTTT, T3GT3G´ and TGTG´ with five different electroactive phases of α-, ε-, δ-, γ- and β (Ruan et al., 2018). The most active phase electrically is the all trans-TTTT zigzag polar β-phase with number of polarization per unit cell is around 8 x 10^{-30} C·m (Roy et al., 2016). Hence, most of the recent works only focused on improving this most electroactive phase by only one technique. Moreover, this work provided the combination of two relatively untypical methods which are introducing a conducting nanofiller followed by electron irradiation.

4.2   Dielectric properties and AC conductivity

To measure AC conductivity and the dielectric properties such as dielectric constant and dielectric loss, an LCR meter model IM 3533 HIOKI was employed in the room temperature along the frequency range of 1 Hz to 100 kHz. The 1 V AC voltage was controlled to produce the electric field and through across the samples that put between two electrodes. The data including conductance (G) and capacitance (C) of the samples as well as its dielectric loss can be generated. Hence, the dielectric constant (ε_r) as well as AC conductivity (σ_{ac}) could be determined using equations:

$$\varepsilon_r = (C.\ d) / \varepsilon_0\ A), \tag{19}$$

$$\sigma_{ac} = (G.\ d) / A, \tag{20}$$

where d is the sample thickness, while ε_0 and A are permittivity in vacuum of 8.854×10^{-12} F m^{-1} and the electrode area, respectively (Thakur et al., 2015).

(a)   (b)
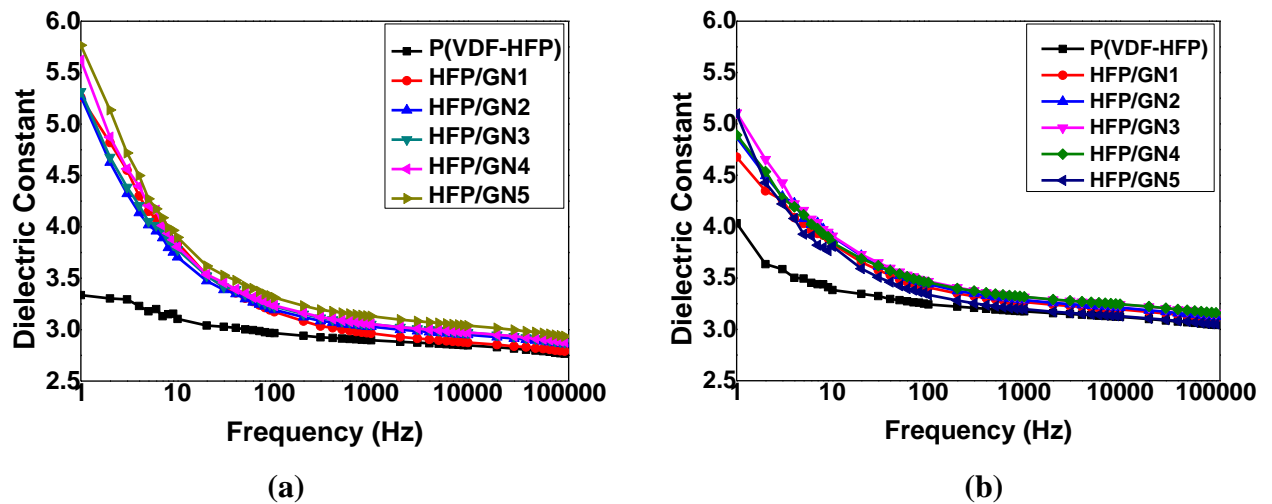
Figure 4.1. Dielectric constant dependent on electric field frequency of neat P(VDF-HFP) and its composites for both **(a)** before and **(b)** after irradiated by electron.

(a)   (b)
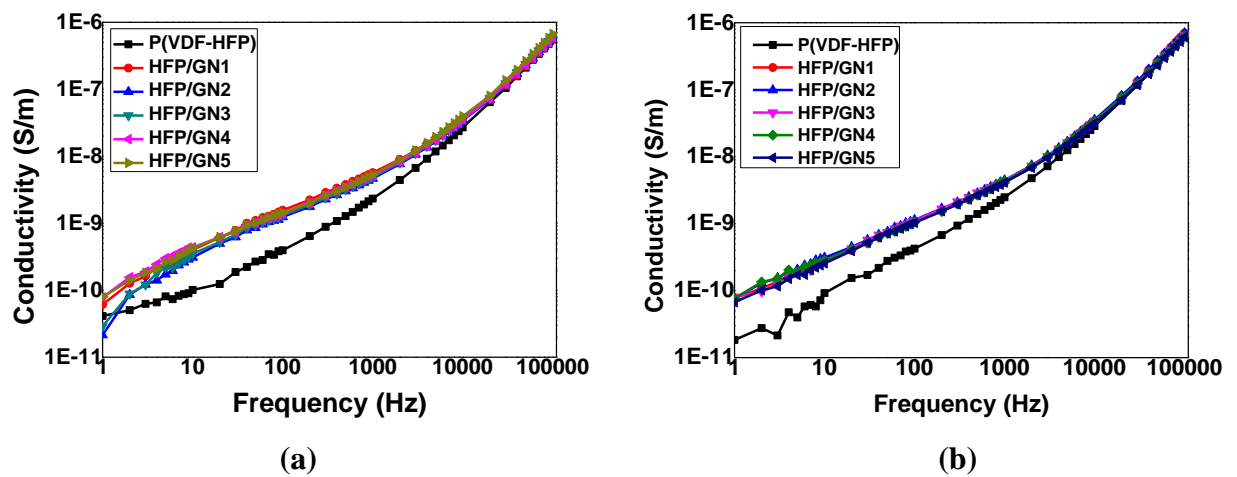
Figure 4.2. AC conductivity dependent on electric field frequency of neat P(VDF-HFP) and its composites for both **(a)** before and **(b)** after irradiated by electron.
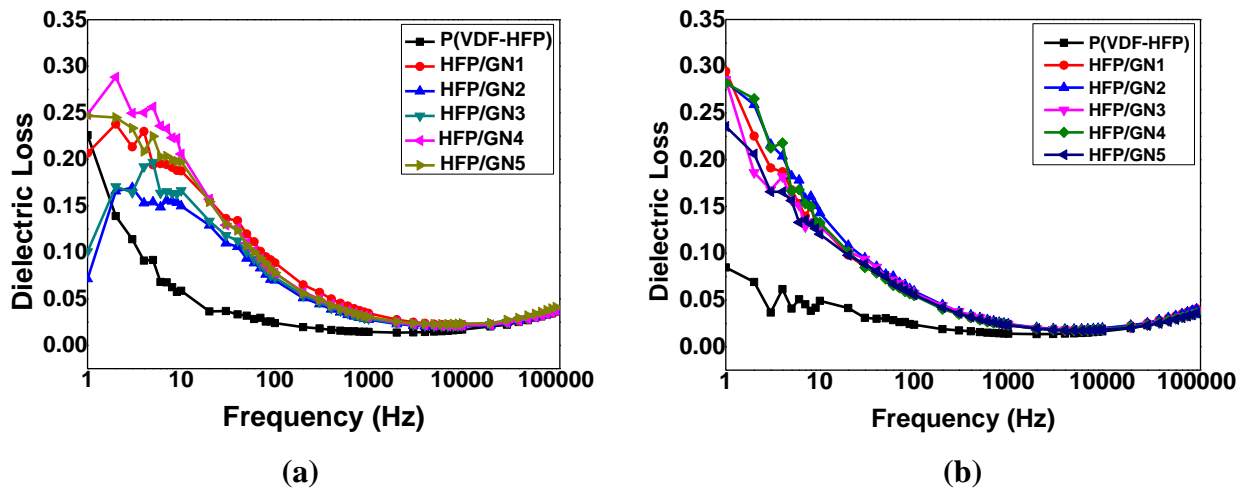
Figure 4.3. Dielectric loss dependent on electric field frequency of neat P(VDF-HFP) and its composites for both **(a)** before and **(b)** after irradiated by electron.
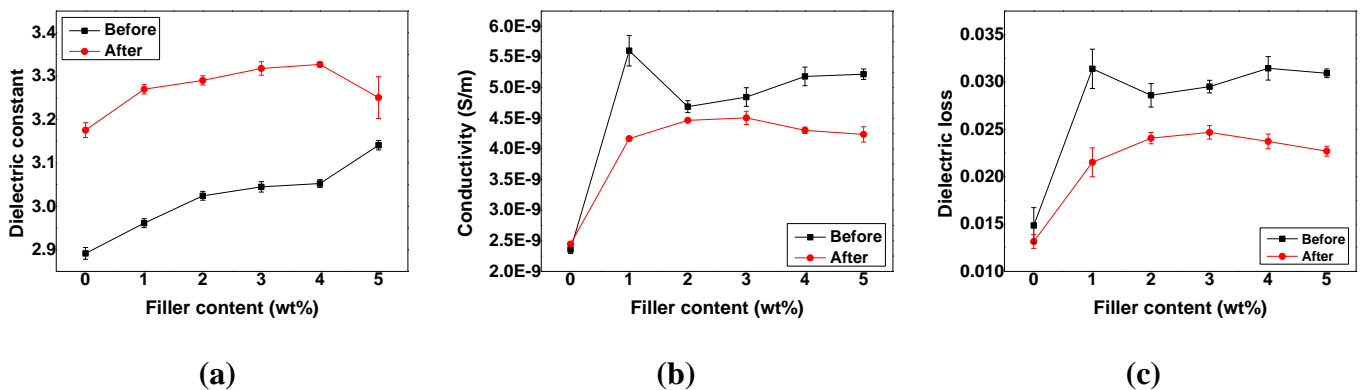
Figure 4.4. (a) Dielectric constant, **(b)** AC conductivity and **(c)** dielectric loss dependent on filler concentration at 1000 Hz before and after irradiated by electron.

Figure 4.1. (a) and **(b)** shows dielectric constant vs electric field frequency of all conditions before and after treated by electron irradiation. As the result, dielectric constant of the composites was much higher that pure polymer. Moreover, after irradiation, the dielectric constant was also improved in whole frequency due to the mechanism that described at chapter 3. The microstructure change and the formation of the mos electroactive crystalline phase finally gain the dipole density resulting on increasing of dielectric constant, charge storage capacity and polarization (He et al., 2016).

As the nucleation agent, GNPs is effective to help the crystallization process. At low frequency of 1 Hz, 1%wt GNP content could improve ε_r from 3.34 to 5.26. This gradual improvement continou with the increasing of filler loading of 2, 3, 4 and 5 wt% to be 5.27, 5.32, 5.62 and 5.77, respectively. In one point, when the frequency increased, the ε_r tend to lower due to the reduction of net polarization. At high frequency, the dipole can not follow the frequency of the applied electric field (Shrivastav, Barde, Mishra, and Phadake, 2013). Besides improving ε_r, GNPs filler could increase dielectric loss and AC conductivity of polymer (**Fig. 4.2** and **4.3).** fortunately, the improvement of those parameter are not significant.

Figure 4.4. (a) shows the dielectric constant at 1000 Hz of all samples conditions. It can be seen clearly that electron irradiation is also effective to gain the ε_r. As described at the previous chapter, the change in microstructure due to irradiation is could be the main reason (George, 2017) especially in transforming α-phase to β-phases (Gérard, 2018).On the other hands, opposite to the improvement of the ε_r, electron irradiation can dramatically reduce undesired AC conductivity and dielectric loss of (**Fig. 4.4. (b)** and **(c)**). A prior study reported the effects on chemical pinning caused by the electron that reducing crystal domains (Yang et al., 2013). Even the exact mechanism is still unclear, but it is strongly caused by cross-linking that enlarge the distance between each chain in the polymer after cut by the electron. This crystal reduction will make the dipoles more flexible during charging and discharging process (Tan et al., 2013).

4.3 Conclusion

Improving the capacity of storage charge as well as its dipole density is one of the effects brought by GNPs charged surface that facilitate the contribution of the charge-movement. As results, β-phase content was improved resulting on improving dielectric constant as well at all range of electric field frequency. Conductive GNPs could improve undesired AC conductivity and dielectric loss. Fortunately, electron beam irradiation shows the attractive role on both improving dielectric constant and decreasing undesired AC conductivity and dielectric loss due to its ability on pinning the crystal/domain size that improve the dipoles flexibility to rotate during discharging process.

Chapter 5 Ferroelectricity P-E loops, energy efficiency properties and electrocaloric effect of electron irradiated GNPs/P(VDF-HFP) composites

5.1 Introduction

Normally, exsusting dielectric materials possess relatively big amount of power density that is useful for faster charging and discharging (Feng et al., 2019). Unfortunately, their lower desired energy storage density limits their ability to be applied in energy-based devices. For example, BOPP materials or biaxially oriented polypropylene that known as the most common polymer for capacitors, with high electrical breakdown of 700 MV/m completed by low dielectric loss of 0.0002 at 1 kH, has not a good behavior for energy density as well as efficiency (Thakur and Gupta, 2016) due to its low permittivity. On the other hands, PVDF-based materials contain relatively higher permittivity and electrical that desired for energy devices (Wang et al., 2017). Nevertheless, one of disadvantages of these materials is their dielectric loss that leads to higher energy loss as well.

To solve this problem, GNPs were exploited as filler. It is due to GNPs advantages over other carbon-based filler such as nanotubes and carbon fibers or even pure graphene (Cataldi, 2018). The ferroelectric matrix that have big crystal domains with packed aligned dipoles shows relatively huge ferroelectric hysteresis loop, describing the energy loss. Hence, reducing this energy loss is should be one of the main focuses too. as proposed, electron irradiation has been employed because of its behavior on dropping dielectric and energy loss by cutting large ferroelectric domains to be much smaller (Yang et al., 2013). Another work also reported that this micron-sized crystal reduction can be created either by positive or negative charges (Plecenik et al., 2012). Further, electron probe of widely used SEM can be employed with some additional benefits of easier in irradiation position control and lower contamination of the hydrocarbon (Gregor et al., 2014). So that, at least there are two main factors to get higher energy efficiency, boosting permittivity and dropping its dielectric, simultaneously.

5.2   P-E loops

As semi-crystalline ferroelectric polymer that containing both crystal and amorphous, P(VDF-HFP) also shows the hysteresis loop during charging and discharging process. High content of β-phase will influence the hysteresis loop as well. With high spontaneously packed of dipoles in ferroelectric domain makes the loop size tend to bigger. As consequence, high polarization response will be obtained but high energy loss can not be denied as well.
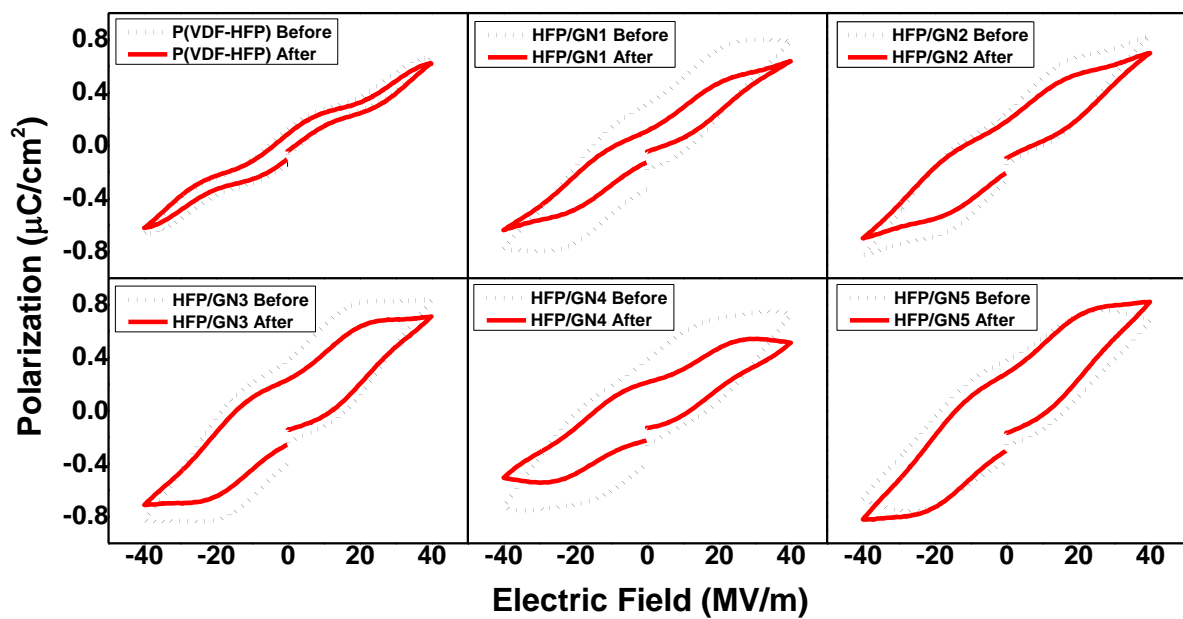
Figure 5.1. Ferroelectricity P-E loops of neat P(VDF-HFP) and its composites both before and after electron irradiation.

Measured under fixed electric field of 40 MV m^{-1} by high voltage amplifier model Trek 601E, the hysteresis loops of all sample conditions were obtained. The measurement was conducted by varying temperature from 21 $^{\circ}$C to 140 $^{\circ}$C at frequency of 10 Hz. The obtained loop then be analyzed to generate the value of storage energy density and energy loss. Further, discharge energy efficiency can be determined by equation:

$$\eta = (U_e) / (U_e + U_l), \tag{21}$$

where η is discharge energy efficiency, U_e is desired energy density while U_l represents undesired energy loss (Zhu et al., 2017) .

Charging process occur when external E was applied resulting on more order dipoles with maximum polarization (P_{max}) on the thin films. While, when external E was removed out, some dipoles will be back to the random state resulting on reduction of polarization. However, during discharging process, huge domain makes some dipoles stillbeen polarized even the E was zero or well known as remnant polarization (P_r). As shown by **Figure 5.1**, the hysteresis loop size was going bigger after adding GNPs for all loadings indicating higher loss. Hence, the interaction force that exist between each domain will bigger too and resulting on higher (P_r) (Soulestin et al., 2017). Nevertheless, the advantages of irradiation over adding GNPs is its ability on slimming the loop indicating smaller both dielectric and energy loss as reported by prior study (Zhu et al., 2017). It is related to pinning process in all-*trans* conformation to be much smaller resulting on increasing reversibility (Yang et al., 2013). Further, the dielectric loss can be spressed resulting on slimmer loop (**Fig. 5.1**).

5.3   Energy efficiency

As explained in chapter 4, the disadvantages of introducing GNPs is its effect on enhancing conductivity and dielectric loss. This was confirmed by P-E loop that finally affect energy properties of the materials. Enhancing hysteresis loop means enhancing of undesired energy loss and limited storage energy density as shown by **Figure 5.2. (a)** and **(b)**. Fortunately, this energy properties reduction that caused by GNPs can be healed by electron irradiation. It can enhance desired energy density with lowering undesired energy loss as indicated by the reduction of P_r so that some charges can be released from the film (Tan et al., 2013).

Changing on energy density as well as its loss finally will affect the discharge energy efficiency of the thin films. From **Figure 5.2. (c)** can be seen clearly that along with increasing energy density and lowering its loss, electron irradiation also lead to boost up the energy efficiency of the pure polymer and its composites for all filler concentration. As an instance, energy efficiency of irradiated pure polymer was improved to 74.66 from 68.11 %, that is literally bigger than reported previously (Guan, Pan, Wang, Wang, and Zhu, 2010) of 58 % for unirradiated P(VDF-HFP) and

30.2 % for pure PVDF (Li et al., 2010). Moreover, the energy efficiency for all composites were also enhanced after irradiation to be almost doubled. Respectively, they were improve from 26.65, 37.10, 16.98, 16.16 and 18.75 %, for 1, 2, 3, 4 and 5 wt% filler content to 57.7, 44.23, 31.34, 30.59 and 32.06 %.
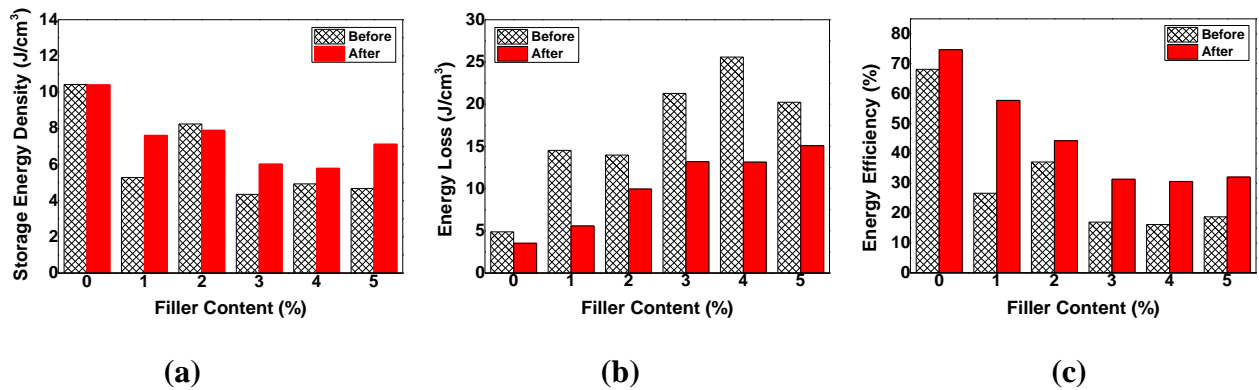
Figure 5.2. **(a)** Desired Storage energy density, **(b)** undesired loss and **(c)** energy efficiency of neat P(VDF-HFP) and its composites before and after electron irradiation

5.4   Electrocaloric effect

As aforementioned at chapter 1, there are two ways that can be conducted to measure electrocaloric effect rather direct on indirect method (Asbani et al., 2015).
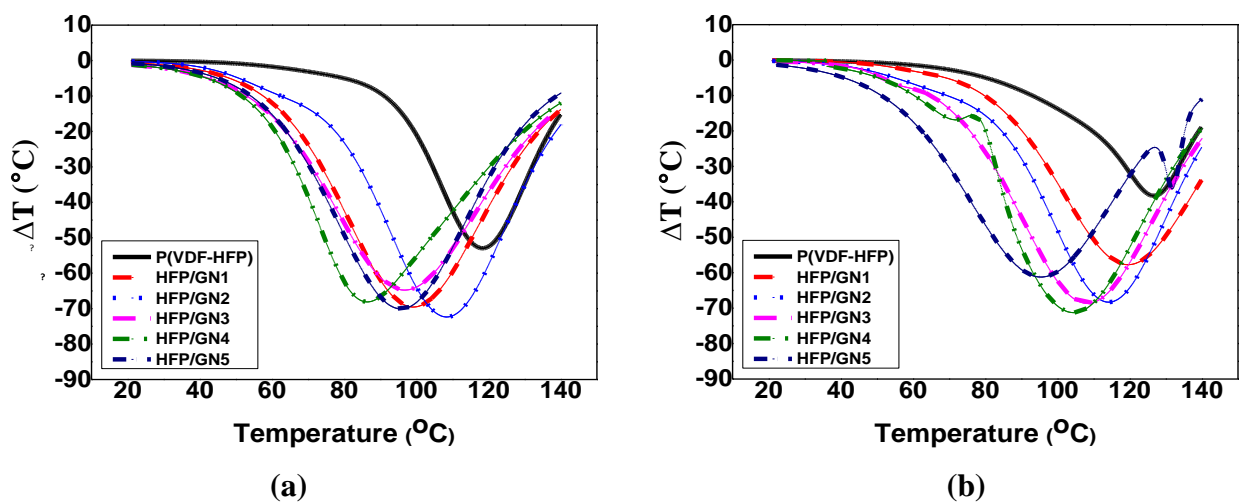
Figure 5.3. The ΔT of neat P(VDF-HFP) and its composites both **(a)** before and **(b)** after irradiated by electron.

For thin films and other materials with the small volume samples, the electrocaloric direct measurement tends to be lack of precision due to heat transfer and heat capacity nonuniformity (Lubomirsky and Stafsudd, 2012). Nevertheless, for most electrocaloric materials, there is no significant different result between direct and indirect method (Maiwa, 2015). **Figure 5.3** shows the ΔT electrocaloric effect of neat P(VDF-HFP) and its composites, both before and after electron beam irradiation. It has been analyzed from the polarization change toward the temperature change that recorded by P-E loop measurements. The polarization change was measured every single degree from 20 to 140 ^{o}C by keeping the constant electric field of 40 MV m^{-1}. The figure shows that the absolute value of the ΔT increase by the increasing of the temperature. This phenomenon is still continuing until reach the peak at the specific temperature. Interestingly, beyond those temperature, the absolute value of the ΔT tends to decrease. Those critical points called Curie temperature (T_c), the temperature when the polymer ferroelectric material change to be paraelectric. In this state, the ΔT reach the maximum value (ΔT_{max}). Each condition of the sample has different ΔT_{max} at different critical points temperature as well.

Figure 5.3. (a) presents the ΔT of the neat P(VDF-HFP) and HFP/GN composites before electron beam irradiation as a function of temperature. From this figure, it can be seen clearly that neat P(VDF-HFP) possess the lowest ΔT compared to the HFP/GN at all loadings. Adding small amount of GNPs conducting nanofillerrs bring the benefit for the electrocaloric effect improvement that indicated by the improvement of ΔT value. The range of the calculated maximum ΔT of the composites is (-64.75) to (-72.34) ^{o}C, much higher than that of the neat P(VDF-HFP) of (-52.95).

Besides the ΔT value, the Curie temperature (T_c) of each condition should be considered too. For the real application, the electrocaloric cooling system will be operated at room temperature. Hence, discovering electrocaloric materials that possess high ΔT at room temperature or at least nearby to is becoming another attention. For the neat P(VDF-HFP) itself shows a quite high T_c of 118.32 ^{o}C. Fortunately, this number is drastically decreased after adding small amount of GNPs conducting nanofillers to the polymers as shown by **Fig. 5.3. (a)**. The T_c of HFP/GN composites before electron irradiation is much lower that that of neat P(VDF-HFP) at

all loadings. The lowest T_c value was shown by HFP/GN4 of 86.28 ^{o}C. Although the T_c at room temperature can not be gained, but it shows a good indication and can be used as a guidance for the future work. Moreover, these results indicated that adding GNPs conducting nanofiller at small loadings could improve electrocalic effect properties of P(VDF-HFP) copolymers in term of both increasing ΔT and dropping T_c.

Along with **Fig. 5.3. (a)**, **Fig. 5.3. (b)** that represents the electrocaloric effect of the polymer and its composites after electron beam irradiation also shows the similar trends. Neat P(VDF-HFP) possesses the lowest ΔT but highest T_c value compared to those of HFP/GN composites. It means that the effect of GNPs conducting nanofillers still exists after irradiation. Nevertheless, for electrocaloric effect, electron irradiation bring the different even the opposite to the GNPs nanofillers effects. Instead of improving ΔT and dropping T_c like GNPs, electron beam irradiation work with the opposite way, lowering ΔT and boosting T_c. This comparation can be seen clearly from **Fig. 5.4. (a)** and **(b)**. The maximum ΔT of neat P(VDF-HFP) after irradiation is (-38.32 ^{o}C), much lower that that of before irradiation of (-52.95 ^{o}C). On the other hands, the T_c of neat P(VDF-HFP) after irradiation was gained from 18.32 ^{o}C to 126.66 ^{o}C.
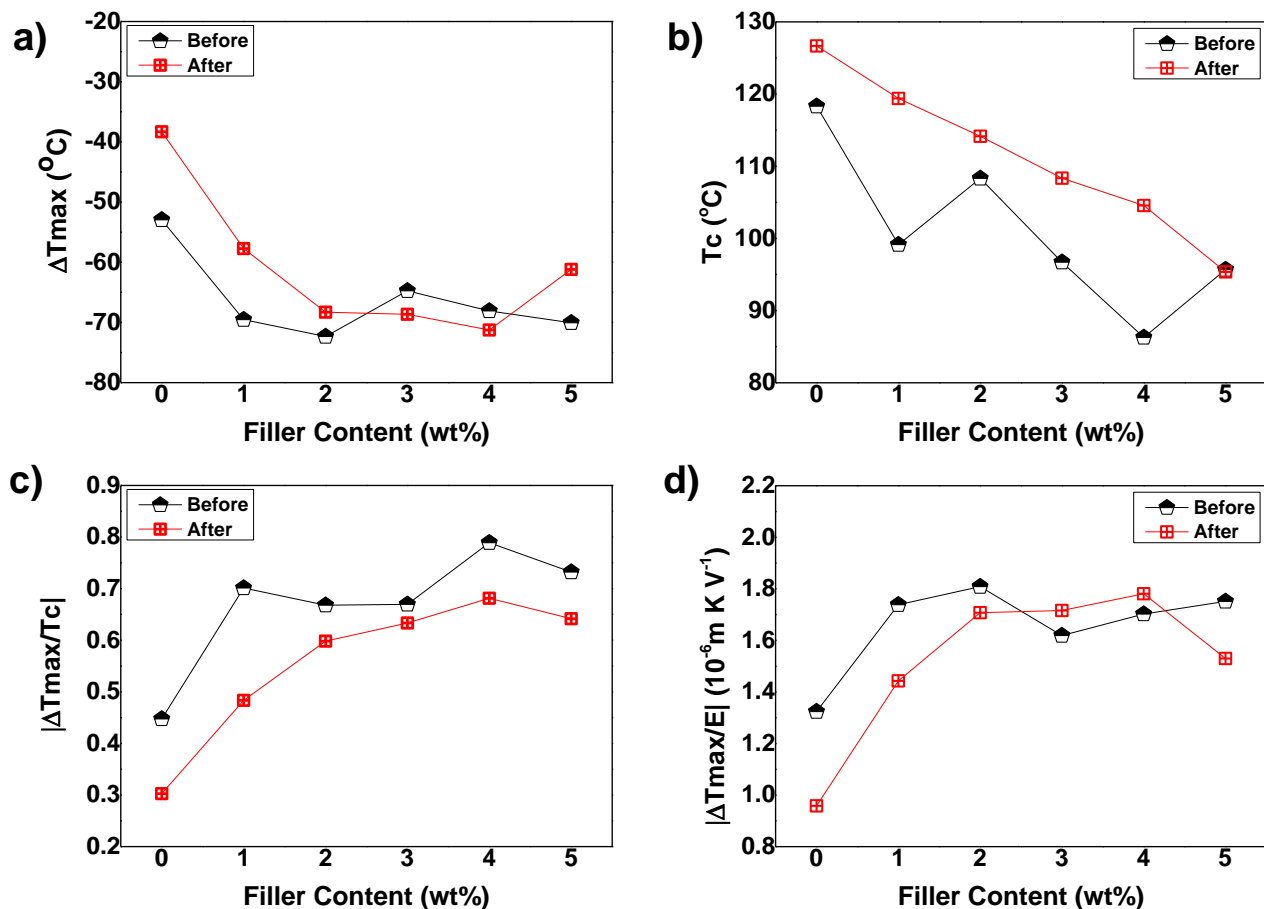
Figure 5.4. (a) ΔT_{max}; **(b)** T_c; **(c)** $|\Delta T_{max}/T_c|$ and **(d)** $|\Delta T_{max}/E|$ of neat P(VDF-HFP) and its composites before and after irradiated by electron.

Since the electrocaloric effect could be determined by two parameters, ΔT and T_c, the comparation ratio of those two parameters might help to select the better codition. **Fig. 5.4. (c)** shows the absolute ratio between ΔT and T_c for all conditions before and after electron beam irradiation. From this graph can be conclude that adding GNPs conducting nanofillers is effective to improve the electrocaloric behaviour of P(VDF-HFP) copolymers. The best propertiy was shown by HFP/GN4 that has almost twice of the $|\Delta T_{max}/T_c|$ ratio of neat P(VDF-HFP). Moreover, for all conditions, neat P(VDF-HFP) and HFP/GN composites all loadings, electron beam irradiation could not help to gain more improvement on it. The electrocaloric of the polymer and its composites was dropped after electron beam irradiation. These results were supported also by the ratio calculation of maximum ΔT and E as shown by **Fig. 5.4. (d)**. from this graph, it can be seen that absolute ratio $|\Delta T_{max}/E|$ of neat P(VDF-

HFP) and HFP/GN composites before electron beam irradiation is higher than that of after irradiation samples.

As stated by prevous works, the mechanism of electron beam irradiation is not comprehensively clear (Baer and Zhu, 2017; Zhu et al., 2017). Nevertheless, this phenomenon might be caused by the difference of the microstructural change that caused by electron beam irradiation and adding GNPs conducting nanofillers. It was proven that both GNPs and electron beam irradiation are effective to improve dielectric constant by inducing the charge that can change the crystalline phase of the polymers.

Not only enhancing the dielectric constant due to the strong interaction between the positive carbon of GNPs and negatively CF_2 bonds of P(VDF-HFP), introducing the fillers to the matrix will also affect to the microstructural change. The GNPs filler will fill the gap that exist in the polymers matrix that might leads to enlarge the distance between the polymers inter-chain. As the consequence, this inter-chain enlargement could weaken the reciprocity of the inter-chain itself in the polymer matrix (Zhu et al., 2017). Thus, introducing GNPs conducting nanofillers could lowering the Curi Temperature (T_c) that represents the energy barrier as shown by **Fig. 5.4. (b)**. Further, the crystallinity and crystal size could also be more exploited to help to understand the mechanism. Our prior work has been reported that the reducement of ΔT in the stretched P(VDF-HFP) might be caused by the drastical improvement of the cristallinity (Salea, Chaipo, Permana, Jehlaeh, and Putson, 2020). Nevertheless, in this work, the crystallinity of the polymer and its composites before and after electron beam irradiation is not significantly different, as presented by **table 3.1** at chapter 3. In the opposite, the crystal size of the polymer and its composites was dropped to almost a half after irradiation. This crystal size reduction could be another key factor to answer why adding GNPs nanofillers show the different effect on electrocaloric behaviour compared to electron beam irradiation.

The larger crystal size of the HFP/GN compared to neat P(VDF-HFP) with the higher spontaneous dipoles that packed in the ferroelectric domain leads to increase the net polarization even the external electric field was removed out. This bigger slope of the polarization change as the function of temperature change affects to bigger ΔT as well. So that, the ΔT of the composites are higher than that of the

polymer. It is different with the electron beam that chopped the crystal size to be smaller that resulting in to flexibility of the dipoles. Hence, when the electric field was removed, only small amounts of dipoles that are still reoriented. It could be lowering the slope of polarization change as the function of temperature change. As the results, the ΔT of the polymer and its composites was decreased after electron beam irradiaton.

5.5   Conclusion

As assumed, introducing conducting fillers such as GNPs will improve both AC conductivity of the polymer as well as its dielectric loss. Hence, huge size of ferroelectric loop can not be denied. As consequence, the HFP/GN composites showed undesired result on energy properties, high loss bu low discharge energy density. Fortunately, as the main key factor of this work, electron irradiation shows the opposite result that was effective on reducing ferroelectric crystal size, considerably boost up permittivity aalong with dropping AC conductivity and dielectric loss. Therefore, energy loss of all samples tend to decrease after electron irradiation. So that, higher both discharge storage energy and its energy efficiency can be reached for neat P(VDF-HFP) as well as its composites for all conditions. Here, after irradiated by electron, energy efficiency of neat P(VDF-HFP) copolymers was improved from 68.11 to 74.66%. this number is literally higher than reported by another work of 58%. Morover, the energy efficiency improvement was also achieved by the composties at all percentage consentration that almost doubled after irradiation. On the other hands, adding GNPs conducting nanofiller at small loadings could also improve electrocalic effect properties of P(VDF-HFP) copolymers in term of both increasing ΔT and dropping T_c. nevertheless, instead of improving ΔT and dropping T_c like GNPs, electron beam irradiation work with the opposite way, lowering ΔT and boosting T_c. hence, adding GNPs conducting nanofillers bring the benefit for dielectric and electrocaloric properties, while electron beam irradiation shows the outstanding performance on dielectric, ferroelectric behavior and energy properties.

Chapter 6 Conclusions and future work

6.1   Main conclusions

Combining two different techniques: introducing small amount of GNP conducting nanofillers and shooting the electron beam are the cores of this work. Some parameters have been observed by a plenty of measurements and characterizations. For the surface properties, GNPs presented a good spreading along the P(VDF-HFP) matrix. For the HFP/GN composites, a strong electrostatic interaction of between them resulted on smaller spherulites and a rougher surface topography compared to that of the neat polymer. Further, appearing of GNPs nanofiller is effective on reducing the pores of the polymer matrix that leads to more compact and homogeneous film. Along with the effect of adding GNPs nanofillers, shooting electron beam could also boost up the surface roughness of both neat polymer and composites. As the consequence, a more hydrophobic surface could be obtained. Hence, the water contact angle for neat P(VDF-HFP) and HFP/GN composites that measured after electron beam irradiation shows various number from 113° to 116°, respectively. Compared to the previously reported by another work of 90° for PVDF, those numbers were much higher, indicating a better performance for self cleaning ability.

Take a look on the microstructure inside, both choosen techniques were effective in facilitating and transforming the non-polar TGTG α-phase to the most electroactive TTTT β-phase by which the dielectric constants of all conditions improved. Unfortunately, introducing small amount of GNP also boosted up AC conductivity and dielectric loss of the polymer, leading to a bigger P-E hysteresis loop. As a highlight, it must be noted that the HFP/GN composites presented lower energy density and higher undesired energy loss. Interestingly, opposite to the effect of adding GNPs nanofillers, however, electron beam irradiation considerably improved the dielectric constant and reduced AC conductivity as well as dielectric loss in the same time. This happens by its effective role on reducing the crystal size. Therefore, energy loss tended to be lower after electron beam irradiation leading to much better desired storage energy density and storage energy efficiency of both neat

P(VDF-HFP) and HFP/GN composites at all loadings. After electron beam irradiation, the energy efficiency of neat P(VDF-HFP) was incrased from 68.11 to 74.66%, which is much higher than previously reported of 58%. Meanwhile, the energy efficiency was increased by two times for the HFP/GN composites.

For another application, electrocaloric cooling system, adding GNPs nanofillers shows a better role compared to electron beam irradiation. This electrocaloric effect improvement caused by GNPs was indicated by both increasing ΔT and dropping T_c. Considering those two electrocaloric parameters, the $| \Delta T_{max} / T_c |$ ratio for HFP/GN composites was improved to almost two times of the neat P(VDF-HFP).

In a simple term, adding GNPs nanofillers to the P(VDF-HFP) copolymers shows a good performance for dielectric and electrocaloric applications with additional advantages of hydrophobicity for self cleaning materialls, while electron beam irradiation shows an outstanding performance on dielectric constant, ferroelectricity and storage energy density and efficiency for a better smart energy device with self cleaning ability addition.

6.2   Future work

This work studied about the microstructure change and its effect on surface, electrical, ferroelectric and energy properties as well as electrocaloric effect behavior. The results show that there is a relation between all of them. According to the results of this work, the following issues could be considered for the future work:

a)   To gain a higher dielectric constant of the polymer, investigating other conducting materials and techniques that can facilitate β-phase formation and dipoles improvements should be conducted in advance.

b)   For energy application, higher storage energy density and efficiency could be generated by improving the flexibility of the dipoles. Hence, deeply exploration of electron beam irradiation and understanding its mechanism will be very useful to find the parallel techniques either by chemical or physical pinning.

c)   To generate a better electrocaloric cooling materials, improving ΔT and lowering T_c to be near room temperature is a necessary.

d)   This work used indirect measurement for electrocaloric effect. Hence, its direct measurements could be conducted as a comparison.

e)   This work can be extended for energy harvesting study.

REFERENCES

Abdessalem, M. B, Kriaa, I., Aydi, A., and Abdelmoula, N. (2018). Large electrocaloric effect in lead-free $Ba_{1-x}Ca_xTi_{1-y}Zr_yO_3$ ceramics under strong electric field at room-temperature. *Ceramics International*, *44*(12), 13595–13601. https://doi.org/10.1016/j.ceramint.2018.04.194

Aronov, D., and Rosenman, G. (2007). Surface energy modification by electron beam. *Surface Science*, *601*, 5042–5049. https://doi.org/10.1016/j.susc.2007.09.003

Asbani, B., Dellis, J. L., Gagou, Y., Kaddoussi, H., Lahmar, A., Amjoud, M., and Marssi, M. (2015). Electrocaloric effect in $Ba_{0.2}Ca_{0.8}Ti_{0.95}Ge_{0.05}O_3$ determined by a new pyroelectric method. *EPL (Europhysics Letters)*, *111*(5), 57008. https://doi.org/10.1209/0295-5075/111/57008

Baer, E., and Zhu, L. (2017). 50th Anniversary Perspective : Dielectric Phenomena in Polymers and Multilayered Dielectric Films. *Macromolecules*, *50(6)*, 2239–2256. https://doi.org/10.1021/acs.macromol.6b02669

Cataldi, P. (2018). Graphene Nanoplatelets-Based Advanced Materials and Recent Progress in Sustainable Applications. *Applied Science*, *8*, 1438. https://doi.org/10.3390/app8091438

Chenyang, X., and Zhao, M. (2013). Ionic liquid modified poly(vinylidene fluoride): crystalline structures, miscibility, and physical properties. *Polymer Chemistry*, *4*, 5726-5734. https://doi.org/10.1039/c3py00466j

Chinaglia, D. L., Gregorio, R., Stefanello, J. C., Altafim, R. A. P., Wirges, Werner Wirges, 2., Wang, F., and Gerhard, R. (2010). Influence of the Solvent Evaporation Rate on the Crystalline Phases of Solution-Cast Poly(Vinylidene Fluoride) Films. *Journal of Applied Polymer Science*, *116*, 785–791. https://doi.org/10.1002/app

Correia, T., and Zhang, Q. (2014). *Engineering Materials Electrocaloric Materials*.

REFERENCES (CONT.)

Daneshkhah, A., Shrestha, S., Siegel, A., Varahramyan, K., and Agarwal, M. (2017). Cross-selectivity enhancement of poly(vinylidene fluoride-hexafluoropropylene)-based sensor arrays for detecting acetone and ethanol. *Sensors (Switzerland)*, *17*(3), 595. https://doi.org/10.3390/s17030595

Fan, Q., and Xiao, C. (2008). Effects of Crosslinking Density on Structure and Properties of Interpenetrating Polymer Networks From Polyurethane and Nitroguar Gum. *Polymer Composites, 29(7)*. 758-767. https://doi.org/10.1002/pc.20451

Feng, Y., Li, J., Li, W., Li, M., Chi, Q., and Zhang, T. (2019). Effect of $BaTiO_3$ nanowire distribution on the dielectric and energy storage performance of double-layer PVDF-based composites. *Composites Part A*, *125*, 105524. https://doi.org/10.1016/j.compositesa.2019.105524

George, B. K. (2017). PVDF-ionic liquid modified clay nanocomposites: Phase changes and shish-kebab structure. *Polymer*, *115*, 70–76. https://doi.org/10.1016/j.polymer.2017.03.026

Gérard, J. (2018). Structural dependence of cations and anions to building the polar phase of PVDF. *European Polymer Journal*, *107*, 236–248. https://doi.org/10.1016/j.eurpolymj.2018.08.022

Gregor, M., Plecenik, T., Tofail, S. A. M., Zahoran, M., Truchly, M., Vargova, M., and Plecenik, A. (2014). Hydrophobicity of electron beam modified surface of hydroxyapatite films. *Applied Surface Science, 337*, 249-253. https://doi.org/10.1016/j.apsusc.2014.05.221

Guan, F., Pan, J., Wang, J., Wang, Q., and Zhu, L. (2010). Crystal Orientation Effect on Electric Energy Storage in Poly (vinylidene fluoride-co-hexafluoropropylene) Copolymers. *Macromolucules*, *43*, 384–392. https://doi.org/10.1021/ma901921h

REFERENCES (CONT.)

Guan, F., Yuan, Z., Shu, E. W., Zhu, L., Guan, F., Yuan, Z., and Zhu, L. (2013). Fast discharge speed in poly (vinylidene fluoride) graft copolymer dielectric films achieved by confined ferroelectricity. *Applied Physics Letters*, *052907*(2009), 10–13. https://doi.org/10.1063/1.3079332

Hartono, A., Satira, S., and Djamal, M. (2016). Electric Field Poling 2GV / m to Improve Piezoelectricity of PVDF Thin Film. *AIP Conf. Proc.*, *030021*, 2–6. https://doi.org/10.1063/1.4943716

He, F. A., Lin, K., Shi, D. L., Wu, H. J., Huang, H. K., Chen, J. J., and Lam, K. H. (2016). Preparation of organosilicate/PVDF composites with enhanced piezoelectricity and pyroelectricity by stretching. *Composites Science and Technology*, *137*, 138–147. https://doi.org/10.1016/j.compscitech.2016.10.031

IUPAC Provision Recomendation. (2004).

Jenkins, A. D., Kratochvíl, P., Stepto, R. F. T., and Suter, U. W. (1996). Glossary of basic terms in polymer science (IUPAC Recommendations 1996). *Pure and Applied Chemistry*, *68*(12), 2287-2311. https://doi.org/10.1351/pac199668122287

Jia, Y., Namiki, T., Kasai, S., Li, L., and Nishimura, K. (2018). Magnetic anisotropy and large low fi eld rotating magnetocaloric effect in NdGa single crystal. *Journal of Alloys and Compounds*, *757*, 44–48. https://doi.org/10.1016/j.jallcom.2018.05.028

Khalifa, M., Mahendran, A., and Anandhan, S. (2016). Probing the synergism of halloysite nanotubes and electrospinning on crystallinity, polymorphism and piezoelectric performance of poly(vinylidene fluoride. *RSC Advances*, *6*, 114052–114060. https://doi.org/10.1039/C6RA20599B

REFERENCES (CONT.)

Kitabata, M., Taddese, T., and Okazaki, S. (2018). Molecular Dynamics Study on Wettability of Poly(vinylidene fluoride) Crystalline and Amorphous Surfaces. *Langmuir*, *34*(40), 12214–12223. https://doi.org/10.1021/acs.langmuir.8b02286

Kitanovski, A., Tu, J., and Poredo, A. (2014). Electrocaloric vs. magnetocaloric energy conversion Comparaisons des conversions d'énergie électrocalorique et magnétocalorique. *International Journal of Refrigeration, 37*, 16-27. https://doi.org/10.1016/j.ijrefrig.2013.07.001

Kitanovski, A., Tu, J., and Poredo, A. (2014). Electrocaloric refrigeration: Thermodynamics, state of the art and future perspectives Froid électrocalorique : Aspects thermodynamiques, état de l'art et perspectives futures. *International Journal of Refrigeration, 40*, 174-188. https://doi.org/10.1016/j.ijrefrig.2013.11.007

Kuvardina, E. V., Novokshonova, L. A., Lomakin, S. M., Timan, S. A., and Tchmutin, I. A. (2013). Effect of the graphite nanoplatelet size on the mechanical, thermal, and electrical properties of polypropylene/exfoliated graphite nanocomposites. *Journal of Applied Polymer Science*, *128*(3), 1417–1424. https://doi.org/10.1002/app.38237

Li, Q., and Wang, Q. (2016). Ferroelectric Polymers and Their Energy-Related Applications. *Macromolecular Chemistry and Physics*, *217*(11), 1228–1244. https://doi.org/10.1002/macp.201500503

Li, W., Meng, Q., Zheng, Y., Zhang, Z., Xia, W., Xu, Z., and Zheng, Y. (2010). Electric energy storage properties of poly(vinylidene fluoride). *Applied Physics Letter*, *96*, 192905. https://doi.org/10.1063/1.3428656

Li, X., Lu, S. G., Chen, X. Z., Gu, H., Qian, X. S., and Zhang, Q. M. (2013). Pyroelectric and electrocaloric materials. *Journal of Materials Chemistry C*, *1*(1), 23–37. https://doi.org/10.1039/c2tc00283c

REFERENCES (CONT.)

Lu, S. G., Zhang, Q. M., and Kutnjak, Z. (2010). Comparison of directly and indirectly measured electrocaloric effect in relaxor ferroelectric polymers. *Applied Physics Letters, 97(20),* 202901. https://doi.org/10.1063/1.3514255

Lu, Z., Hu, W., Xie, F., Zhuo, L., and Yang, B. (2017). Sol-gel synthesis of nanosilica-coated: Para -aramid fibers and their application in the preparation of paper-based friction materials. *RSC Advances*, *7*(49), 30632–30639. https://doi.org/10.1039/c7ra05142e

Lubomirsky, I., and Stafsudd, O. (2012). Invited Review Article : Practical guide for pyroelectric measurements. *Review of Scientific Instruments, 83*, 051101. https://doi.org/10.1063/1.4709621

Magalhaes, R. Duraes,N. Silva, M. (2011). The role of solvent evaporation in the microstructure of electroactive β-Poly(vinylidene fluoride) membranes obtained by isothermal crystallization. *Soft Materials*, *9(1),* 1-14. https://doi.org/10.1080/1539445X.2010.525442

Maiwa, H. (2015). Characterization of electrocaloric properties by indirect estimation and direct measurement of temperature – electric field hysteresis loops. *Japanese Journal of Applied Physics*, *54*, 10NB08. https://doi.org/http://dx.doi.org/10.7567/JJAP.54.10NB08

Malmonge, L. F., Malmonge, J. A., and Sakamoto, W. K. (2003). Study of pyroelectric activity of PZT/PVDF-HFP composite. *Materials Research*, *6*(4), 469–473. https://doi.org/10.1590/S1516-14392003000400007

Mansouri, S., Sheikholeslami, T. F., and Behzadmehr, A. (2019). Investigation on the electrospun PVDF/NP-ZnO nanofibers for application in environmental energy harvesting. *Journal of Materials Research and Technology*, *8*(2), 1608–1615. https://doi.org/10.1016/j.jmrt.2018.07.024

REFERENCES (CONT.)

Martins, P., Lopes, A. C., and Lanceros-Mendez, S. (2014). Electroactive phases of poly(vinylidene fluoride): Determination, processing and applications. *Progress in Polymer Science*, *39*(4), 683–706. https://doi.org/10.1016/j.progpolymsci.2013.07.006

Mischenko, A. S. (2006). Giant Electrocaloric Effect in Thin-Film $PbZr_{0.95}Ti_{0.05}O_3$. *American Association for the Advancement of Science,311(5765).* 1270-1. https://doi: 10.1126/science.1123811

Moradi, R., Karimi-sabet, J., Shariaty-niassar, M., and Koochaki, M. A. (2015). Preparation and Characterization of Polyvinylidene Fluoride/Graphene Superhydrophobic Fibrous Films. *Polymers*, *7*, 1444–1463. https://doi.org/10.3390/polym7081444

Neese, B., Chu, B., Lu, S., Wang, Y., Furman, E., and Zhang, Q. M. (2018). Large Electrocaloric Effect in Ferroelectric Polymers Near Room Temperature. *American Association for the Advancement of Science, 321*(5890), 821–823. https://doi.org/10.1126/science.1159655

Pakhomov, O. V, Karmanenko, S. F., Semenov, A. A., and Starkov, A. S. (2010). Thermodynamic Estimation of Cooling Efficiency Using an Electrocaloric Solid State Line, *55*(8), 1155–1160. https://doi.org/10.1134/S106378421008013X

Pandya, S., Wilbur, J. D., Bhatia, B., Damodaran, A. R., Monachon, C., Dasgupta, A. and Martin, L. W. (2017). Direct Measurement of Pyroelectric and Electrocaloric Effects in Thin Films. *Physical Review Applied*, *7*(3), 034025. https://doi.org/10.1103/PhysRevApplied.7.034025

Plecenik, T., Tofail, S. A. M., Gregor, M., Zahoran, M., Truchly, M., Plecenik, T.and Roch, T. (2012). Direct creation of microdomains with positive and negative surface potential on hydroxyapatite coatings. *Applied Physics Letters*, *98*, 113701. https://doi.org/10.1063/1.3567532

REFERENCES (CONT.)

Review, P., War, W., and States, U. (1988). Linear dielectric-breakdown electrostatics. *Physical Review B*, *38*(13), 9005–9010. https://doi.org/10.1103/physrevb.38.9005

Ribeiro, C., Costa, C. M., Correia, D. M., Nunes-pereira, J., Oliveira, J., Martins, P., and Lanceros-méndez, S. (2018). Electroactive poly (vinylidene fluoride)-based structures for advanced applications. *Nature Publishing Group*, *13*(4), 681–704. https://doi.org/10.1038/nprot.2017.157

Roy, A., Dutta, B., and Bhattacharya, S. (2016). Electroactive phase nucleation and non-isothermal crystallization kinetics study in [DEMM][TFSI] ionic liquid incorporated P(VDF-HFP) co-polymer membranes. *Journal of Materials Science*, *51*(17), 7814–7830. https://doi.org/10.1007/s10853-016-9978-4

Roy, S., Thakur, P., Hoque, N. A., Bagchi, B., and Das, S. (2016). Enhanced electroactive β-phase nucleation and dielectric properties of PVdF-HFP thin films influenced by montmorillonite and Ni(OH)2nanoparticle modified montmorillonite. *RSC Advances*, *6*(26), 21881–21894. https://doi.org/10.1039/c6ra00864j

Ruan, L., Yao, X., Chang, Y., Zhou, L., Qin, G., and Zhang, X. (2018). Properties and applications of the β phase poly(vinylidene fluoride). *Polymers*, *10*(3), 1–27. https://doi.org/10.3390/polym10030228

Lu, S. L., Li, X. Y., Cheng, J. P., Gorny, L., and Zhang, Q. M. (2011). Giant Electrocaloric Effect in High-Energy Electron Irradiated P(VDF-TrFE) Copolymers. *Material Research Society*, *1310*(5), 1001–1006. https://doi.org/10.1557/opl.2011.

Sachdeva, G., and Jain, V. (2016). Comparative Exergy Analysis of Vapor Compression Refrigeration System Using Alternative Refrigerants, *10*(6), 1081–1088.

REFERENCES (CONT.)

Salea, A., Chaipo, S., Permana, A. A., Jehlaeh, K., and Putson, C. (2020). The microstructure of negative electrocaloric Polyvinylidene fluoride-hexafluoropropylene copolymer on graphene loading for eco-friendly cooling technology. *Journal of Cleaner Production*, *251*, 119730. https://doi.org/10.1016/j.jclepro.2019.119730

Shrivastav, B. D., Barde, R., Mishra, A., and Phadake, S. (2013). Frequency and Temperature Dependence of Dielectric Properties of Fish Scales Tissues. *Research Journal of Physical Sciences*, *1*(6), 24–29.

Soulestin, T., Ladmiral, V., Dos Santos, F. D., and Améduri, B. (2017). Vinylidene fluoride- and trifluoroethylene-containing fluorinated electroactive copolymers. How does chemistry impact properties? *Progress in Polymer Science*, *72*, 16–60. https://doi.org/10.1016/j.progpolymsci.2017.04.004

Sousa, R. E., Nunes-pereira, J., Ferreira, J. C. C., Costa, C. M., Machado, A. V, Silva, M. M., and Lanceros-mendez, S. (2014). Microstructural variations of poly(vinylidene fluoride co-hexa fluoropropylene) and their influence on the thermal, dielectric and piezoelectric properties. *Polymer Testing*, *40*, 245–255. https://doi.org/10.1016/j.polymertesting.2014.09.012

Su, J., and Zhang, J. (2017). Improvement of electrical properties and thermal conductivity of ethylene propylene diene monomer (EPDM)/barium titanate (BaTiO$_3$) by carbon blacks and carbon fibers. *Journal of Materials Science: Materials in Electronics*, *28*(7), 5250–5261. https://doi.org/10.1007/s10854-016-6182-x

Tan, S., Hu, X., Ding, S., Zhang, Z., Li, H., and Yang, L. (2013). Significantly improving dielectric and energy storage properties via uniaxially stretching crosslinked P(VDF-co-TrFE) films. *Journal of Materials Chemistry A*, *1*(35), 10353–10361. https://doi.org/10.1039/c3ta11484h

REFERENCES (CONT.)

Thakur, P., Kool, A., Bagchi, B., Das, S., and Nandy, P. (2014). Enhancement of β phase crystallization and dielectric behavior of kaolinite/halloysite modified poly(vinylidene fluoride) thin films. *Applied Clay Science, 99,* 149-159. https://doi.org/10.1016/j.clay.2014.06.025

Thakur, P., Kool, A., Bagchi, B., Das, S., and Nandy, P. (2015). Effect of in situ synthesized Fe_2O_3 and Co_3O_4 nanoparticles on electroactive β phase crystallization and dielectric properties of poly(vinylidene fluoride) thin films. *Physical Chemistry Chemical Physics, 17(2),* 1368-1378. https://doi.org/10.1039/C4CP04006F

Thakur, V. K., and Gupta, R. K. (2016). Recent Progress on Ferroelectric Polymer-Based Nanocomposites for High Energy Density Capacitors : Synthesis, Dielectric Properties, and Future Aspects. *Chemical Reviews*, *116*, 4260–4317. https://doi.org/10.1021/acs.chemrev.5b00495

Tiwari, V. K., Prasad, A. K., Singh, V., Jana, K. K., Misra, M., Prasad, C. D., and Maiti, P. (2013). Nanoparticle and process induced super toughened piezoelectric hybrid materials: The effect of stretching on filled system. *Macromolecules*, *46*(14), 5595–5603. https://doi.org/10.1021/ma400603h

Verma, V. P. (2018). Microstructural, thermal and electrical properties of electron irradiated Li_2CO_3 doped PVA. *Indian Journal of Pure and Applied Physics, 56(08)*. 616-620.

Vienneau, D., De Hoogh, K., Hauri, D., Vicedo-Cabrera, A. M., Schindler, C., Huss, A., and Röösli, M. (2017). Effects of radon and UV exposure on skin cancer mortality in Switzerland. *Environmental Health Perspectives*, *125*(6), 1–9. https://doi.org/10.1289/EHP825

REFERENCES (CONT.)

Vuarnoz, D., Kitanovski, A., Gonin, C., and Egolf, P. W. (2012). Thermodynamic and exergy efficiencies of magnetocaloric energy conversion utilising industrial waste heat. *International Journal of Exergy*, *10*(4), 365–378. https://doi.org/10.1504/IJEX.2012.047508

Wang, X., Xiao, C., Liu, H., Huang, Q., Hao, J., and Fu, H. (2018). Poly(vinylidene Fluoride-Hexafluoropropylene) Porous Membrane with Controllable Structure and Applications in Efficient Oil/Water Separation. *Materials*, *11*(443), 1–12. https://doi.org/10.3390/ma11030443

Wang, Y., Huang, X., Li, T., Wang, Z., Li, L., Guo, X., and Jiang, P. (2017). Novel crosslinkable high-k copolymer dielectrics for high-energy-density capacitors and organic field-effect transistor applications. *Journal of Materials Chemistry A: Materials for Energy and Sustainability*, *5*, 20737–20746. https://doi.org/10.1039/C7TA06005J

Witkowska, B., and Frydrych, I. (2004). A comparative analysis of tear strength methods. *Fibres and Textiles in Eastern Europe*, *12*(2), 42–47.

Yang, D., Xu, H., Yu, W., Wang, J., and Gong, X. (2017). Dielectric properties and thermal conductivity of graphene nanoplatelet filled poly(vinylidene fluoride) (PVDF)/poly(methyl methacrylate) (PMMA) blend. *Journal of Materials Science: Materials in Electronics*, *28*(17), 13006–13012. https://doi.org/10.1007/s10854-017-7132-y

Yang, L., Li, X., Allahyarov, E., Taylor, P. L., Zhang, Q. M., and Zhu, L. (2013). Novel polymer ferroelectric behavior via crystal isomorphism and the nanoconfinement effect. *Polymer*, *54*(7), 1709–1728. https://doi.org/10.1016/j.polymer.2013.01.035

REFERENCES (CONT.)

Zhu, L. (2014). Exploring Strategies for High Dielectric Constant and Low Loss Polymer Dielectrics. *The Journal of Physical Chemistry Letters*, *5(21)*, 3677–3687. https://doi.org/10.1021/jz501831q

Zhu, Y., Jiang, P., Zhang, Z., and Huang, X. (2017). Dielectric phenomena and electrical energy storage of poly (vinylidene fluoride) based high-k polymers. *Chinese Chemical Letters*, *28*(11), 2027–2035. https://doi.org/10.1016/j.cclet.2017.08.053

Paper I (Published)

The microstructure of negative electrocaloric Polyvinylidene fluoride-hexafluoropropylene copolymer on graphene loading for eco-friendly cooling technology

Ahamad Salea, Suphita Chaipo, **Ardian Agus Permana**, Kunthisa Jehlaeh and
Chatchai Putson

The microstructure of negative electrocaloric Polyvinylidene fluoride-hexafluoropropylene copolymer on graphene loading for eco-friendly cooling technology
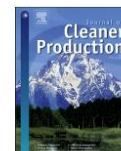
Ahamad Salea, Suphita Chaipo, Ardian Agus Permana, Kunthisa Jehlaeh, Chatchai Putson[*]

Materials-Physics Laboratory, Physics Department, Faculty of Science, Prince of Songkla University, Songkhla, 90112, Thailand

ABSTRACT

Extraordinarily negative electrocaloric materials are desirable for environment-friendly cooling applications. Stretched and unstretched Polyvinylidene fluoride-hexafluoropropylene thin films with suitable graphene contents have been studied in this work. The thin films were fabricated by solution casting method. Crystallinity was induced by stretching technique resulting a translucent film, with increasing dielectric constant, dielectric loss, conductivity and ferroelectric properties. By increasing the filler content, the maximum negative temperature change was intensified, and Curie temperature was decreased by 20 °C. However, a good electrocaloric effect was achieved without stretching, although stretching could stabilize Curie temperature to a smooth curve. The best performance in this work was found with graphene of 1 wt% (weight fraction of 0.01), which had an enhanced electrocaloric effect with a potential for electrocaloric cooling applications.

© 2019 Elsevier Ltd. All rights reserved.

1. Introduction

Cooling systems are very important in various applications to increase heat transfer rates. The conventional cooling systems used in refrigeration and air conditioning might be replaced by novel technologies. Electrocaloric cooling (ECC) is recently interesting as innovative cooling system with green technology that releases no CFC emissions (Goupil et al., 2012; Scott, 2011). It has high energy conversion efficiency that is better than conventional cooling (Pakhomov et al., 2010). ECC can be potentially applied in micro-electronic circuits, integrated circuit (ICs), automobiles, air-conditioners and refrigerators. ECC is based on both electrocaloric and pyroelectric effects, stemming from the cross-coupling of temperature and polarization change in an insulating dielectric material. The mechanism of electrocaloric effect (ECE) is started with heat energy that can be released or absorbed by applied electric field. As the consequence, it can reorient the dipole moments on the material. On the other hand, the reversed way of that

phenomenon called pyroelectric effect that still obeying Maxwell relations (Lines and Glass, 1977). ECC has been found in insulating dielectric-ferroelectric materials. In ferroelectric materials, ECE can be observed in term of the changing of both entropy (ΔS) and temperature (ΔT) when applying external electric field (E). The highest ΔT is usually found near the phase transition temperature or Curie temperature (T_c). A large ΔT with comparatively small E is beneficial for ECE. Moreover, large dielectric constant (ε_r) with small dielectric loss ($\varepsilon_r^{"}$) are desired for ECE according to the Maxwell relations.

ECE materials have been extensively applied to the innovative electrocaloric cooling system in particular high electrocaloric efficiency regarded to the ferroelectric ceramic, namely positive ECE such as $BaTiO_3$ with $\Delta T = 1.6$ K (1 MV/m) (Bai et al., 2012), $Pb_{0.97}La_{0.02}(Zr_{0.66}Sn_{0.23}Ti_{0.11})O_3$ with $\Delta T = 0.6$ K (30 MV/m) (Zhuo et al., 2017), and negative ECE such as $(Pb_{0.88}Sr_{0.08})$ $[Nb_{0.08}(Zr_{0.53}Ti_{0.47})_{0.92}]O_3$ with $\Delta T = -0.38$ K (1.5 MV/m) (Chen et al., 2017), NBT with $\Delta T = -1.6$ K (7 MV/m) (Jiang et al., 2014), $Pb_{0.97}La_{0.02}(Zr_{0.80}Sn_{0.14}Ti_{0.06})O_3$ with $\Delta T = -5.5$ K (11 MV/m) (Zhuo et al., 2018), etc. It found that most of ferroelectric ceramic have love electrical breakdown. This is the main disadvantages to consider on ferroelectric ceramic, requiring low ΔS and ΔT,

---

respectively. The brittle and heavyweight are also another disadvantages to fabricate thin film. Recently, the ceramics are replaced with polymers due to they are flexible, modifier shape, lightweight, easy to process and low cost. Importantly, the larger electrical breakdown of ferroelectric polymer is a key point to enlarge ΔT for electrocaloric performances, such as P(VDF-TrFE)55/45 with ΔT = 12.6 K (209 MV/m) (Neese et al., 2008).

However, not many research to date has focused on the ferroelectric polymers (Neese et al., 2008), i.e. Polyvinylidene Fluoride (PVDF) ferroelectric polymers or PVDF family. PVDF is a semicrystalline polymer containing Fluorine (F), Hydrogen (H), and a Carbon (C) backbone in the units $-(C_2H_2F_2)_n-$. β phase (TTTT conformation) has the most dipoles in PVDF, giving large net dipole moment, polarization, and dielectric constant, and producing a large ECE (Lu et al., 2011). Polyvinylidene fluoride-hexafluoropropylene (PVDF-HFP) is also one of interesting PVDF family that possess some advantages such as good flexibility, chemically resistance, excellent electromechanical properties and low cost (He et al., 2005; Huan et al., 2007; Neese et al., 2007).

Many different approaches have been proposed to improve this performance. Tailored polarization by electron-beam or gamma irradiation (Bauer, 2010; Parangusan et al., 2018b; Zhang et al., 1998), self-rearranged polarization by electrospinning (Parangusan et al., 2018a; Tohluebaji et al., 2019), rearranged polarization by poling at given temperature (Sencadas et al., 2004), modified crystal structure by stretching technique at given temperature (Tan et al., 2013), combination of polar and charge distributions on polymer composite by adding filler (Choolaei et al., 2017), are examples. However, stretching technique and adding filler are the most convenient way to improve these properties without using advanced tools as gamma source and high voltage. The combination of stretching technique and polymer composite by adding filler are interesting to study.

Stretching is one of technique to improve the configuration of the dipoles (Salimi and Yousefi, 2003). It has improved on dielectric and ferroelectric properties. S. Tan and coworkers (Tan et al., 2013) studied the reduction of crystallite size on stretched films and his results agree with other author's finding in this area (He et al., 2016; Zhao et al., 2009). He provided an improving dielectric and ferroelectric properties of stretched PVDF-TrFE film. He highlighted that the stretched films reduce crystallite size, improve crystal orientation polarization and overall crystallinity. As a result, they exhibited a dramatic increased dielectric constant, slightly increased dielectric loss, and smaller remnant polarization (P_r) as slimmer ferroelectric loop with enhanced relaxation speed of crystal grains. So far researchers have only found innovative ways to relate crystallite size reduction with dielectric and ferroelectric properties, but in this paper make a further contribution by showing that crystallinity reduction improve electrocaloric behavior.

On the other hand, many researches have been occurred on PVDF polymer with nanofillers. V. Goodarzi and coworkers (Goodarzi et al., 2014) studied nanofiller effect on crystallization behavior on mechanical PVDF nanocomposites properties. They found that the nanocomposite has a small greater than the pure polymer. V. Goodarzi continuously confirmed the effect on semicrystalline PVDF-HFP structure by adding LDH nanoparticles filler (Shojaei et al., 2018). They proved that most of crystallite size on PVDF-HFP are decreased with LDH loading. As yet, a solution of crystallite size effect on ECE has not found, although ECE have been made. Furtherly, they investigated the crystallite sizes of PVDF-HFP copolymer filled by Graphene Oxide (GO) (Choolaei et al., 2017). As a result, the crystallite size on β phase decreased by increasing GO content. It seems that crystal growth in a particular crystallographic direction is against by GO nanoparticle.

Besides GO, Graphene nanoplatelets is one of graphene family materials that have electrical and thermal conductor. Some works about graphene nanoplatelets have been reported on fluid heat transfer system (Bahiraei and Heshmatian, 2019; Bahiraei and Mazaheri, 2018; Bahiraei et al., 2019). The graphene nanoplatelets is clearly improved heat transfer efficiency, showing at the highest graphene concentration on that graphene nanofluid system. Besides its excellent properties on heat transfer, it is also interesting to study graphene nanoplatelets effect on electrical properties. Since it is included as great electrical conductor, graphene family materials also have potential roles to induce electroactive phase on electroactive polymer with crystallite size reduction. As reported, electrical conductive filler of graphene are the most interesting for improving dielectric PVDF polymers compared with other fillers (Li et al., 2009, 2010; Yang et al., 2016)

The aim of the present work is to fabricate a stretched PVDF-HFP/graphene nanoplatelets by two techniques of stretching film and adding graphene nanofiller, and to find a new electrocaloric relation in the amount of crystallite size and crystallinity formed. PVDF-HFP was blended with graphene nanoplatelets by using solution casting technique. Appropriate graphene contents for ECE were sought. Saturation of the electrocaloric effect will determine the suitable filler content. Both unstretched and stretched samples are compared, assessing the PVDF-HFP microstructure effects. The results of the comparison between the effects of the two techniques (i.e., adding graphene and stretching) encourage and propose to relationship between the structure morphology, crystallinity (X_c), crystallite size, dielectric properties and electrocaloric behavior. This new relation will be able to design and predict the advanced capacitor and electrocaloric cooling system in future.

2. Materials and methods

Graphene nanoplatelets powder was purchased from Sigma-Aldrich Ltd, Singapore, having 12.01 g/mol (806633 ALDRICH), and was ultra-sonicated in 200 W N,N-dimethylformamide with ≥ 99% purity (DMF), from RCI Labscan Limited, Thailand, for 20 min to prevent formation of agglomerates. Then, it was mixed with Polyvinylidene fluoride-hexafluoropropylene P(VDF-HFP) powder from Solvay Solexis, Belgium with a 10 wt % HFP (Solef 11010/1001) and then stirred at 30 °C around 12 h to get homogeneous solution. Then, the composite solution was casted on glass plate with an adjustable film applicator (Sheen S/N 102503/2, lncl, Shims) before evaporating DMF by drying at 80 °C 12 h in the oven (Asset positively identifiable T410353 Binder). The thickness of each composites thin film was about 100 μm after peeled off from the glass plates. This step has to drop a few DI water when peeling the film out for preventing the crack formation on films. Afterwards, the thin films were observed before stretched with original length ratio (L/L_0) of four times, from 20 mm to 80 mm elongation length. The stretching rate of 2.5 mm/min was used by adjustable step motor at 100 °C to about 30 μm. A suitable stretching force and temperature could induce large X_c in this PVDF-HFP, as reported in a prior study (Sukwisute et al., 2013). The stretched composite thin films with graphene filler loadings of 1, 2, 3, 4 and 5 wt% (0.01, 0.02, 0.03, 0.04, and 0.05, respectively by weight fraction) in PVDF-HFP were labeled GPN1ST, GPN2ST, GPN3ST, GPN4ST, and GPN5ST, respectively. Similarly, GPN1NST, GPN2NST, GPN3NST, GPN4NST, and GPN5NST, by loading level, were the labels used for cast film samples of 30 μm thickness without stretching. Pure PVDF-HFP thin films, with and without stretching were labeled as pureST and pureNST, were compared as the control cases.

3. Results and discussion

3.1. Macroscopic structure

Surface Morphology. Graphene distribution on the surface of a composite thin film was detected by SEM (FEI Quanta 400, USA). As Fig. 1(a)-(b), stretching changed pure PVDF-HFP to translucent material. Possibly crystalline regions were formed by stretching (He et al., 2016; Tan et al., 2013). Fig. 1(c) presents the distribution of filler in PVDF-HFP in TEM images. The filler was well dispersed in the polymer. The white color represents the insulating PVDF-HFP polymer while the darker color regions are graphene particles in the sample of GPN1NST. The graphene filler was surrounded by semicrystalline PVDF-HFP, as seen in Fig. 1(d), having both crystalline and amorphous parts. Furthermore, graphene filler directly darkens the film in a manner dependent on graphene content.

XRD diffraction. Film composites were investigated by using an X-ray diffractometer (XRD, X'Pert MPD, Philips, Netherlands). The 2θ was scanned from $14°$ to $38°$ with $0.05°$ s^{-1} scaning rate by Cu–K radiation (wavelength 0.154 nm) under 40 kV voltage. The crystallite size (L) were calculated following Equation (1) by Scherrer (1918). Where λ, FWHM, and θ, are the X-ray wavelength (0.154 nm), the full width at half maximum for diffraction peaks, and the corresponding diffraction angle, respectively.

$$L_{2\theta}(nm) = \frac{0.91\lambda}{FWHM \cdot \cos\theta} \qquad (1)$$

An XRD patterns presents in Fig. 2(a). PureNST, pureST, GPN1ST, GPN2ST, GPN3ST, GPN4ST, and GPN5ST were investigated. The strongest diffraction on PVDF-HFP exhibits at $2\theta = 20.5°$ of β phase with (110)/(200) crystallographic planes. Diffraction peak $2\theta = 18.3°$ is associated with α phase (020) plane (Patro et al., 2008). The β phase (TTTT) produces the highest net polarization compared with α (TGTG′) and γ (TTTGTTTG′) phases.

XRD by filler loading. Graphene nanoplatelets diffraction at $2\theta = 26.5°$ increased with graphene content. However, adding filler had not significantly observed crystallite size reduction in both 2θ of $18.3°$ and $20.5°$ (Fig. 2 (b)), while previous study reported crystallite size reduction by adding filler (Choolaei et al., 2017). In this work, a few interval of graphene content has not enough to significantly differentiate on crystallite size. For $2\theta = 20.5°$, GPN5ST seemed the biggest crystallite size (0.123 nm) compared with pureST (0.087 nm), GPN1ST (0.094 nm), GPN2ST (0.082 nm), GPN3ST (0.091 nm), and GPN4ST (0.081 nm) due to excessive filler. In fact, crystallite size can be reduced with modified PVDF fillers (Choolaei et al., 2017) and stretching (Tan et al., 2013).

XRD by stretched case. It is seen that stretching significantly decrease crystallite size for $2\theta = 18.3°$, as in Fig. 2(b). After stretching film, the crystallite size was considerably decreased from 0.507 nm of pureNST to 0.042 nm of pureST. The stretching force have possibly energy to cut crystallite size into smaller pieces. This tendency is matched with prior study (Tan et al., 2013). They explained that crystallite size is reduced after stretching PVDF polymer with increasing crystallinity.

DSC analysis. To characterize the samples for thermal stability, Differential Scanning Calorimeter (DSC, Simultaneous Thermal Analyzer, STA8000, PerkinElmer, USA) was used. The heat was applied to the samples from 120 °C to 180 °C at 10.00 °C/min in ambient atmospheric air. This experiment can determine the melting temperature (T_m) around 160 °C. The thermal stability was observed from the area under the endothermic peak, i.e., the melting enthalpy (ΔH_m). The crystallinity (X_c) was calculated from Equation (2), where $\varnothing$ is the filler's weight fraction in the composites. ΔH_m and ΔH_m^0 are the observed enthalpy of melting and that for 100% crystalline PVDF-HFP, which equals 104.6 J g^{-1} (He et al., 2017).

$$X_c(\%) = \frac{\Delta H_m}{(1 - \varnothing)\Delta H_m^0} \times 100 \qquad (2)$$

DSC by filler loading. Fig. 3(a-b) exhibits the DSC results, including X_c (Fig. 3(c)) and T_m (Fig. 3(d)). It is seen that X_c and T_m increase with graphene content until they reach a peak in 2–3 wt%. Afterwards they gradually decreased at 4–5 wt%, because excessive filler decreased X_c along with T_m. In addition, X_c of GPN5ST suddenly dropped to 44.91%, whereas crystallite size on $2\theta = 20.5°$ increased, seen in XRD result. It can seem that excessive filler of GPN5ST decreases X_c and increases crystallite size.

DSC by stretched case. It seems that the stretched films produce higher X_c, seen in Fig. 3(c). Stretching possibly changes the amorphous to crystalline phase in polymer causing unstable crystalline phase, matching translucent in Fig. 1(a–b). T_m seemly decreased after stretching. It is possibly that stretching force induced overall X_c and reduced the crystallite size, resulting to increase X_c and decrease T_m, respectively. The result is in agreement with a prior study (Fatou, 1971; Sukwisute et al., 2013; Tan et al., 2013). After stretching, X_c reduction on 5 wt% graphene is possibly the maximum limit in this work.

3.2. Dielectric properties

The samples were measured for dielectric properties across frequencies from 1 to 10^5 Hz by using an IM 3533 LCR meter (HIOKI, Japan) by setting the voltage across sample of 1 V ac, with 5 mm diameter electrodes and 30 μm sample thickness. The capacitance (C), loss tangent or dielectric loss (ε_r''), and electrical conductivity (σ_{ac}) were recorded at room temperature. Subsequently, dielectric constant (ε_r) and σ_{ac} were calculated from Equations (3) and (4), respectively. Here d refers to the thickness, A refers to the electrode area, f refers to the ac frequency in Hz, and ε_0 refers to free space permittivity equaling 8.853×10^{-12} F m^{-1} (Thakur et al., 2015). The ε_r, ε_r'', and σ_{ac} for unstretched and stretched samples are shown in Fig. 4(a-c), (d-f), and (g-i), respectively.

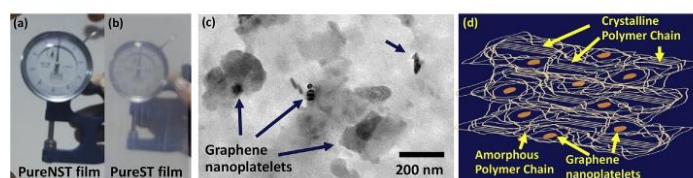$$\varepsilon_r = Cd/\varepsilon_0 A \qquad (3)$$

Fig. 1. Appearances of a pure PVDF-HFP film when (a) unstretched and (b) stretched. The composite film structure in (c) TEM image of the GPN1NST, (d) schematic idealization.
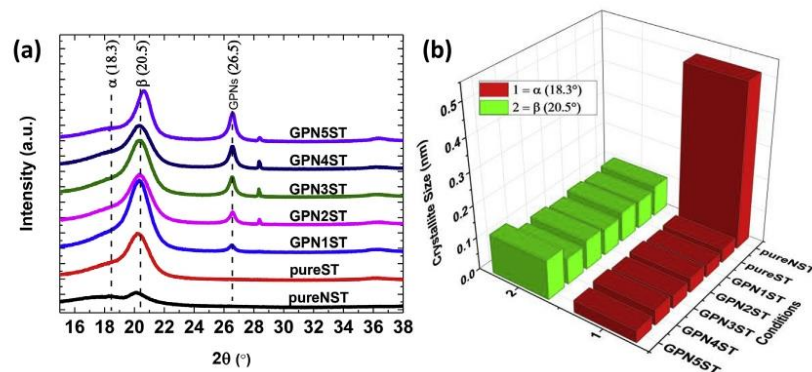
Fig. 2. (a) XRD diffraction at $2\theta = 15° - 38°$ of pureNST, pureST, GPN1ST, GPN2ST, GPN3ST, GPN4ST, and GPN5ST, (b) crystallite size of PVDF-HFP at $2\theta = 18.3°$ and $20.5°$, referring to α and β phases.
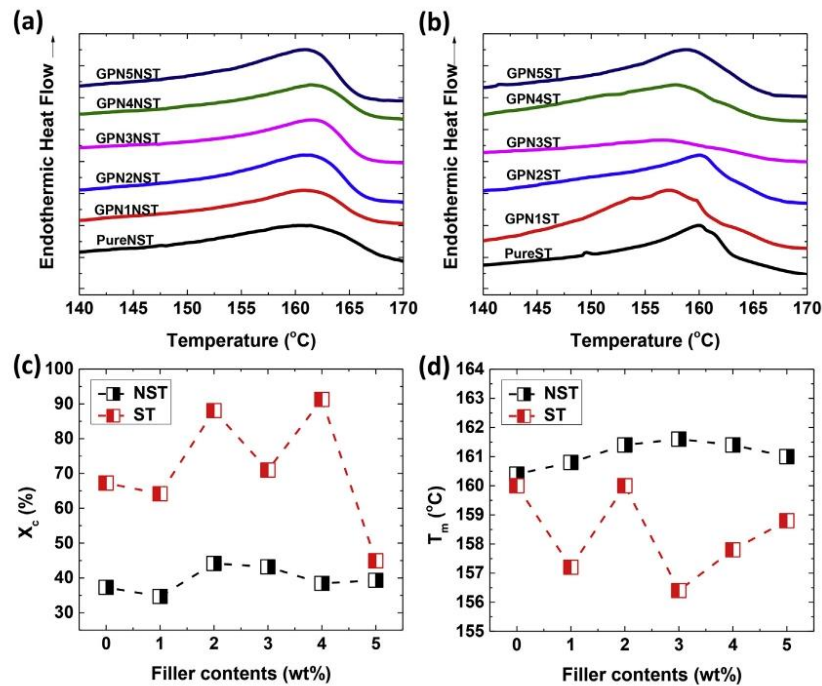
Fig. 3. DSC thermographs of (a) unstretched, and (b) stretched thin film composites, and dependence of (c) X_c, and (d) T_m on filler loading.

$$\sigma_{ac} = 2\pi f \varepsilon_0 \varepsilon_r \varepsilon_r^{''} \tag{4}$$

The ε_r at various frequencies is seen in Fig. 4(a)–(b) for unstretched and stretched cases with various filler contents. The orientational polarizability is represent by ε_r that generally decreases with frequency (Kasap, 2006). The dipoles could rapidly reorient following the alternating electric field at comparatively low

frequencies, giving the maximum ε_r. In contrast, when the electric field changes too rapidly at high frequencies, the dipoles could not follow it. As a result, the ε_r decreased with frequency. The interfacial polarization effects is explained by the Maxwell-Wagner-Sillars (MWS) theory (Tsangaris et al., 1998). The ε_r at high graphene loadings of 3–5 wt% was increased at any frequency, while the films with 1 or 2 wt% graphene produce lower ε_r than pure PVDF-HFP at

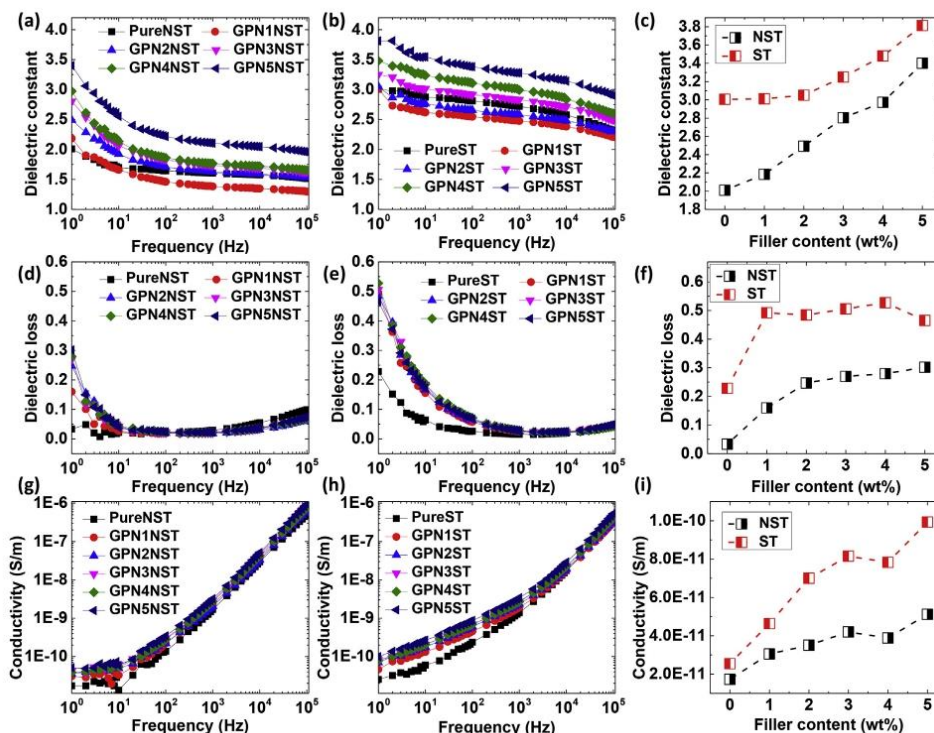**Fig. 4.** Dielectric properties of composite thin films with graphene filler in PVDF-HFP in unstretched and stretched cases. Dielectric constant against frequency for (a) unstretched films, and (b) stretched films, and (c) dielectric constant by filler loading at 1 Hz. (d)–(f) dielectric loss, (g)–(i) conductivity in similar plots.

high frequencies. The largest ε_r (at 1 Hz) is shown in Fig. 4(c). According to these results, the ε_r increased with graphene content, likely because of enhanced interfacial polarization and improved the orientational polarizability of graphene charge, seen in Fig. 4. Moreover, excessive filler still increased ε_r although X_c decreased. The ε_r increase with conductive filler (Huang et al., 2009; Paik et al., 2015) is explained by the logarithmic law for heterogeneous phases (Lichtenecker, 1931). In addition, the $\varepsilon_r^{''}$ in Fig. 4(d–f) represents the energy loss as dipoles are oriented in an alternating electric field (Kasap, 2006). The $\varepsilon_r^{''}$ is decreased with frequency. Commonly the dipoles at low frequencies with an applied electric field give a high ε_r and $\varepsilon_r^{''}$ as well, while these both decrease with frequency. In Fig. 4(f), the $\varepsilon_r^{''}$ is increased with graphene content because of the effects on interfacial polarization, or MWS effect. The σ_{ac} was measured as shown in Fig. 4(g–i). It relates to the number of charge carriers, or electron mobility and electrical resistance in the heterogeneous dielectric material, which dissipates energy from the electric field to the heat. The σ_{ac} is increased with frequency and with graphene content. The lowest and highest σ_{ac} were observed for pure PVDF-HFP and 5 wt% filled case, respectively. The increase in σ_{ac} with frequency can be explained by hopping space-charges between the phases. The space charge mechanism is described by the MWS model (Tsangaris et al., 1998). When conductive graphene filler was added in PVDF-HFP, it generated a second phase in this material, making the composite heterogeneous and increasing σ_{ac}. This also increased the $\varepsilon_r^{''}$ in a highly heterogeneous microstructure (Tsangaris et al., 1998). According to some prior studies (Ardimas

et al., 2018; Putson et al., 2012) adding a conductive filler into PU dielectric polymer increased the number of charge carries. In this current study, the 5 wt% loading, which produced the maximum σ_{ac}, was chosen for further experiments. In addition, stretching made a significant difference as seen in Fig. 4(e), (f), and (i). The stretched films have much larger ε_r, $\varepsilon_r^{''}$ and σ_{ac} than the unstretched films, caused by decreased crystallite size, improved the orientational polarizability of crystal domains (Tan et al., 2013), and increased overall X_c. As a result, the dielectric properties were improved.

The basic improvement of dielectric properties in both adding filler and stretching technique is crystallite size reduction. However, it seems that the majority influence of dielectric improvement on adding filler technique is conductive graphene loading.

3.3. Ferroelectric properties

The samples were measured for polarization and electric field measurements (P-E loop) using ferroelectric polarization loop and dielectric breakdown test system (PK-CPE1701, USA). The recoverable (U_e) and unrecoverable (U_l) energies are found from integrated areas of charge and discharge phases in Fig. 5. The energy storage efficiency of the materials can be evaluated from Equation (5). Remnant polarization (P_r, μC/cm^2) at 10 Hz frequency in 40 MV/m electric field was characterized using a Ferroelectric analyzer.

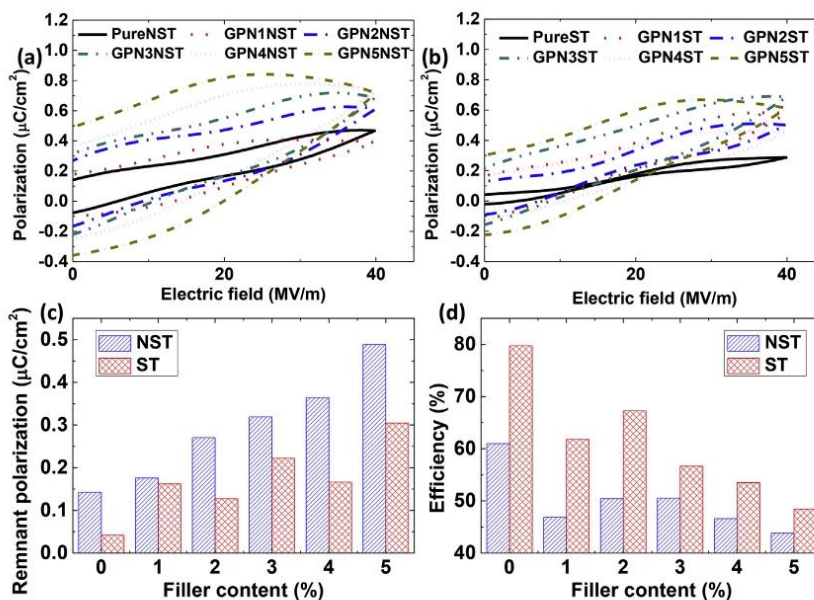$$Efficiency\ (\eta, \%) = U_e \times 100/(U_e + U_l) \tag{5}$$

Fig. 5. P—E loops (a) unstretched, and (b) stretched ferroelectric material composites with various filler contents. (c) Remnant polarization, and (d) efficiency.

Ferroelectric properties by filler loading. When the electric field is sufficiently high as 40 MV/m, P-E loops were occurred. P-E loops with various filler contents were showed by Fig. 5(a–b). The loops seem to be antiferroelectric being slim (Yang et al., 2013). Obviously the loop size changed to be bigger loop with graphene content, corresponding to give larger P_r as Fig. 5(c), give lesser U_e than U_l, and steadily produce low energy storage efficiency, η, as seen in Fig. 5(d). On the adding filler technique in PVDF-HFP ferroelectric polymer, the conductive graphene filler is seemly majority influences while the crystallite size reduction on adding filler is the minority influences, resulting bigger loop from conductive filler instead of from crystallite size reduction. This reason is matched with the explanation of dielectric properties above. The disconnected initial-final P-E loop points were larger with graphene content. For example, at under zero external electric field (E = 0), the initial-final polarization is more disconnected because of the larger U_l from conductive graphene loading.

Ferroelectric properties of stretched samples. Comparing unstretched and stretched cases shows clear differences. The loops are totally seemed to be slimmer after stretching, correspond to smaller P_r, resulting greater U_e than U_l, and steadily produce high energy storage efficiency, η. On the stretching technique in PVDF-HFP ferroelectric polymer, the crystallite size reduction is seemly being main influences, resulting a narrower loop from crystallite size reduction. It was possible to describe that the crystallite size reduction is easy to switch the orientation polarization along the direction of the external electric field. It is causing the slimmer loops with enhanced relaxation speed of crystal grains, which is also corroborated by previous studies (He et al., 2016; Tan et al., 2013). This reason is matched with the explanation of dielectric properties above.

Basic improvement of slimmer ferroelectric loop in both adding filler and stretching technique is because of crystallite size reduction. However, it seems that the majority influence of bigger

ferroelectric loop on adding filler technique is the conductive graphene loading.

3.4. Electrocaloric properties

The P-E loops for each sample were recorded at temperatures from 30 to 140 °C in a controlled oven, to record P_r at 1 °C intervals. The slope at each point was calculated to obtain the adiabatic temperature change (ΔT) from Maxwell relations, according to Equations (6) and (7), where ΔS, P, T, ρ, C_E, and E are entropy change, polarization, temperature, density, specific heat capacity of PVDF-HFP (1600 J/kg/°C) and the electric field, respectively.

$$\Delta S = \int_{E_1}^{E_2} \left(\frac{\partial P}{\partial T} \right) dE \qquad (6)$$

$$\Delta T = -\frac{1}{\rho C_E} \int_{E_1}^{E_2} T \left(\frac{\partial P}{\partial T} \right) dE \qquad (7)$$

The loops became gradually larger with temperature as shown in supplementary material Fig. S1(a-b). The P_r then rapidly increased around 120 °C matching the T_c reported in a previous paper (Thetpraphi et al., 2015). Possibly, these samples show T_c from an anti-ferroelectric phase to normal loops of ferroelectric phase (Yang et al., 2013) resulting negative electrocaloric. The maximum ΔT (ΔT$_{max}$) is typically at T_c following Equations (6) and (7).

Electrocaloric properties by filler loading. Fig. 6(a-b) presents the relationship between ΔT and temperature with various filler contents. ΔT seems to be negatively electrocaloric effect. Practically, a negative ΔT$_{max}$ directly intensified with graphene content at 1 wt%
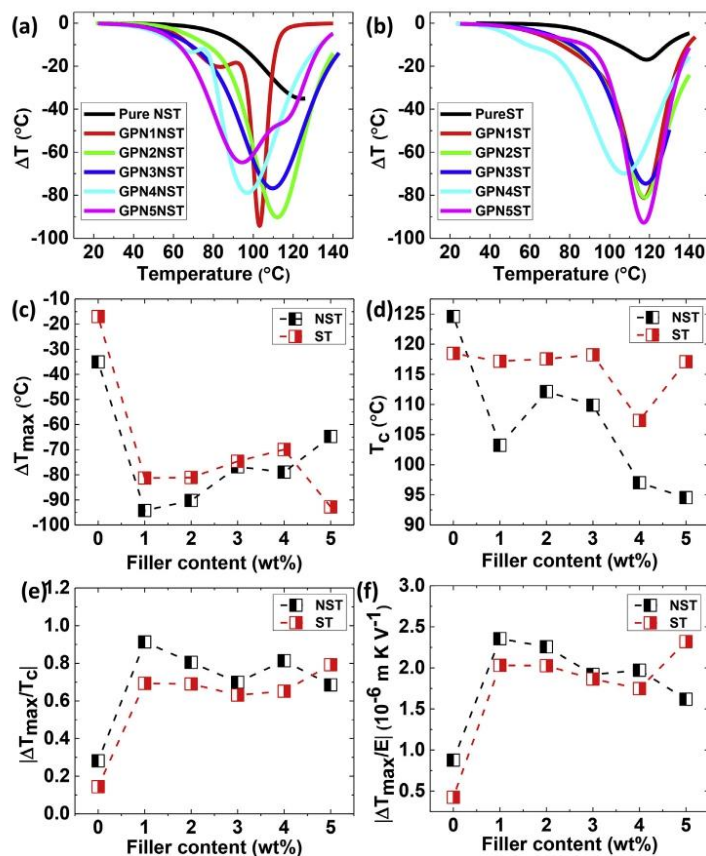
Fig. 6. Electrocaloric behavior with various graphene contents, (a)–(b) the negative ΔT of unstretched and stretched cases at various temperatures, (c) ΔT_{max}, (d) T_c, (e) $|\Delta T_{max}/T_c|$, and (f) $|\Delta T_{max}/E|$.

from -26 to $-88\ °C$ approximately and then slightly decreased to around $-76\ °C$ at 3 wt%, as seen in Fig. 6(c). The graphene fixed polymer chain to get a large net of dipole moment and made them easily following external E (free dipolar orientational polarizability). Consequently, they intensify negative ΔT_{max}. The T_c decreased with graphene content in Fig. 6(d), because graphene particle might able to slightly change anti-ferroelectric phase in PVDF-HFP to ferroelectric phase, in relation with a prior study (Zouari et al., 2018). Hence, T_c could be easily shifted at a lower temperature with increasing graphene content.

Electrocaloric properties of stretched cases. The unstretched and stretched cases differed in properties. Stretching was clearly effective in stabilizing T_c because of uniformity of dipolar orientational of polarizability that reducing the crystallite size and increasing the X_c. For example, the curves were smooth for 2, 4, and 5 wt% cases. The samples that producing maximum σ_{ac} that is larger than GPN5ST as Fig. 4(h), are unable to be measured because of easy to breakdown at high E (Chu et al., 2006). However, the negative ΔT_{max} reduced with stretching technique because of increased overall X_c for other filler contents, except 5 wt% as seen in

Fig. 6(c). The sample with 5 wt% graphene suddenly dropped overall X_c as in Fig. 3(c), giving a large negative ΔT_{max}. On the other hand, stretching slightly increased T_c because of larger overall X_c that hardly followed by E especially at the phase transition. Whereas, the unstretched cases had rapidly decreasing T_c in Fig. 6(d). The maximum of both absolute $|\Delta T_{max}/T_c|$ and $|\Delta T_{max}/E|$ were obtained especially with 1 wt% for both types of samples before the gradual decrease in Fig. 6(e)–(f). Excessive filler at 5 wt% with stretching eventually caused an improvement. For unstretched cases, less X_c had mostly better electrocaloric properties than the stretched cases. GPN1NST composites gave a large absolute $|\Delta T_{max}/E|$ value of about $2.36 \times 10^{-6}\ m\ K\ V^{-1}$, which is larger than that of ferroelectric ceramic $PbZr_{0.95}Ti_{0.05}O_3$ thin-film ($0.25 \times 10^{-6}\ m\ K\ V^{-1}$) (Mischenko et al., 2006). However, L. Yang and colleagues (Yang et al., 2016) have reported the T_c of PVDF/graphene composite that is lesser than reported on this current study.

The improvement of electrocaloric properties in adding filler technique is mainly depended on the suitable of a few graphene loading as 1 wt% before it is gradually reducing with graphene

content. Too much graphene content will reduce ΔT_{max} and T_c, corresponding to decrease $|\Delta T_{max}/T_c|$ as well as $|\Delta T_{max}/E|$. It seems that the majority influence of electrocaloric improvement on stretching technique is caused by X_c reduction. The crystallite size reduction possibly has less influence on electrocaloric properties, resulting in no significant relation in both adding filler and stretching techniques.

4. Conclusion

Composite thin films of PVDF-HFP with various graphene filler contents (0-5 wt%) were fabricated by solution casting technique. The comparison of adding filler and stretching technique were considered. Well dispersed graphene in PVDF-HFP thin films were observed. Stretching induced crysrtallinity and made the film translucent. The crystalline enlargement was observed by DSC analysis. Adding filler to $2-3$ wt% produced the maximum crystallinity before gradually decreased around 5 wt% due to excessive filler loading; while, stretching technique dramatically increased crystallinity. Both adding filler and stretching technique also induced crystallite size reduction as well. It resulting in great dielectric constant, dielectric loss, and conductivity. In stretching technique, smaller crystallite size produces slimmer ferroelectric loop, corresponding to lesser remnant polarization, smaller unrecoverable energy and larger recoverable energy and energy storage efficiency. The main influence on adding filler case is conductive graphene loading rather than crystallite size reduction that resulting in bigger ferroelectric loop, larger remnant polarization, higher unrecoverable energy and smaller recoverable energy and energy storage efficiency. The antiferroelectric was observed, giving maximum negative ΔT at T_c 120 °C. On the adding filler case, negative ΔT_{max} was intensified as well as T_c reduction to a lower temperature by 20 °C before electrocaloric properties as $|\Delta T_{max}/T_c|$ gradually decreased with graphene content due to agglomeration. For stretching technique, the electrocaloric properties are reduced with crystalline enlargement although the stretching technique could stabilize T_c to a smooth curve. Adding filler cases is attractive for dielectric and electrocaloric improvement but undesirable for ferroelectric properties; while, the stretching technique is attractive for improving dielectric and ferroelectric properties, but undesirable for electrocaloric properties. Those two techniques facilitate for their adoption in advanced capacitor and electrocaloric refrigerators with suitable energy storage efficiency in the future.

Declaration of competing interest

The authors declare that they have no known competing financial interests or personal relationships that could have appeared to influence the work reported in this paper.

Acknowledgements

Appendix A. Supplementary data

Supplementary data to this article can be found online at https://doi.org/10.1016/j.clepro.2019.119730.

References

Ardimas, Putson, C., Muensit, N., 2018. High electromechanical performance of modified electrostrictive polyurethane three-phase composites. Compos. Sci. Technol. 158, 164–174. https://doi.org/10.1016/j.compscitech.2018.02.012.

Bahiraei, M., Heshmatian, S., 2019. Graphene family nanofluids: a critical review and future research directions. Energy Convers. Manag. 196, 1222–1256. https://doi.org/10.1016/j.enconman.2019.06.076.

Bahiraei, M., Mazaheri, N., 2018. Application of a novel hybrid nanofluid containing graphene–platinum nanoparticles in a chaotic twisted geometry for utilization in miniature devices: thermal and energy efficiency considerations. Int. J. Mech. Sci. 138–139, 337–349. https://doi.org/10.1016/j.ijmecsci.2018.02.030.

Bahiraei, M., Mazaheri, N., Rizehvandi, A., 2019. Application of a hybrid nanofluid containing graphene nanoplatelet–platinum composite powder in a triple-tube heat exchanger equipped with inserted ribs. Appl. Therm. Eng. 149, 588–601. https://doi.org/10.1016/j.applthermaleng.2018.12.072.

Bai, Y., Ding, K., Zheng, G.-P., Shi, S.-Q., Qiao, L., 2012. Entropy-change measurement of electrocaloric effect of BaTiO$_3$ single crystal. Phys. Status Solidi A 209 (5), 941–944. https://doi.org/10.1002/pssa.201127695.

Bauer, F., 2010. Relaxor fluorinated polymers: novel applications and recent developments. IEEE Trans. Dielectr. Electr. Insul. 17 (4), 1106–1112. https://doi.org/10.1109/TDEI.2010.5539681.

Chen, C., Liang, R., Liu, Z., Yan, S., Nie, X., Zhou, Z., Dong, X., 2017. Coexistence of negative and positive electrocaloric effect in Sr and Nb co-doped Pb(Zr,Ti)O$_3$ ferroelectric ceramics. Mater. Lett. 189, 303–306. https://doi.org/10.1016/j.matlet.2016.11.006.

Choolaei, M., Goodarzi, V., Khonakdar, H.A., Jafari, S.H., Seyfi, J., Saeb, M.R., Häußler, L., Boldt, R., 2017. Influence of graphene Oxide on crystallization behavior and chain folding surface free energy of poly(vinylidenefluoride-co-hexafluoropropylene). Macromol. Chem. Phys. 218 (19), 1700103 https://doi.org/10.1002/macp.201700103.

Chu, B., Zhou, X., Ren, K., Neese, B., Lin, M., Wang, Q., Bauer, F., Zhang, Q.M., 2006. A dielectric polymer with high electric energy density and fast discharge speed. Science 313 (5785), 334–336. https://doi.org/10.1126/science.1127798.

Fatou, J.G., 1971. Melting temperature and enthalpy of isotactic polypropylene. Eur. Polym. J. 7 (8), 1057–1064. https://doi.org/10.1016/0014-3057(71)90138-8.

Goodarzi, V., Kokabi, M., Razzaghi Kashani, M., Reza Bahramian, A., 2014. Prediction of long-term mechanical properties of PVDF/BaTiO$_3$ nanocomposite. J. Appl. Polym. Sci. 131 (16) https://doi.org/10.1002/app.40596.

Goupil, F.L., Berenov, A., Axelsson, A.-K., Valant, M., Alford, N.M., 2012. Direct and indirect electrocaloric measurements on ⟨001⟩-PbMg$_{1/3}$Nb$_{2/3}$O$_3$-30PbTiO$_3$ single crystals. J. Appl. Phys. 111 (12), 124109 https://doi.org/10.1063/1.4730338.

He, F.-A., Lin, K., Shi, D.-L., Wu, H.-J., Huang, H.-K., Chen, J.-J., Chen, F., Lam, K.-H., 2016. Preparation of organosilicate/PVDF composites with enhanced piezoelectricity and pyroelectricity by stretching. Compos. Sci. Technol. 137, 138–147. https://doi.org/10.1016/j.compscitech.2016.10.031.

He, X.J., Yao, K., Gan, B.K., 2005. Phase transition and properties of a ferroelectric poly(vinylidene fluoride-hexafluoropropylene) copolymer. J. Appl. Phys. 97 (8), 084101 https://doi.org/10.1063/1.1862323.

He, Z., Cao, Q., Jing, B., Wang, X., Deng, Y., 2017. Gel electrolytes based on poly(vinylidenefluoride-co-hexafluoropropylene)/thermoplastic polyurethane/poly(methyl methacrylate) with in situ SiO$_2$ for polymer lithium batteries. RSC Adv. 7 (6), 3240–3248. https://doi.org/10.1039/C6RA25062A.

Huan, Y., Liu, Y., Yang, Y., 2007. Simultaneous stretching and static electric field poling of poly(vinylidene fluoride-hexafluoropropylene) copolymer films. Polym. Eng. Sci. 47 (10), 1630–1633. https://doi.org/10.1002/pen.20843.

Huang, X.Y., Jiang, P.K., Xie, L.Y., 2009. Ferroelectric polymer/silver nanocomposites with high dielectric constant and high thermal conductivity. Appl. Phys. Lett. 95 (24), 242901 https://doi.org/10.1063/1.3273368.

Jiang, X., Luo, L., Wang, B., Li, W., Chen, H., 2014. Electrocaloric effect based on the depolarization transition in (1−x)Bi$_{0.5}$Na$_{0.5}$TiO$_3$–xKNbO$_3$ lead-free ceramics. Ceram. Int. 40 (2), 2627–2634. https://doi.org/10.1016/j.ceramint.2013.10.066.

Kasap, S.O., 2006. Principles of Electronic Materials and Devices. McGraw-Hill, New York.

Li, J., Khanchaitit, P., Han, K., Wang, Q., 2010. New route toward high-energy-density nanocomposites based on chain-end functionalized ferroelectric polymers. Chem. Mater. 22 (18), 5350–5357. https://doi.org/10.1021/cm101614p.

Li, J., Seok, S.I., Chu, B., Dogan, F., Zhang, Q., Wang, Q., 2009. Nanocomposites of ferroelectric polymers with TiO$_2$ nanoparticles exhibiting significantly enhanced electrical energy density. Adv. Mater. 21 (2), 217–221. https://doi.org/10.1002/adma.200801106.

Lichtenecker, K., 1931. Die Herleitung des logarithmischen Mischungsgesetzes aus allgemeinen Prinzipien der Stationaren Stromung. Phys. Z. 32, 255–260.

Lines, M.E., Glass, A.M., 1977. Principles and Applications of Ferroelectrics and Related Materials. Oxford university press.

Lu, S.G., Zhang, Q.M., Kutnjak, Z., 2011. 15 - the electrocaloric effect (ECE) in ferroelectric polymer films. In: Cao, Z. (Ed.), Thin Film Growth. Woodhead Publishing, pp. 364–383.

Mischenko, A., Zhang, Q., Scott, J., Whatmore, R., Mathur, N., 2006. Giant electrocaloric effect in thin-film PbZr$_{0.95}$Ti$_{0.05}$O$_3$. Science 311 (5765), 1270–1271. https://doi.org/10.1126/science.1123811.

Neese, B., Chu, B., Lu, S.-G., Wang, Y., Furman, E., Zhang, Q.M., 2008. Large electrocaloric effect in ferroelectric polymers near room temperature. Science 321 (5890), 821–823. https://doi.org/10.1126/science.1159655.

Neese, B., Wang, Y., Chu, B., Ren, K., Liu, S., Zhang, Q.M., Huang, C., West, J., 2007. Piezoelectric responses in poly(vinylidene fluoride/hexafluoropropylene) co-polymers. Appl. Phys. Lett. 90 (24), 242917 https://doi.org/10.1063/1.2748076.

Paik, H., Choi, Y.Y., Hong, S., No, K., 2015. Effect of Ag nanoparticle concentration on the electrical and ferroelectric properties of Ag/P(VDF-TrFE) composite films. Sci. Rep. 5, 13209 https://doi.org/10.1038/srep13209.

Pakhomov, O.V., Karmanenko, S.F., Semenov, A.A., Starkov, A.S., Es'kov, A.V., 2010. Thermodynamic estimation of cooling efficiency using an electrocaloric solid-state line. Tech. Phys. 55 (8), 1155–1160. https://doi.org/10.1134/S106378421008013x.

Parangusan, H., Ponnamma, D., Al-Maadeed, M.A.A., 2018a. Stretchable electrospun PVDF-HFP/Co-ZnO nanofibers as piezoelectric nanogenerators. Sci. Rep. 8 (1), 754. https://doi.org/10.1038/s41598-017-19082-3.

Parangusan, H., Ponnamma, D., AlMaadeed, M.A.A., 2018b. Investigation on the effect of γ-irradiation on the dielectric and piezoelectric properties of stretch-able PVDF/Fe–ZnO nanocomposites for self-powering devices. Soft Matter 14 (43), 8803–8813. https://doi.org/10.1039/C8SM01655K.

Patro, T.U., Mhalgi, M.V., Khakhar, D.V., Misra, A., 2008. Studies on poly(vinylidene fluoride)–clay nanocomposites: effect of different clay modifiers. Polymer 49 (16), 3486–3499. https://doi.org/10.1016/j.polymer.2008.05.034.

Putson, C., Jaaoh, D., Meauma, N., Muensit, N., 2012. Effect of micro- and nano-particle fillers at low percolation threshold on the dielectric and mechanical properties of polyurethane/copper composites. J. Inorg. Organomet. Polym. Mater. 22 (6), 1300–1307. https://doi.org/10.1007/s10904-012-9755-z.

Salimi, A., Yousefi, A.A., 2003. Analysis Method: FTIR studies of β-phase crystal formation in stretched PVDF films. Polym. Test. 22 (6), 699–704. https://doi.org/10.1016/S0142-9418(03)00003-5.

Scherrer, P., 1918. Bestimmung der Größe und der inneren Struktur von Kolloid-teilchen mittels Röntgenstrahlen. Nachr. Ges. Wiss. Goettingen Math. Phys. Kl. 1918, 98–100.

Scott, J.F., 2011. Electrocaloric materials. Annu. Rev. Mater. Res. 41 (1), 229–240. https://doi.org/10.1146/annurev-matsci-062910-100341.

Sencadas, V., Lanceros-Méndez, S., Mano, J.F., 2004. Characterization of poled and non-poled β-PVDF films using thermal analysis techniques. Thermochim. Acta 424 (1), 201–207. https://doi.org/10.1016/j.tca.2004.06.006.

Shojaei, L., Goodarzi, V., Otadi, M., Khonakdar, H.A., Jafari, S.H., Asghari, G.h., Reuter, U., 2018. Temperature and frequency-dependent creep and recovery studies on PVDF-HFP/organo-modified layered double hydroxides nano-composites. J. Appl. Polym. Sci. 135 (23), 46352 https://doi.org/10.1002/app.46352.

Sukwisute, P., Muensit, N., Soontaranon, S., Rugmai, S., 2013. Micropower energy harvesting using poly(vinylidene fluoride hexafluoropropylene). Appl. Phys. Lett. 103 (6), 063905 https://doi.org/10.1063/1.4818339.

Tan, S., Hu, X., Ding, S., Zhang, Z., Li, H., Yang, L., 2013. Significantly improving dielectric and energy storage properties via uniaxially stretching crosslinked

P(VDF-co-TrFE) films. J. Mater. Chem. 1 (35), 10353–10361. https://doi.org/10.1039/C3TA11484H.

Thakur, P., Kool, A., Bagchi, B., Hoque, N.A., Das, S., Nandy, P., 2015. The role of cerium(iii)/yttrium(iii) nitrate hexahydrate salts on electroactive β phase nucleation and dielectric properties of poly(vinylidene fluoride) thin films. RSC Adv. 5 (36), 28487–28496. https://doi.org/10.1039/C5RA03524D.

Thetpraphi, K., Putson, C., Muensit, N., 2015. Dependence of mechanical and dielectric properties on temperature of poly(vinylidene fluoride-hexa-fluoropropylene). Appl. Mech. Mater. 749, 129–133. https://doi.org/10.4028/www.scientific.net/AMM.749.129.

Tohluebaji, N., Putson, C., Muensit, N., 2019. High electromechanical deformation based on structural beta-phase content and electrostrictive properties of elec-trospun poly(vinylidene fluoride- hexafluoropropylene) nanofibers. Polymers 11 (11), 1817. https://doi.org/10.3390/polym11111817.

Tsangaris, G.M., Psarras, G.C., Kouloumbi, N., 1998. Electric modulus and interfacial polarization in composite polymeric systems. J. Mater. Sci. 33 (8), 2027–2037. https://doi.org/10.1023/a:1004398514901.

Yang, L., Li, X., Allahyarov, E., Taylor, P.L., Zhang, Q.M., Zhu, L., 2013. Novel polymer ferroelectric behavior via crystal isomorphism and the nanoconfinement effect. Polymer 54 (7), 1709–1728. https://doi.org/10.1016/j.polymer.2013.01.035.

Yang, L., Qian, X., Koo, C., Hou, Y., Zhang, T., Zhou, Y., Lin, M., Qiu, J.-H., Zhang, Q.M., 2016. Graphene enabled percolative nanocomposites with large electrocaloric efficient under low electric fields over a broad temperature range. Nano Energy 22, 461–467. https://doi.org/10.1016/j.nanoen.2016.02.026.

Zhang, Q.M., Bharti, V., Zhao, X., 1998. Giant electrostriction and relaxor ferroelectric behavior in electron-irradiated poly(vinylidene fluoride-trifluoroethylene) copolymer. Science 280 (5372), 2101. https://doi.org/10.1126/science.280.5372.2101.

Zhao, C., Guo, M., Lu, Y., Wang, Q., 2009. Ferroelectric poly(vinylidene fluoride-trifluoroethylene-chlorotrifluoroethylene)s: effect of molecular weight on dielectric property. Macromol. Symp. 279 (1), 52–58. https://doi.org/10.1002/masy.200950508.

Zhuo, F., Li, Q., Gao, J., Ji, Y., Yan, Q., Zhang, Y., Wu, H.-H., Xi, X.-Q., Chu, X., Cao, W., 2018. Giant negative electrocaloric effect in (Pb,La)(Zr,Sn,Ti)O₃ antiferroelectrics near room temperature. ACS Appl. Mater. Interfaces 10 (14), 11747–11755. https://doi.org/10.1021/acsami.8b00744.

Zhuo, F., Li, Q., Gao, J., Yan, Q., Zhang, Y., Xi, X., Chu, X., 2017. Phase transformations, anisotropic pyroelectric energy harvesting and electrocaloric properties of (Pb,La)(Zr,Sn,Ti)O₃ single crystals. Phys. Chem. Chem. Phys. 19 (21), 13534–13546. https://doi.org/10.1039/C7CP01762F.

Zouari, I., Sassi, Z., Seveyrat, L., Abdelmoula, N., Lebrun, L., Khemakhem, H., 2018. Structural, dielectric, piezoelectric, ferroelectric and electro-caloric properties of Ba₁₋ₓCaₓTi₀.₉₇₅(Nb₀.₅Yb₀.₅)₀.₀₂₅O₃ lead-free ceramics. Ceram. Int. 44 (7), 8018–8025. https://doi.org/10.1016/j.ceramint.2018.01.242.

Paper II (Published)

Electron beam irradiation for boosting storage energy density of tuned poly(vinylidene fluoride-hexafluoropropylene)/graphene nanoplatelet polymer composites

Ardian Agus Permana, Somyot Chirasatitsin and Chatchai Putson

crystals

MDPI

Article

Electron-Beam Irradiation for Boosting Storage Energy Density of Tuned Poly(vinylidene fluoride-hexafluoropropylene)/Graphene Nanoplatelet Polymer Composites

Ardian Agus Permana [1], Somyot Chirasatitsin [2] and Chatchai Putson [1,*]

[1] Department of Physics, Faculty of Science, Prince of Songkla University (PSU), Hat Yai, Songkhla 90112, Thailand; ardianaguspermana@gmail.com

[2] Institute of Biomedical Engineering, Faculty of Medicine, Prince of Songkla University (PSU), Hat Yai, Songkhla 90110, Thailand; somjot.c@psu.ac.th

* Correspondence: chatchai.p@psu.ac.th

check for updates

Abstract: In current, the energy storage materials based on electrets and ferroelectric polymers are urgently demanded for electric power supply and renewable energy applications. The high energy storage density can be enhanced by conducting or inorganic fillers to ferroelectric polymer matrix. However, agglomeration, phase separation of fillers, interfacial phase regions and crystallinity of matrix remain the main factors for the improvement of energy storage density in those composites. Poly(vinylidene fluoride-hexafluoropropylene) was modified with graphene nanoplatelets for enhanced the dielectric properties and energy storage density, which combines the irradiated by electron beam. Tuning effect of the crystalline regions and polar phases with graphene nanoplatelets and electron irradiation on its surface, structure, electrical and energy storage properties were observed. The film homogeneity was increased by reducing the pores, along with the improvement of surface roughness and hydrophobicity, which related with the dielectric properties and energy storage density. The β-phase fraction and crystallinity improvement significantly affect electrical properties by improving polarization and dielectric constant. As a core, electron beam dramatically reduce the crystals size by two times. Hence, energy storage density of composites was enhanced, while energy loss was reduced under operating conditions. Results on the improvement of energy efficiency were from 68.11 to 74.66% for neat poly(vinylidene fluoride-hexafluoropropylene) (P(VDF-HFP)), much higher than previously reported of 58%, and doubled for P(VDF-HFP)/GNPs composites which will be discussed and evaluated for the practical energy storage materials.

Keywords: electrical properties; storage energy density; poly(vinylidene fluoride-hexafluoropropylene); graphene nanoplatelet; electron-beam irradiation

---

1. Introduction

The demand for energy storage components such as capacitors and batteries for electric power supply and renewable energy applications is growing drastically [1]. Finding effective ways of improving the energy efficiency of these components is becoming a focus of attention [2]. When produced on a large-scale, especially for miniaturized devices, they need to combine high power output, storage energy density and efficiency with low energy loss in a compact, durable, inexpensive and lightweight form. Moreover, other properties that relate to their surface characteristics, such as self-cleaning, are also important [3].

In general, dielectric materials have high power density which accommodates fast charging and discharging process [4]. Nevertheless, their application in energy storage components is limited by their low energy density. For instance, biaxially oriented polypropylene (BOPP), the polymer most often used in capacitors, has a high breakdown strength (7500 kV/cm) [5] and a low dielectric loss at 1 kHz (0.0002), but a low energy density and therefore poor energy efficiency [6]. The low energy density of BOPP is associated with its low dielectric constant. In contrast, the relatively high dielectric constant and breakdown strength of polyvinylidene fluoride (PVDF) and its copolymers and terpolymers are excellent electroactive properties for energy storage components [7], but, despite being considered superior to other dielectric ferroelectric materials, PVDF-based materials have a relatively high dielectric loss and high energy loss, which limits their applications. A brief summary of the electrical properties of some various polymers was presented by Table 1.

Table 1. The electrical properties comparison of different various polymers.

Polymer Materials	Breakdown Strength (kV/cm)	Dielectric Loss (1 kHz)	Storage Energy Density (J/cm^3)	Energy Efficiency (%)	References
Polyvinyl chloride (PVC)	400	0.018			[6]
PMMA	2500	0.05	1.5 (at ~3300 kV/cm)		[8–10]
BOPP	7500	0.0002	3 (at 5000 kV/cm)		[5]
High-density polyethylene (HDPE)	222.9	0.0002–0.0007			[6,10]
PVDF	1500–5000	0.04	2.8 (at 4500 kV/cm)		[6,11]
PVDF (alpha)	4000	0.025	4 (at 3000 kV/cm)	30.2	[12]
PVDF (beta)	2000		1.5 (at 1500 kV/cm)	75	[12]
PVDF (gamma)	5000	0.025	14	59.57	[12]
P(VDF-HFP) (96/4 mol %)	6000	0.4	12.5	58	[13]
P(VDF-TrFE) (50/50 mol %)	1621	<0.1	1.13 (at 1300 kV/cm)		[14,15]
Irradiated P(VDF-TrFE) (50/50 mol %) @80-Mrad		0.06			[15]
Polyvinyl alcohol	1000	0.3			[16]
Polyurethane	200	0.02			[6]
Epoxy	250–450	0.015			[6,10]

These examples illustrate two key aspects for achieving higher energy efficiency: improving the dielectric constant and simultaneously lowering its loss. The following approaches to improve the dielectric constant of materials have been reported: poling, or high voltage polarization [17], adding nanofillers [18], electrospinning [19] and mechanical stretching [20]. However, the vital factors on which they have all focused are microstructural changes in crystallinity and crystal phase transition from the most stable α-phase to the most electroactive polar β-phase. Among the three modes of molecular conformation denoted as TTTT, T$_3$GT$_3$G′ and TGTG′ and the five crystalline phases known as the α-, ε-, δ-, γ- and β-phase in PVDF [20], the α- and ε–phase are the most stable due to the anti-parallel alignment of their dipole moments. The most electrically active phase is the polar all trans-TTTT zigzag β-phase, which has a high polarization per unit cell of 8 × 10–30 C·m [18].

Whereas most recent studies have only focused on one approach to improving the electroactive properties of materials, this paper presents the combined use of two relatively untypical approaches: adding a nanofiller and electron-beam irradiation. In the first approach, graphene nanoplatelets (GNPs) were used as the nanofiller. It was chosen due to its benefit to apply in wide area. For the example, the work related to GNPs on modifying electrocaloric effect for the cooling system is currently reported by our prior work [21]. For the other applications, their unique characteristics make them one of the most promising candidates for nanocomposite storage, batteries and supercapacitors [1]. Compared with carbon nanotubes, carbon fibers, pure graphene and other carbon-based materials, GNPs are more suitable for low-cost mass production [22]. The positive charge of the carbon in GNPs will interact with the negative charge of the fluorine in the poly(vinylidene fluoride-hexafluoropropylene) (P(VDF-HFP)) matrix. The polar β-phase once constructed, should improve polarization and the dielectric constant [23].

The obtained ferroelectric material, while having huge domains of spontaneously aligned dipoles, exhibited a relatively large hysteresis loop, which described its energy loss. Reducing energy loss was, therefore, an important objective. Electron-beam irradiation was employed to achieve it since it was reported to be effective at reducing dielectric loss by breaking large domains into smaller ones [24] and micron-sized ferroelectric domains had been previously created by both positive and negative charges [25]. Interestingly, electron-beam irradiation was effectively carried out by the electron probe [26] of a conventional scanning electron microscope (SEM) and had the benefits of control over the position and focus of the electron-beam and lower hydrocarbon contamination of materials during low-energy irradiation.

This work reports the effects of GNP nanofillers and electron-beam irradiation on poly(vinylidene fluoride-hexafluoropropylene) (P(VDF-HFP)), a relative low-cost material that demonstrated outstanding breakdown strength, allowing it to generate an energy efficiency of 58% [13], compared to 30.2% for PVDF [12]. In addition to modified energy and electrical properties, this study also observed changes in micro-domains, which affected parameters such as surface roughness, microstructure and hydrophobicity of the material. These changes can be important since certain surface parameters, such as hydrophobicity, bring benefits to smart material applications in terms of their anti-sticking and self-cleaning abilities [3]. Even though these surface properties are not directly related to energy efficiency, they are characteristics that support the potential application of P(VDF-HFP) in smart electronic devices.

2. Materials and Methods

2.1. Materials

Solef 11010/1001P(VDF-HFP) copolymer powders were from Solvay Solexis, Brussels, Belgium. *N,N*-Dimethylformamide (≥99% purity DMF solvent) was from RCI Labscan, Bangkok, Thailand. 306633-25G GNP powder was from Sigma Aldrich, St. Louis, MO, USA.

2.2. Film Preparation Method

Neat P(VDF-HFP) and P(VDF-HFP)/GNP composite, referred to as HFP/GN, were investigated in this study. All samples were produced by the solution casting method. Neat P(VDF-HFP) thin film was fabricated by mixing P(VDF-HFP) powder with 10% of HFP monomer and DMF solvent at room temperature for 16 h using a magnetic stirrer. The copolymer concentration in the solution was 20 wt% with the ratio between copolymer and solvent was 1:4. The solution was then rested for 1 h to allow the dispersion of bubbles. Next, glass plates were prepared and the solution was cast on them using a blade of the desired thickness. The cast solution was then dried in an oven for 12 h at 80 °C. The final thickness of all samples was controlled to a tolerance of 30 ± 5 μm. In the preparation of HFP/GN composite films, GNP powder was first dispersed in DMF using a sonicator for 20 min before being mixed with P(VDF-HFP) powder and stirred for 16 h. HFP/GN films were then prepared as described above. The GNP nanofiller powder loading was varied at 1, 2, 3, 4 and 5% by weight. These films were denoted HFP/GN1, HFP/GN2, HFP/GN3, HFP/GN4 and HFP/GN5, respectively.

2.3. Electron-Beam Irradiation

The surfaces of all samples were irradiated by an electron beam using an SEM (HITACHI TM3030Plus, Tokyo, Japan) at an acceleration voltage AV of 15 kV. The 15 keV energy of electron beam was emitted to the irradiation areas of 3 mm × 4 mm of the samples. The exposition time was fixed for all condition at 300 s. The electron beam current of 42.5 μA could generate the electron charge dose by 106.25×10^3 μC/cm^2 which emitted to the thin films in a vacuum chamber.

2.4. Characterization

Atomic force microscopy (AFM) measurements were carried out with an Easyscan 2 (Nanosurf AG, Liestal, Switzerland) operated in dynamic force mode to characterize the interfacial morphology and the surface area topography of the samples. The water contact angle was determined using a contact angle device, model OCA 15EC (Dataphysics, Filderstadt, Germany). Measurements were taken using an input power of 55 W, 12 V DC voltage and a 6.3 AT fuse with the liquid volume controlled at 2 μL. Morphological structure and dispersion were observed with an SEM (TM3030Plus, Hitachi, Germany) using various magnifications.

The phase of crystalline materials was determined by X-ray diffractometry (XRD) (Empyrean, PANalytical, The Netherlands). Samples were scanned over range (2θ) of 5 to 90° using a 0.154 nm (CuKα) wavelength with a speed of 0.04° s^{-1} in the Cu tube at 30 mA and 40 kV. Structural aspects of functional groups were identified by Fourier transform infrared spectrometry (FTIR VERTEX 70, Bruker, Germany). Spectra were recorded from 4000 to 400 cm^{-1} in attenuated total reflectance (ATR) mode.

Thermal behavior was characterized by differential scanning calorimetry (DSC 7, Perkin Elmer, Waltham, USA). Measurements were conducted on 1–3 mg of thin film from 20 to 200 °C. The heating rate was controplled at 10 °C min^{-1} in a nitrogen atmosphere. The value of the melting enthalpy (ΔH_m) was generated from the area of the peak, while the maximum endothermic peak was associated with the melting temperature (T_m). Crystallinity (X_c) was calculated based on the equation:

$$X_c = \Delta H_m / ((1-\phi)\, \Delta H_{100\%}) \times 100 \tag{1}$$

where ΔH_m and $\Delta H_{100\%}$ denote the measured melting enthalpy and fusion enthalpy of 100% P(VDF-HFP) crystals, 104.6 J g^{-1}, respectively, while ϕ refers to the mass fraction of the fillers in the matrix [27].

AC conductivity, as well as dielectric properties were measured using an LCR meter (IM 3533 HIOKI). Measurements were taken at frequencies from 1 Hz to 100 kHz at room temperature by connecting a voltage of 1 V AC to the samples through two electrodes. Conductance (G), capacitance (C) and dielectric loss were measured directly while the dielectric constant (ε_r) and AC conductivity (σac) were calculated from the following equations:

$$\varepsilon_r = (C\, d) / \varepsilon_0\, A \tag{2}$$

and

$$\sigma_{ac} = (G\, d) / A \tag{3}$$

where C is the measured capacitance, d is the thickness of the films, ε_0 and A are permittivity of vacuum (8.854 × 10^{-12} F m^{-1}) and the area, respectively. G represents the measured conductance [27].

The hysteresis loops representing polarization (P) vs electric field (E) were produced using a high voltage power amplifier (Trek 601E) with a low current. All samples were subjected to an E of 40 MV m^{-1} at 10 Hz at temperatures from 21 °C to 140 °C. The loops obtained were analyzed by calculating the area inside and outside which denoted the ferroelectric energy loss and storage, respectively. Energy efficiency was calculated from the equation:

$$\eta = (U_e)/(U_e + U_l) \tag{4}$$

where η is energy efficiency, U_e is energy density and U_l is energy loss [28].

3. Results and Discussion

3.1. AFM Measurements

AFM produced topographic images which providing information about the structural formation of the spherulites. Figure 1a shows topographic image of neat P(VDF-HFP) before electron-beam

irradiation. Large spherulites were presented with relatively big gaps between them. These relatively big spherulites were associated to the non-polar α-phase conformation mode that strongly affected by the film preparation technique. Ribeiro et al. have reported the effect of the different preparation methods, including solvent casting method, to the crystalline phase nucleation [29]. In this case, the solution was casted on the glass plate by using blade and was put in the oven to evaporate the solvents. High evaporation temperature, more than 70 °C, could increase the material's evaporation rate. So that the stability of the material is quite high, leading to α-phase crystallization [30].
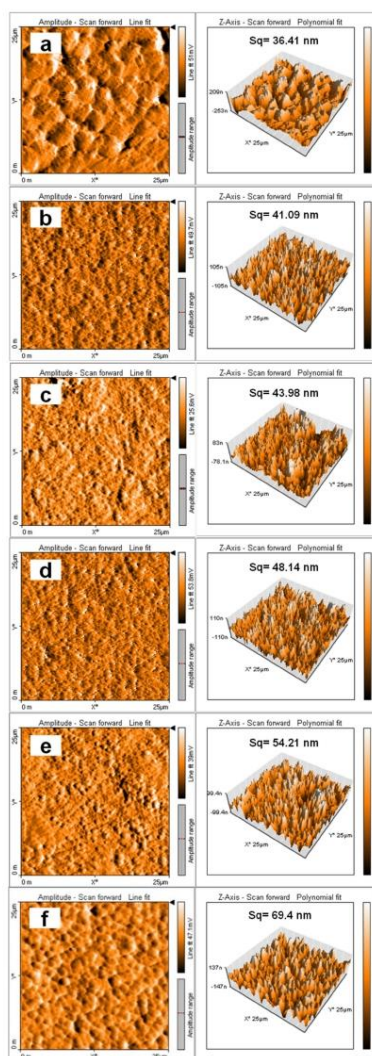

Figure 1. AFM topography images of: (**a**) neat P(VDF-HFP); (**b**) HFP/GN1; (**c**) HFP/GN2; (**d**) HFP/GN3; (**e**) HFP/GN4; and (**f**) HFP/GN5 before electron-beam irradiation.

After introducing GNPs conducting nanofillers, the large gaps observed in neat P(VDF-HFP) tended to be filled with GNPs in the HFP/GN composites. Hence, a network of smaller parallel spherulites could be formed. This spherulites reduction was strongly caused by the interface reduction that occurs between each spherulites [31]. The spherulitic microstructures of HFP/GN composites were similar to that of neat P(VDF-HFP) (Figure 1b–f), but with smaller spherulites. This observation was consistent with a previous work reporting that adding compatible fillers in the gaps between particles of composite materials is effective to increase its cross-linking density, which is the density of a small area where parts of polymer chains are connected [32].

GNPs demonstrated good adhesion with the polymer matrix since there were no significant gaps at the interface of GNPs and polymer. Adding a small amount of GNPs produced good dispersion and efficient electrostatic interaction preventing significant agglomeration [33]. The strong electrostatic interaction between GNPs and polymer chains was associated with the strong dipole moment of the nanofillers and the size reduction of the spherulites [33]. This morphological change also influenced other properties, such as the dielectric constant, which will be discussed below.

Adding GNP conducting nanofillers not only affected the spherulite size but also the surface topography of the composites, specifically the surface roughness (Sq). In neat P(VDF-HFP), the Sq value was lower because its surface comprised of a dense skin [3]. The Sqs of all HFP/GN composites before electron-beam irradiation were higher than that of neat P(VDF-HFP). This property was associated to the full exfoliation of the GNPs, which help their dispersion in the P(VDF-HFP) copolymer matrix. Good dispersion of nanofillers in the matrix tended to generate a good interfacial strength between the nanofillers and the matrix. It was also confirmed by an prior work, which addressing a morphological change from a micro- to nano-structure and an improvement of its surface roughness [3]. After irradiation, there were no significant changes in surface topography or spherulites that observed. It shows the same trend with the AFM result before electron-beam irradiation; the spherulites of neat P(VDF-HFP) after electron-beam irradiation were also bigger than that of all HFP/GN composites (Figure 2a–f).

Nevertheless, according to the Sq parameter, the roughness of neat P(VDF-HFP) copolymer and HFP/GN composites was increased after electron-beam irradiation. This rougher surface topography was derived from radial lamellar structures of the arrangement of the spherulites [33] and may also be related to the electron beam's ability to cut and break the polymer chains [24]. This finding confirms the early work reported by Gregor et al. (2014). The creation of micro-domains after electron-beam irradiation improved the surface roughness of materials [26].

3.2. SEM Results

P(VDF-HFP) copolymers were dispersed in the DMF solvent (Figure 3a). It shows that neat P(VDF-HFP) thin films with 20 wt% concentration in the solution possess a relative compact structure morphology with addition of small pores that spread out along the film. The black zones in Figure 3a referred to the pores. The pores were ascribed from the gap that left by the DMF solvent during evaporation time. The morphology of P(VDF-HFP) was reported in a prior work that studied about the influence of concentration loading of the polymer and the evaporation temperature on P(VDF-HFP) matrix [34]. Along with this work, the stated prior work also reported that higher concentration of P(VDF-HFP) leads to decrease the pore size of the matrix. On the other hands, a high evaporation temperature (in this case is 80 °C) can also decrease the pore size by improving the evaporation rate in DMF solvents and the polymer chain was able to occupy and fill out the space left by the DMF solvent during evaporation. As the result, this also affected the diffusion of polymers and the mobility of polymer chains [35]. It is resulting in more compact film that separated by those small pores, along with the AFM results in Figure 1 above, that describing the spherulitics.
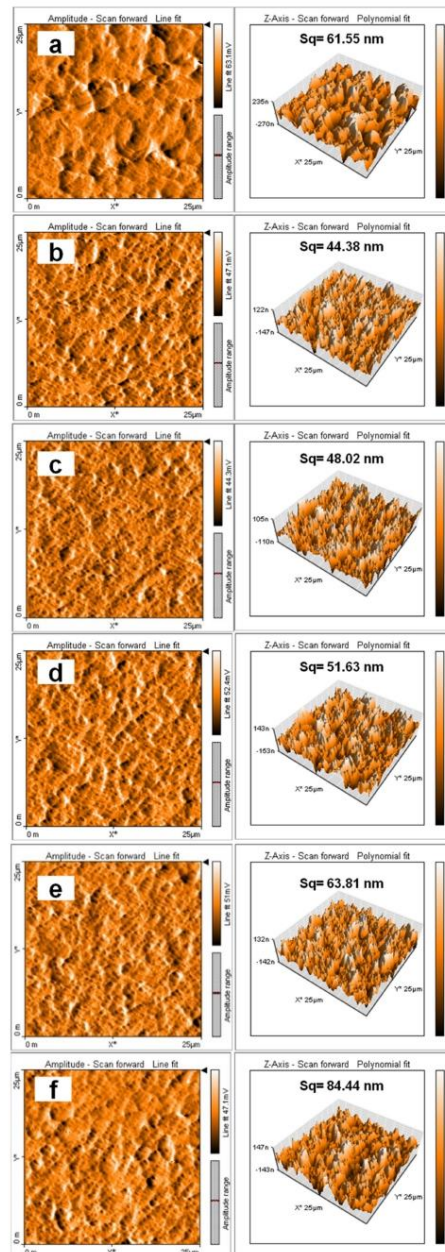
Figure 2. AFM topography images of: (**a**) neat P(VDF-HFP); (**b**) HFP/GN1; (**c**) HFP/GN2; (**d**) HFP/GN3; (**e**) HFP/GN4; and (**f**) HFP/GN5 after electron-beam irradiation.
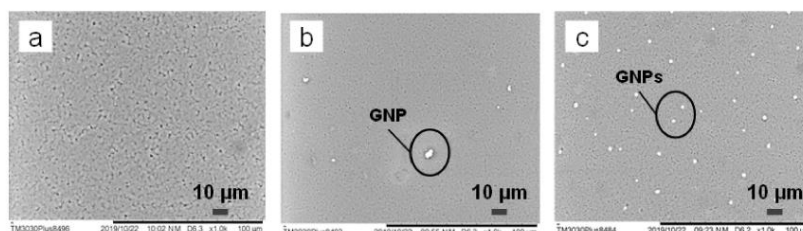
Figure 3. SEM morphology images of: (**a**) neat P(VDF-HFP); (**b**) HFP/GN1; and (**c**) HFP/GN5 composites.

Moreover, the morphology of the composites was also observed. GNPs particles were spread out within the P(VDF-HFP) matrix (Figure 3b,c). The presence of GNPs in the P(VDF-HFP) dielectric matrix causing some properties of the matrix to change. In respect of the electrical properties, such as the dielectric constant, AC conductivity and dielectric loss, the mechanism can be analogized to the mechanism of a capacitor, where the GNPs closed to each other acts as the electrode, and the P(VDF-HFP) matrix between them as the dielectric material. Further, the composite films acted as a large group of micro-capacitors.

In Figure 3b, there were only a few white spots indicating GNPs since the nanofiller content was only 1 wt%. However, there were more white spots in Figure 3c since the nanofiller content was increased to 5 wt%, which imaging many micro-capacitors that formed. The comparison of Figure 3b,c reveals that the gaps between each GNPs were much smaller at higher loading of the fillers. Thus, adding a higher percentage of GNPs conducting filler to the P(VDF-HFP) matrix could improve overall electrical properties that will be explained in the more detail below.

In addition to the spreading pattern of the filler, another factor that can be observed in Figure 3 is the homogeneity of the matrix itself. In neat P(VDF-HFP) thin film, it can be seen clearly that the matrix (Figure 3a) containing the pores/holes that represented by the black zones. In the opposite, the gaps or pores in the composites (Figure 3b,c) were much smaller compared to those of the neat P(VDF-HFP). Thus, the SEM images also show the similar results and confirming the AFM results. Due to a good dispersal of the GNP nanofillers in the P(VDF-HFP) matrix, the nano-sized GNPs (0.34–100 nm) [22] could easily fill the gaps or holes in the P(VDF-HFP) matrix and thus successfully alter its microstructure, resulting in more homogeneous and flexible films [22]. It firmed GNPs ability as one of the most attractive materials to use in nanocomposites since they show a good dispersion performance, especially when used with a solvent. In addition to its homogeneous dispersion, GNP fillers are also well known for their affinity for radicals and excellent exfoliation in the polymer matrix.

3.3. Water Contact Angle

PVDF and its copolymers are categorized as environmentally and chemically stable, hydrophobic fluorinated polymers. In simple term, hydrophobicity is a combination of two things. The first is chemical low surface energy that was defined as the measured unrealized bond energy. This is usually addressed to the molecular level of the materials. Second, the physical nano- or micro-scaled surface structure that usually quantified by surface roughness/topography measurement [3]. The hydrophobicity of a material is usually determined by the water contact angle. There are two main ways of increasing hydrophobicity either by reducing the surface energy of a material with high surface roughness, or improving the surface roughness of a material with low surface energy.

Before irradiation, the water contact angle of neat P(VDF-HFP) that observed in this work was around 110°, much higher than that of a previously reported PVDF polymer (around 90°) [36]. Emulsion polymerization of the HFP monomer on the PVDF polymer [37] not only improved mechanical strength and solubility but also increased its hydrophobicity. Further, adding a small amount of GNPs to the copolymer matrix increased its water contact angle as well (Figure 4). In simple terms,

hydrophobicity is the opposite of surface energy, which depends on the type of chemical bonds created on a surface. When the more energy is required to break strong chemical bonds, such as metallic bonds, so their surface energy are also high. Then, the hydrophobicity is low. In contrast, the energy required to break weak chemical bonds, such as those in hydrocarbons, is low, so the surface energy is also low and the hydrophobicity is high.
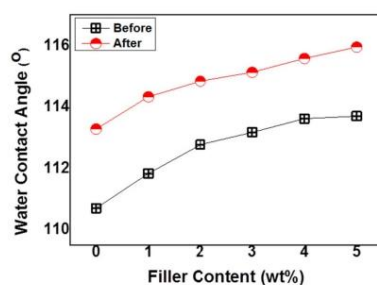

Figure 4. The water contact angle of neat P(VDF-HFP) and HFP/GN composites before and after electron-beam irradiation.

P(VDF-HFP) is categorized as a hydrophobic material since it has weak hydrocarbon bonds. GNPs with their high density of carbon were effective at modifying the structure and producing surface roughness, as shown by the AFM results. Therefore, improving the surface roughness of hydrophobic materials with low surface energy will significantly affect the water contact angle and improve its hydrophobicity [3]. If the surface of hydrophobic materials is roughened, the total surface area will increase so that when water drips onto such a surface, more air can be trapped on it, resulting in a higher contact angle [3].

The water contact angle of all samples was increased after electron-beam irradiation (Figure 4). This result confirmed those of other works that reporting the improvement of water contact angles after electron-beam irradiation [26,38]. Electron-beam irradiation could modify hydrophobicity by cutting chemical bonds either by chemical contamination or electron charge induction [38]. During electron-beam irradiation, charge induction begins with the pairing of electrons with holes inside the dielectric materials. The localized states of the amorphous areas trap the weak and heavy mobile holes and the electrons can then fill the dielectric bulk much more deeply. The electrons trapped on the bulk level will generate a negative charge, while a positive charge will be generated by localized holes around the surface.

Gregor et al. (2014) suggested that hydrophobicity improvement may be associated with the creation of micro-domains [26], in which case much higher hydrophobicity would be detected. This micro- to nano-structure change could boost hydrophobicity without any change in morphology. The creation of microdomain leads to improve surface roughness after electron-beam irradiation. Thus, higher water contact angle could be obtained through that mechanism.

3.4. XRD Results

As a semi-crystalline material, PVDF and its composites, including P(VDF-HFP), consist of both crystalline and amorphous areas. After casting, they are well known to present a dominant α-phase whereas the crystalline phase with the most useful piezoelectrical and dielectric properties is the planar zig-zag/TTTT β-phase conformation mode [39]. In common with this present work, many previous studies have focused on how to change the α-phase to the polar β-phase. In some cases, the two phases will only be detected in specific characteristic peaks. At those peaks, it is impossible to find other crystalline phases.

90

In the diffraction patterns of neat P(VDF-HFP) and HFP/GN composites before and after electron-beam irradiation, the intensity of the diffraction peak at 17.7° that associated to (100) crystallographic plane specifically corresponds to the non-polar α- and δ-phase (Figure 5). At that peak, there is no possibility of overlapping with the γ- or β-phase. However, the intensity of these diffraction peaks in the patterns of HFP/GN composites was significantly reduced from 4755 in the neat P(VDF-HFP) to 4530. This means that adding GNP conducting nanofillers lowered the intensity of the non-polar α-phase. Physically, this α-phase intensity reduction is an indicator that introducing GNPs conducting nanofillers to the P(VDF-HFP) matrix could manipulate the crystalline phase of the polymer matrix. It was suggesting that GNPs is effective to interact with the amorphous region of the P(VDF-HFP) chains and its inter-phases [23]. As the consequence, the P(VDF-HFP) segments diffusion could be prohibited towards the crystallization fronts.
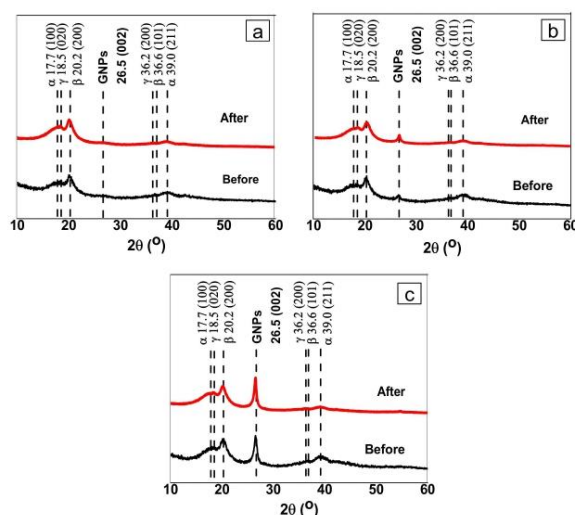

Figure 5. XRD patterns of: (**a**) neat P(VDF-HFP); (**b**) HFP/GN1; and (**c**) HFP/GN5 composites before and after electron-beam irradiation.

Other non-polar α-phase diffraction peaks are found at 18.5° and 39.0°, corresponding to the (020) and (211) crystallographic planes, respectively. Along with the previous mentioned, the intensity of these characteristic α-phase peaks was also lower after adding GNPs conducting nanofillers. Moreover, the characteristic peak of the γ-phase was also detected at 18.5° and 36.2° and referred respectively to the (020) and (200) crystal planes [40].

Interestingly, while the α-phase characteristic diffraction peaks were reduced, the polar β-phase diffraction peak intensity shows the opposite trend. The peak intensity of the β-phase at 36.6°, corresponding to the (101) crystal plane was increased from 1151 to 1225. Another observed diffraction peak that was also attributed to the polar β-phase appears at 20.2° associated to the (200) crystal plane [23,33]. Physically, these diffraction peak improvements of the polar β-phase ascribed to the formation of more regular and order molecules in the P(VDF-HFP) matrix that promoted by GNPs loading addition. Hence, this most electroactive polar phase formation could be generated. In addition to the change on diffraction peak intensity of polymer crystalline phases, introducing GNPs also significantly boosted up the diffraction peak at 26.5°, which was identified as the GNPs characteristic of the (002) crystal plane [23].

Over those aforementioned above, the most significant effect was shown by electron-beam irradiation. At 39.0°, the intensity of the non-polar α-phase diffraction peak referred to (211) crystal plane was significantly reduced and even get nearly disappeared for both neat P(VDF-HFP) and HFP/GN composites. It indicates that electron beam could facilitate the more polar β-phase and stabilize it at the same time.

To confirm the XRD results, FTIR analysis was conducted. This method was very useful in determining the β-phase fraction in the material and a combination of XRD and FTIR measurements helped to determine the microstructural changes which occurred inside the material during electron-beam irradiation.

3.5. FTIR Results

Figure 6a shows the FTIR spectra of neat P(VDF-HFP) and HFP/GN composites before irradiation. The characteristic absorption peaks of the α-phase at 532, 613, 764 and 978 cm^{-1} were attributed to the vibration mode of CH_2 and CF_2 groups in neat P(VDF-HFP) [23,33]. Peaks were also detected at 875, 1069 and 1402 cm^{-1} that referred to the CF_2 stretching mode in pure P(VDF-HFP) [39]. The peak at 875 cm^{-1} is attributed to the C-C group of the α-phase in the P(VDF-HFP). Hence, at that wavenumber, it is impossible to find any other crystalline phase. However, the absorption peak at 1170 cm^{-1} can be assigned to γ- and α-phases.
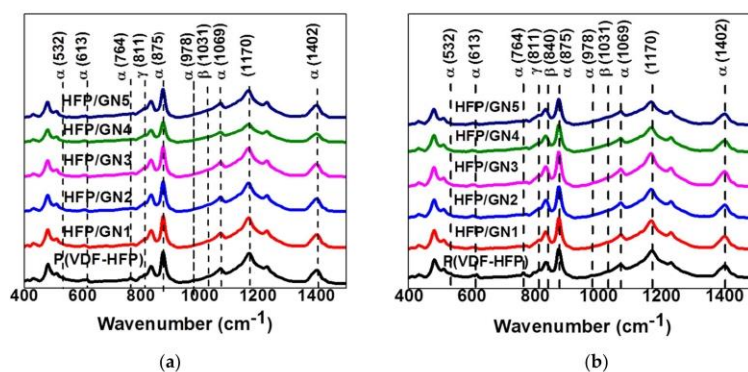

Figure 6. FTIR spectra of neat P(VDF-HFP) and HFP/GN composites: (**a**) before; and (**b**) after electron-beam irradiation.

Absorption at peaks attributed to the α-phase was slightly decreased for HFP/GN composites. For example, the intensity of α-phase absorption peaks at wavenumber of 875, 1069 and 1402 cm^{-1} in the P(VDF-HFP) were decreased from 0.71, 0.34 and 0.30 to 0.63, 0.32 and 0.27, respectively, in HFP/GN5. Further, as predicted, the reduction of α-phase absorption peaks at several wavenumbers tends to affect the intensity of the absorption peaks at 811 and 1031 cm^{-1}, that corresponded to γ- and β-phases, respectively. The absorption peak at 1031 itself refers to the CF_2 bending vibration modes of the β-phase [40]. The intensity at those wavenumbers was increased slightly from 0.19 and 0.16 to 0.21 and 0.17, respectively. Those intensity changing indicates that the GNPs ability on prohibiting the non-polar α-phases as well as tailoring and transforming the most order β-phase conformation mode. Hence, these FTIR results strongly confirm and support the XRD results that firstly described.

Electron-beam irradiation also caused structural changes in the crystallinity of P(VDF-HFP) and HFP/GN composites. In the spectra of P(VDF-HFP), the α-phase absorption peaks at 875, 1069 and 1402 cm^{-1} before irradiation (Figure 6a) are reduced from 0.71, 0.34 and 0.30 to 0.54, 0.25 and 0.23, respectively, after electron-beam irradiation (Figure 6b). Similar reductions in α-phase absorption peaks also occurred in the HFP/GN composites. The FTIR absorption data were used to calculate the

crystalline fraction of the polar β-phase (*F(β)*) in P(VDF-HFP) and HFP/GN composites by assuming it is in an agreement with the Lambert–Beer law expressed in the following equation:

$$F(\beta) = A_\beta / ((K_\beta / K_\alpha) A_\alpha + A_\beta) \tag{5}$$

where A_α and A_β are the absorbance at wavenumber of 764 cm^{-1} and 840 cm^{-1}, while the absorption coefficients at those wave numbers are K_α equal to 6.1×10^4 cm^2 mol^{-1} and K_β equal to 7.7×10^4 cm^2 mol^{-1}, respectively [27].

The calculated β-phase fractions (*F(β)*) of all loadings before and after irradiation were shown by Figure 7. The graph illustrates the increased β-phase content of the P(VDF-HFP) matrix after the addition of GNPs. Electron-beam irradiation was also effective in optimizing the polar β-phase. In summary, therefore, both GNPs and electron-beam irradiation promoted β-phase formation.
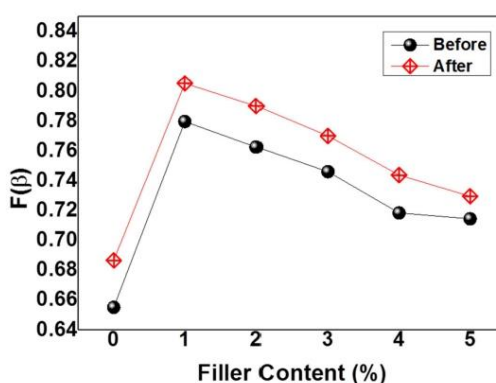

Figure 7. β-phase fractions in neat P(VDF-HFP) and HFP/GN composites before and after electron-beam irradiation.

The increased overall β-phase content of HFP/GN was due to interfacial electrical interactions between positively charged carbon atoms in GNPs and partially negative fluorine atoms in the P(VDF-HFP), which causing a bigger dipole moment. The positively charged carbon in the GNPs tends to rotate the C–F bonds near the C–C chain backbone of the P(VDF-HFP). Hence, the β-phase could form. This result was consistent the findings of He et al. (2016) who used positive organosilicate to modify the β-phase content in PVDF [41].

Irradiating the samples with the electron beam also affected their microstructure because the negative charge of the electron was able to interact with the positive charge of the hydrogen atoms of the P(VDF-HFP) chains. As reported in another work, interactions that occurred between the negative charge of a nanofiller and the positive charge of hydrogen, or between positively charged nanofillers and negatively charged fluorine CF$_2$ groups in PVDF chains generated a polar crystalline phase [42]. In deeply, the negative charge from the electron beam will produce the local electric field in the interface of the P(VDF-HFP). This negative charge will pull the bonds that contain the opposite charges with the specific direction of the dipoles around them. Since CH$_2$ bonds have more positively charge than CF$_2$, the electron beam will rotate the CH$_2$ bonds resulting on more order arrangement of the dipoles. This interface interaction leads to create the β-phase nucleation.

In addition to providing data relating to changes in the crystalline phase from α- to β-phase, XRD measurements also provided useful information about crystal size. According to other studies, electron-beam irradiation could cut crystal domains into smaller sizes [24,28]. Through electron-beam irradiation, the width of the diffraction peaks of the neat P(VDF-HFP) and the HFP/GN composites at

half-maximum gradually increased. These data could be used to control the thickness or size of crystal sheets (*D*) by using the Scherrer formula [43]:

$$D = (K\,\lambda) / (B\,\cos\theta) \tag{6}$$

where *K* (*K* = 0.89) is the Scherrer constant, *λ* (*λ* = 0.154 nm) is the X-ray wavelength and *B* and *θ* are the width of the half-maximum and the location of the diffraction peak.

Table 2 shows the crystallinity (X_c) as well as the width of the diffraction peak of neat P(VDF-HFP) and HFP/GN composites at half-maximum (*B*) and the crystal size (*D*) for all conditions, before and after electron-beam irradiation. The width at half-minimum of neat P(VDF-HFP) had increased from 0.58 rad to 1.02 rad after irradiation while the crystal size had reduced from 0.60 nm to 0.48 nm. The HFP/GN composites also exhibited the same trend. For example, the width at half-minimum of HFP/GN5 had increased from 0.55 rad to 1.10 rad after electron-beam irradiation, whereas, the crystal size of the HFP/GN5 composites had decreased from 1.38 nm to 0.54 nm.

Table 2. The crystallinity (X_c), width at half-maximum (*B*) and crystal size (*D*) of neat P(VDF-HFP) and HFP/GN composites before and after electron-beam irradiation at the 20.2° diffraction peak.

GNP Content (wt%)	X_c (%)		*B* (rad)		*D* (nm)	
	Before	**After**	**Before**	**After**	**Before**	**After**
0	26.52	26.06	0.58	1.02	0.60	0.48
1	35.56	32.24	0.71	0.92	1.46	0.68
2	38.34	30.57	0.39	0.82	2.60	0.81
3	31.47	35.20	0.87	1.07	1.91	0.58
4	27.25	28.07	0.47	0.82	1.07	0.82
5	31.67	32.25	0.55	1.10	1.38	0.54

Crystal size is strongly associated with dielectric loss, which itself relates to the relaxation of the crystal domain with high polarity. In normal ferroelectrics, the β-phase is irreversible since it has a large domain/crystal size. Many researchers have investigated ways to crack or break the crystals to reduce their size and by doing so, change the loop from normal to relaxor ferroelectric, entailing a smaller dielectric loss. Larger crystals lead to a strengthening of the interaction coupling between each domain. Since the electron beam cuts the crystal into smaller domains, the interaction couplings between each domain tended to decrease [44]. This has the advantage of enabling the dipole moment/ crystal grains to be more reversible. Hence, when the external electric field is removed, the relaxation speed of the dipole moment or crystal grains will increase and this is useful for releasing the charge stored on the material's surface. It is for that reason that dielectric loss after electron-beam irradiation decreased along with a decrease in the crystal domain size [43].

3.6. DSC Results

DSC measurements provided useful information about melting temperature (T_m) and melting enthalpy (ΔH_m) of the films. Moreover, the degree of crystallinity (X_c) could also be calculated.

The melting temperatures (T_m) of the HFP/GN composites were higher than that of neat P(VDF-HFP) both before and after irradiation (Figure 8a,b). The T_m is related to the form of the crystalline phase. The increase in melting temperature were associated with the increased β-phase formation in the films [45] and indicated that GNPs induced the formation of the polar β-phase. Furthermore, before irradiation, the melting enthalpy (ΔH_m) of the HFP/GN composites was generally greater than that of the neat P(VDF-HFP) as was the degree of crystallinity (X_c) (Table 2). The ΔH_m itself is related to the nucleation of GNPs with the P(VDF-HFP) matrix [45].
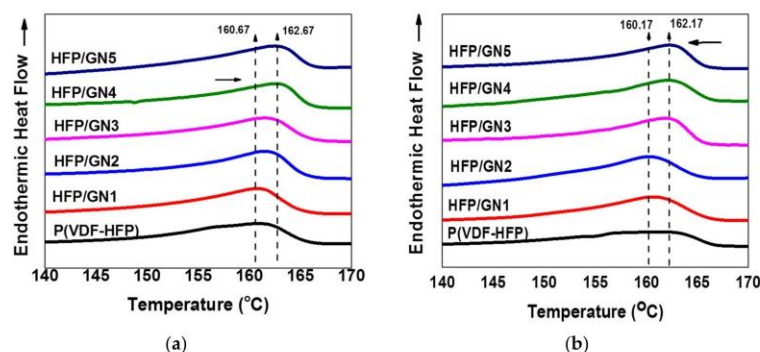
Figure 8. DSC thermograms showing T_m of neat P(VDF-HFP) and HFP/GN composites: (**a**) before; and (**b**) after electron-beam irradiation.

Naturally, smaller fillers such as GNPs will be dispersed more effectively than larger fillers, and the outstanding characteristics of GNPs as a reinforcing agent for polymer nanocomposites will have an impact on the polymer's properties.

Figure 9 presents a schematic of the proposed mechanism of GNPs dispersal within P(VDF-HFP). P(VDF-HFP) is categorized as a semi-crystalline material and this kind of material contains both crystalline and amorphous areas in its structure. Actually, adding nanofillers is only one of the well-known methods to get the most electroactive crystalline phase. Compared to others such as melting process, applying external electric field or ultra-fast cooling, adding nanofillers, which is currently developed, has additional advantages that has no microstructural limitations or causing undesired deformation of the structure [30]. When GNP nanofillers were introduced into the P(VDF-HFP) matrix, the GNPs spread throughout the whole of the polymer matrix in both crystalline and amorphous areas.
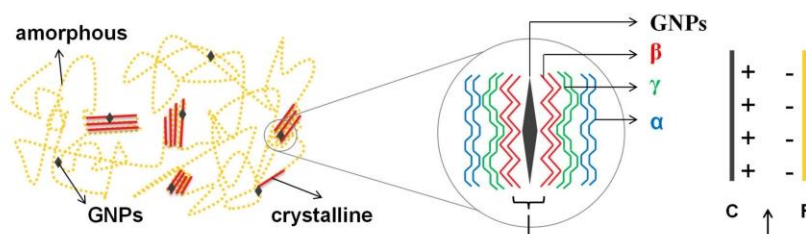

Figure 9. The schematic of the structure of HFP/GN composites.

The mechanism of the specific phase nucleation process cannot be generalized. The prior works have reported that it has also influenced either by the nanofillers size or the nanofillers amount [30]. Nevertheless, all of them are agreed with the dominant role of the interface interactions between the fillers and the matrix. The appearance of GNPs conducting nanofillers will produce local electric field that occurs around the nanoparticles. This electric field then attracting the randomly arranged dipoles of P(VDF-HFP). The nucleation of β-phase could be gained during this process. The dipoles that rotate depend on the type of the nanofillers itself. Simply, more positively charged particles will attract the negative CF_2 groups of the polymer, while the more negatively charged particles will induce the CH_2 group of the polymer.

In the composite containing the lowest GNP content of 1 wt%, the conducting fillers tended to interact with the crystalline areas as a consequence of the positively charged carbon atoms on GNPs, that attracted by the negative charge of the fluorine atoms in P(VDF-HFP). The crystalline areas of the P(VDF-HFP) matrix consisted of five crystalline phases including the α-phase, γ-phase and β-phase [20]. This kind of interface interaction led to the transition of α-phases to β-phases, especially in those areas very closed to GNPs. Further, the γ-phase occurred in areas close to the β-phase and not too distant from GNPs. In areas far away from GNPs, the non-polar α-phase still existed, as illustrated in Figure 9. The polymer chain rotation resulted in planar zig-zag conformation modes. Here, the C–F bond, which has higher electronegativity was reoriented parallel to the opposite side of the C–H bond [18] and that is why the β-phase fraction increased significantly after the addition of only 1 wt% of GNPs, as shown by the FTIR results in Figure 7 of β-phases fraction.

When the filler content was higher than 1 wt%, GNPs not only attracted the crystalline areas but also attracted the amorphous areas of the polymer. In the amorphous areas, the interaction that occurred between the P(VDF-HFP) matrix and the GNP nanofillers led to the creation of new crystalline areas, causing an improvement in overall crystallinity and overall crystalline phases. However, since overall crystallinity increased, the interaction between GNPs and amorphous areas created not only β-phases but also other crystalline phases including the non-polar α-phase formation. Therefore, the percentages of β-phase fraction seem to slightly decline as a proportion of the overall crystalline phases after increasing the GNPs filler content as shown by Figure 7.

Nevertheless, the crystallinity and melting enthalpy of the films decreased after electron-beam irradiation compared to their values before electron-beam irradiation, as shown in Table 2 and Figure 8b, respectively. The T_m of the neat P(VDF-HFP) film decreased from 160.67 to 160.17 after electron irradiation with a similar reduction in the HFP/GN composites. Tan et al. (2013) suggested that the reduction in melting temperature was caused by reduced crystallinity and smaller crystal size, which was confirmed by XRD analysis [43] domain size [43].

3.7. Dielectric Properties and AC Conductivity

At room temperature, before and after electron-beam irradiation, the dielectric constant (ε_r) of neat P(VDF-HFP) and various HFP/GN composites was dependent on the frequency of the electric field from 1 Hz to 100 kHz (Figure 10a,b). The non-irradiated HFP/GN composites had a higher dielectric constant than non-irradiated neat P(VDF-HFP) over the whole frequency range. It indicates that the dielectric constant is also dependent on the fillers content.
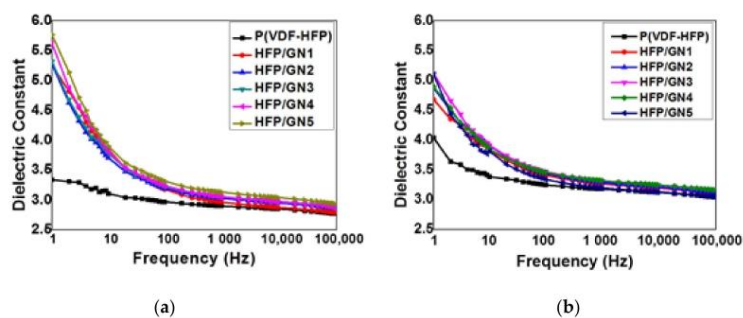

(**a**)   (**b**)

Figure 10. Plots of the dielectric constant vs the frequency of the electric field for neat P(VDF-HFP) and various HFP/GN composites of: (**a**) before; and (**b**) after electron-beam irradiation.

As explained above, GNPs acted as micro-capacitor electrodes closely arranged in serial or parallel to each other but still in isolated systems [23]. As found in a previous study [41], the higher polarization

of HFP/GN composites could improve the dielectric constant in two ways. The charged surface of the GNPs could provide a charge-movement contribution, and the GNPs could facilitate polar β-phase formation, which increased dipole density and charge storage capacity. GNPs acted as nucleation agents that promoted crystallization. In addition, interfacial interactions between GNPs and the P(VDF-HFP) matrix stabilized the β-phase TTTT chain sequences of the P(VDF-HFP) and limited movement of the molecular chains during the process of crystal-formation [41]. The molecular chains located near the β-phase TTTT chain sequences will even change into γ-phase TTTG without the direct influence of the surface of GNPs. Nevertheless, the α-phase TGTG chains were still found in the P(VDF-HFP) molecular chains but only when it is far enough from GNPs.

At low frequency of 1 Hz, the addition of 1%wt GNP increased the dielectric constant from 3.34 for neat P(VDF-HFP) to 5.26. The dielectric constant increased gradually with further GNPs loading to 5.27, 5.32, 5.62 and 5.77 for HFP/GN2, HFP/GN3, HFP/GN4 and HFP/GN5, respectively. In contrast, as the frequency increased, net polarization dropped due to the cessation all polarization mechanisms. The inability of the structural components in all repeat units to couple with the electric field prevented maximum reorientation of the dipoles [46]. Hence, higher frequencies produced a reduction in the dielectric constant.

GNPs also improved AC conductivity of P(VDF-HFP) and dielectric loss (Figures 11 and 12) which represent typical insulating behavior. The AC conductivity of the neat P(VDF-HFP) shows non-monotonous behavior. It can be seen that the AC conductivity increase almost linearly with the increasing of frequency. It might occur because it approaches or is closely the same with the resonance frequency of the charge carriers in the polymer chain. This frequency dependence of AC conductivity could be related to the activated trapped charges release [47].
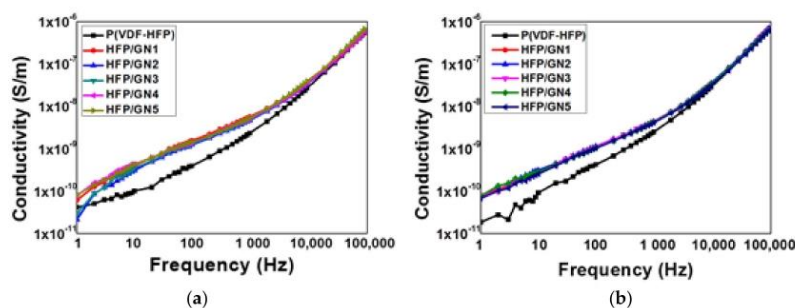

Figure 11. AC conductivity of neat P(VDF-HFP) and HFP/GN composites of: (**a**) before; and (**b**) after electron-beam irradiation depended on the frequency of the electric field.
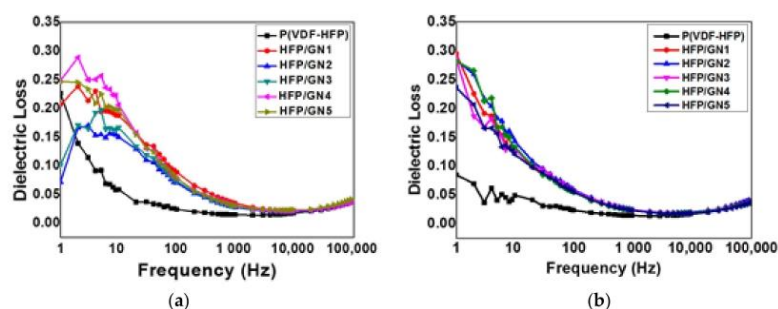

Figure 12. Dielectric loss of neat P(VDF-HFP) and HFP/GN composites of: (**a**) before; and (**b**) after electron-beam irradiation depended on the frequency of the electric field.

The increased AC conductivity in the HFP/GN composites may have been caused by their dipole density and GNPs themselves that are highly conductive. Although it is not significant, this AC conductivity improvement could be affected by several factors such as filler conductivity and filler concentration. Polymers that electrically resistant normally possess the electrical conductivity ranges of 10^{-14} to 10^{-17} S/cm. Those numbers are much lower than that of the Carbon-based fillers of 10^2 to 10^5 S/cm. Hence, the composites that incorporated by conducting filler will have higher conductivity as well. Further, the introduction of the filler into the matrix could gradually decrease the resistivity of the polymer. Nevertheless, the low filler concentration that used in this work does not affect to the conductive path formation that indicated by the very few amount of the GNPs particles that located nearly or contact each other as shown by SEM result in Figure 3. In addition to filler conductivity and its concentration, another factor that influences the HFP/GN AC conductivity improvement is the aspect ratio of the filler. Graphene-based filler itself is well known as the material with high aspect ratio. As the aspect ratio boost up, the conductive path could be reached at lower filler concentration. This work confirmed the prior study that also reporting AC conductivity improvement that caused by GNPs nanofillers [23].

As the fillers content increase (beyond 5 wt%), the formation of micro-capacitor that parallel each other will increase too. Continuously, the possibility of conductive network formation and leakage current will be higher too. So that, in one point, the percolation threshold could be reached. As the mechanism, the polymer's insulating layer that is sandwiched by two GNPs conducting particles will decrease and cased the fillers to almost contact each other. At the percolation threshold or beyond, the dielectric constant and AC conductivity could be slightly improved. Along with the result of this work, a prior work has been reported the AC conductivity improvement that caused by GNPs incorporation [23]. Moreover, it was reported also that the percolation threshold for GNPs conducting nanofillers in PVDF/PMMA matrix was beyond 4 wt%.

As aforementioned, the dielectric properties for both dielectric constant and dielectric loss were dropped as increasing the frequency. Inability of the dipoles to reorient following the applied electric field at high frequency led the reduction of the dielectric loss as well. As shown by Figure 12, the dielectric loss for neat P(VDF-HFP) before and after electron-beam irradiation was decreased as increasing of frequency. When the GNPs conducting nanofillers were introduced to the P(VDF-HFP) matrix, the dielectric loss was increased since dielectric loss are also determined by the material's conducting nature [23]. Nevertheless, as neat P(VDF-HFP), the dielectric loss of the composites was also decreased as increasing of frequency. As well known, the dielectric properties including dielectric constant and dielectric loss for polar materials can be explained by the contribution of several types of polarizability components such as deformational period including electronic and ionic polarization and relaxation period including orientational and interfacial polarization. In low frequency, the total polarization was determined by the sum of those four polarization types. Since the ionic polarization does not play the significant role in the total net polarization, and the orientational polarization that usually take longer time to occur compared to electronic and ionic polarization, will lead to the reduction of the net polarization. Hence, at high frequency range, the polarization was only corresponded to the interfacial polarization.

The dielectric constant of both neat P(VDF-HFP) and the HFP/GN composites was higher after electron-beam irradiation at 1000 Hz (Figure 13a), which was probably a result of the microstructural and morphological changes inside the material caused by the electron beam. As previously explained, microstructural changes in the samples due to electron-beam irradiation also influenced their electrical properties. The positively charged hydrogen atoms inside the P(VDF-HFP) chains attracted negatively charged electrons [42]. Since the most stable non-polar α-phase dominates the original state of P(VDF-HFP) copolymer, the negative charge from the electron beam produced a more ordered crystalline phase and transitioned α-phases to γ-phases and β-phases [33]. In addition, the electron beam helped the GNPs in the HFP/GN composites to act as nucleation agents in the formation of polar β-phases.
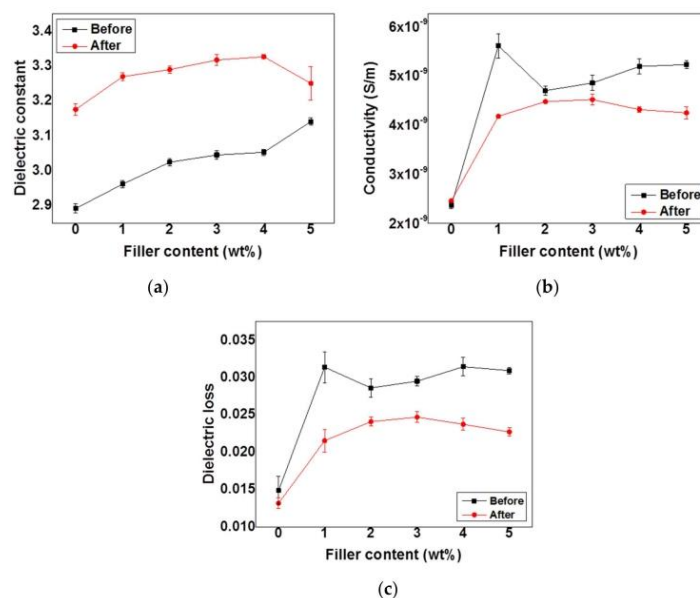
Figure 13. (**a**) Dielectric constant; (**b**) AC conductivity; and (**c**) dielectric loss of neat P(VDF-HFP) and HFP/GN composites as a function of graphene nanoparticle (GNP) content before and after electron-beam irradiation at 1000 Hz.

Both AC conductivity and dielectric loss were also increased after adding GNPs nanofillers to P(VDF-HFP) matrix. This condition could lead to the formation of conductive path and leakage current. It was suggested the GNPs framework interconnection in the P(VDF-HFP) matrix that resulting on charge transfer improvement in the composites. The AC conductivity and dielectric loss improvement of HFP/GN1 composites looks sharper than others. It might be caused by the dispersion of the GNPs in the HFP/GN composites. According to SEM results in Figure 3, the agglomeration of the GNPs filler in HFP/GN1 composites can be observed associated to the bigger size of the GNPs group. It is along with the work that was previously reported that explains that the non-uniform distribution of the filler in the polymer matrix could lead to improve the conductivity, and dielectric loss as well due to the agglomeration [48]. This phenomenon was commonly observed in many polymer composites behavior. Further, the curve of dielectric loss shows the similar pattern to the AC conductivity since it is also well known that the dielectric loss is originally determined by the natural electrical conductivity of the materials [49].

Meanwhile, AC conductivity and dielectric loss of all composites were lower after electron-beam irradiation (Figure 13b,c). A previous study of electron-beam irradiation of Poly(vinylidene fluoride-trifluoroethylene) copolymer with 50 mol% TrFE (P(VDF&HIPHEN;co-TrFE)) reported the effects on chemical pinning of the reduced crystal domains [24]. However, the specific mechanism inside the material by which this occurs is still unclear, although the researchers considered that electron-beam irradiation caused cross-linking in the material. Chemical cross-linking expands the length of the inter-chain and pins polymer chains. As a consequence, it may decrease the crystal domain size and help the dipole moments to rotate during electrical discharge. Hence, the dielectric loss will decrease and the dielectric constant will increase [43]. These electrical properties mechanism finally affect to other parameter such as ferroelectric loop as well as energy properties of the materials. Uniquely, the ability of the electron beam on suppressing the AC conductivity and dielectric loss seems

stronger than the effect of GNPs conducting nanofiller itself on gaining those parameters. Hence, as shown by Figure 13b,c, the AC conductivity and dielectric loss of the composites look not significant change after electron-beam irradiation even though the filler contents were increased.

3.8. P-E Loop

PVDF-based polymers, including P(VDF-HFP), are semi-crystalline materials in which amorphous and crystalline areas moderate the polarization response to an external electric field. Since PVDF-based polymers are ferroelectric materials, the polarization response to the electric field exhibits a ferroelectric hysteresis loop. Normal ferroelectric materials contain a large number of spontaneous dipoles that are packed on a relatively wide ferroelectric crystalline domain. This condition can produce a strong polarization response to an applied electric field.

As regards the mechanism when E is applied to thin films, the dipoles in the film will be rearranged to align with the direction of E, which is known as the charging process until the maximum polarization (P_{max}) value is reached. However, the dipole directions will revert to a random state when E is removed from the system, and polarization will drop until E is equal to zero. This step is known as the discharging process. Nevertheless, not all the dipoles will rearrange themselves in their original state and larger crystalline domains will retain some charge, which is trapped and cannot be released. As a consequence, some dipoles will still exhibit an ordered orientation and will remain polarized. This state is described as the remnant polarization (P_r), at $E = 0$. Here, polarization is not zero even though there is no longer an applied electric field, and remnant polarization can be high.

The polarization (P) response of neat P(VDF-HFP) and HFP/GN composites to an externally applied electric field (E) was measured at room temperature (30 °C). The P-E hysteresis loop gradually increased in size with increments of GNP and remnant polarization was exhibited (Figure 14). Loop size is an indication of the size of the ferroelectric domain and is closely linked to dipole reversibility. A larger crystal size means a bigger energy loss. A large domain normally formed a large coupling force with other aligned domains nearby [50]. Strong interactions between domains will prevent the relaxation of the dipoles during the discharging process, preventing dipole reorientation once the external E is removed. This was also confirmed by dielectric measurements. Dielectric constant, AC conductivity and dielectric loss all improved after adding GNPs, since the GNPs are a conducting material. As a result, the composites possessed higher remnant polarization resulting in bigger loops compared to the loop of neat P(VDF-HFP).
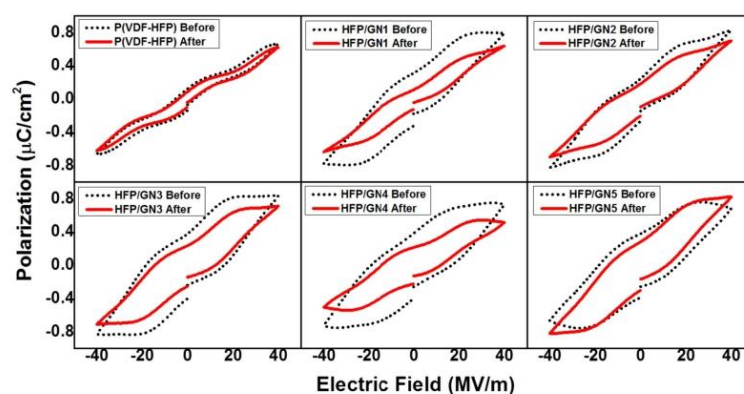

Figure 14. Polarization-applied electric field (P-E) hysteresis loops of neat P(VDF-HFP) and HFP/GN composites before and after electron-beam irradiation.

Electron-beam irradiation had a similar effect to GNPs on the dielectric constant of P(VDF-HFP), promoting β-phase formation. The additional beneficial effects of irradiation included improved dielectric constant and possess better energy storage properties. Previous studies reported that electron-beam irradiation was effective at reducing dielectric loss [28]. Its ability to pin the all-*trans* conformation domain size of neat P(VDF-HFP) and HFP/GN composites improved dipole reversibility [24]. The large domains of normal ferroelectrics can be pinned and cut into smaller domains. Electron-beam irradiation is also able to shorten P(VDF-HFP) segments and facilitate dipolar switching during discharge. After being pinned by the electron-beam, the small domains/crystal sizes were able to reverse freely because the forces holding domains were lower. As a result, dielectric loss decreased. Moreover, the P-E loops (Figure 14) confirmed that remnant polarization also decreased in all composites after electron-beam irradiation. The loops were clearly slimmer after electron-beam irradiation.

3.9. Energy Efficiency

As previously mentioned, even though the GNPs conducting nanofillers improved the dielectric constant by promoting β-phase formation, GNPs also promoted increased dielectric loss. Compared to neat P(VDF-HFP), storage energy density of the composites tended to be lower at all loadings of GNPs from 1 to 5 wt%. The energy density was decreased by the increasing of the filler content. Hence, the energy loss was significantly increased, as shown in (Figure 15a,b). As explained, GNPs could lead the improvement of AC conductivity and dielectric loss as well. Thus, the increasing of the proportion of GNPs in the composites produced a bigger loop indicating bigger energy loss. The reversibility of the dipoles was decreased resulting to the difficulties of the dipoles on following the electric field when it was removed from the system. Hence, this energy loss improvement affected to reduce the storage energy density.
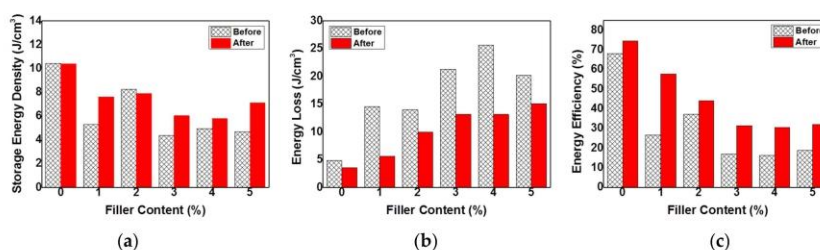

Figure 15. (**a**) Storage energy density; (**b**) energy loss; and (**c**) storage energy efficiency of neat P(VDF-HFP) and HFP/GN composites before and after electron-beam irradiation.

Interestingly, different with the effect of adding GNPs conducting nanofillers, electron-beam irradiation was able to improve the storage energy density but reduce the energy loss of all samples. It also reduced the remnant polarization of the loop, thus assisting the release of the charge stored on the film's surface [43], resulting in lower dielectric and energy loss.

The final parameter considered was energy efficiency, which describes the ratio of storage energy density to energy loss. There are two ways to improve the energy efficiency of materials: increasing the storage energy or decreasing the energy loss. The storage energy density is the energy that can be released per unit volume and is usually calculated during electric field discharge. Energy loss relates to unreleased energy and occurs when energy is transferred from one system, place or condition to another. Mathematically, storage energy density (U_e) and energy loss (U_l) can be expressed by the following equations:

$$U_e = \int EdD = \frac{1}{2}DE = \frac{1}{2}\varepsilon_r\varepsilon_0 E_b^2 \tag{7}$$

and

$$U_l \;=\; \frac{1}{2}\omega\varepsilon''\varepsilon_0 E_b^2 \tag{8}$$

where E and D are respectively the applied electric field and electrical displacement, while ε_r, ε_0 and E_b are the dielectric constant (measured permittivity), vacuum permittivity (8.85×10^{-12} F/m) and electrical breakdown strength, respectively. ω represents frequency and ε'' refers to the dielectric loss [28,43]. According to these equations, in the same applied electric field, storage energy density will depend only on the dielectric constant, while energy loss is closely related to dielectric loss.

Electron-beam irradiation considerably improved the energy efficiency of P(VDF-HFP) and HFP/GN composites (Figure 15c) by increasing the dielectric constant while simultaneously reducing the dielectric loss, thus increasing U_e and reducing U_l. For example, the energy efficiency of neat P(VDF-HFP) increased from 68.11 to 74.66% after irradiation, which is much higher than the efficiency reported by Guan et al. (2010) [13] who only achieved 58% for P(VDF-HFP) without electron-beam irradiation and 30.2% for PVDF [12]. The energy efficiency of HFP/GN1, HFP/GN2, HFP/GN3, HFP/GN4 and HFP/GN5 also increased after electron-beam irradiation, in some cases almost doubling, from 26.65, 37.10, 16.98, 16.16 and 18.75%, to 57.7, 44.23, 31.34, 30.59 and 32.06%, respectively.

4. Conclusions

Two main approaches were adopted in this study: adding GNP conducting nanofillers and electron-beam irradiation. The good spreading and strong electrostatic interactions of GNPs within the polymer matrix produced smaller spherulites and a rougher surface topography compared to the neat P(VDF-HFP). The GNP nanofiller also reduced the pores and resulting in more homogeneous film. Electron-beam irradiation also increased surface roughness of both GNPs and electron-beam irradiation so that it is able to facilitate the formation of a more hydrophobic surface. The measured water contact angle after electron-beam irradiation were varied from 113° to 116° for neat P(VDF-HFP) and HFP/GN composites, respectively. These values were much higher than that of currently reported of 90° for PVDF. In addition, both approaches were effective in facilitating the transformation of the non-polar TGTG α-phase to the polar TTTT β-phase, which improved the dielectric constant. Nevertheless, adding GNP conducting nanofillers boosted AC conductivity and dielectric loss leading to a bigger P-E hysteresis loop. As results, it must be noted that the HFP/GN composites exhibited lower energy density and higher energy loss. Interestingly, however as the core of this work, electron-beam irradiation acted in the opposite way by effectively reducing crystal size, considerably improving the dielectric constant and reducing AC conductivity as well as dielectric loss. Energy loss, therefore, tended to be lower after electron-beam irradiation leading to better storage energy density and storage energy efficiency both for neat P(VDF-HFP) and HFP/GN composites at all loadings. For neat P(VDF-HFP), the energy efficiency was increased from 68.11 to 74.66% after electron irradiation, much higher than previously reported of 58%. Meanwhile, the increasing of it on HFP/GN composites after electron irradiation is almost doubled.

References

1. Qiao, Y.; Yin, X.; Zhu, T.; Li, H.; Tang, C. Dielectric polymers with novel chemistry, compositions and architectures. *Prog. Polym. Sci.* **2018**, *80*, 153–162. [CrossRef]
2. Jiang, J.; Shen, Z.; Qian, J. igh discharge efficiency in multilayered polymer nanocomposites of high energy density. *Energy Storage Mater.* **2019**, *18*, 213–221. [CrossRef]
3. Moradi, R.; Karimi-sabet, J.; Shariaty-niassar, M.; Koochaki, M.A. Preparation and Characterization of Polyvinylidene Fluoride/Graphene Superhydrophobic Fibrous Films. *Polymers* **2015**, *7*, 1444–1463. [CrossRef]
4. Feng, Y.; Li, J.; Li, W.; Li, M.; Chi, Q.; Zhang, T. Effect of BaTiO$_3$ nanowire distribution on the dielectric and energy storage performance of double-layer PVDF-based composites. *Compos. Part A* **2019**, *125*, 105524. [CrossRef]
5. Hardy, C.G.; Islam, Md. S.; Gonzalez-Delozier, D.; Morgan, J.E.; Cash, B.; Benicewicz, B.C.; Ploehn, H.J.; Tang, C. Converting an Electrical Insulator into a Dielectric Capacitor: End-Capping Polystyrene with Oligoanilnie. *Chem. Mater.* **2013**, *25*, 799–807. [CrossRef]
6. Thakur, V.K.; Gupta, R.K. Recent Progress on Ferroelectric Polymer-Based Nanocomposites for High Energy Density Capacitors: Synthesis, Dielectric Properties, and Future Aspects. *Chem. Rev.* **2016**, *116*, 4260–4317.
7. Wang, Y.; Huang, X.; Li, T.; Wang, Z.; Li, L.; Guo, X.; Jiang, P. Novel crosslinkable high-k copolymer dielectrics for high-energy-density capacitors and organic field-effect transistor applications. *J. Mater. Chem. A Mater. Energy Sustain.* **2017**, *5*, 20737–20746. [CrossRef]
8. Xie, L.; Huang, X.; Huang, Y.; Yang, K.; Jamg, P. Core Double-Shell Structured BaTiO 3—Polymer Nanocomposites with High Dielectric Constant and Low Dielectric Loss for Energy Storage Application. *J. Phys. Chem. C* **2013**, *117*, 22525–22537. [CrossRef]
9. Gross, S.; Camozzo, D.; Di Noto, V.; Armelao, L.; Tondello, E. PMMA: A key macromolecular component for dielectric low-k hybrid inorganic–organic polymer films. *Eur. Polym. J.* **2007**, *43*, 673–696. [CrossRef]
10. Huang, X.; Jiang, P.; Tanaka, T. A Review of Dielectric Polymer Composites With High Thermal. *IEEE Electr. Insul. Mag.* **2011**, *27*, 8–16. [CrossRef]
11. Song, Y.; Shen, Y.; Liu, H.; Lin, Y.; Li, M.; Nan, C. Improving the dielectric constants and breakdown strength of polymer composites: Effects of the shape of the BaTiO$_3$ nanoinclusions, surface modification and polymer matrix. *J. Mater. Chem.* **2012**, *22*, 16491–16498. [CrossRef]
12. Guan, F.; Pan, J.; Wang, J.; Wang, Q.; Zhu, L. Crystal Orientation Effect on Electric Energy Storage in Poly(vinylidene fluoride-co-hexafluoropropylene) Copolymers. *Macromolucules* **2010**, *43*, 384–392. [CrossRef]
13. Li, W.; Meng, Q.; Zheng, Y.; Zhang, Z.; Xia, W.; Xu, Z. Electric energy storage properties of poly(vinylidene fluoride). *Appl. Phys. Lett.* **2010**, *96*, 192905.
14. Xu, H. Dielectric Properties and Ferroelectric Behavior of Poly(vinylidene fluoride-trifluoroethylene) 50/50 Copolymer Ultrathin Films. *J. Appl. Polym. Sci.* **2001**, *80*, 2259–2266. [CrossRef]
15. Bharti, V.; Zhao, X.Z.; Zhang, Q.M.; Romotowski, T.; Tito, F.; Ting, R. Ultrahigh field induced strain and polarization response in electron irradiated poly(vinylidene fluoride-trifluoroethylene) copolymer. *Mat. Res. Innov.* **1998**, *2*, 57–63. [CrossRef]
16. Das, A.K.; Sinha, S.; Mukherjee, A.; Meikap, A.K. Enhanced dielectric properties in polyvinyl alcohol-Multiwall carbon nanotube composites. *Mater. Chem. Phys.* **2015**, *167*, 286–294. [CrossRef]
17. Hartono, A.; Satira, S.; Djamal, M. Electric Field Poling 2GV/m to Improve Piezoelectricity of PVDF Thin Film. *AIP Conf. Proc.* **2016**, *1719*(030021), 2–6.
18. Roy, S.; Thakur, P.; Hoque, N.A.; Bagchi, B.; Das, S. Enhanced electroactive β-phase nucleation and dielectric properties of PVdF-HFP thin films influenced by montmorillonite and Ni(OH)$_2$ nanoparticle modified montmorillonite. *RSC Adv.* **2016**, *6*, 21881–21894. [CrossRef]
19. Mansouri, S.; Sheikholeslami, T.F.; Behzadmehr, A. Investigation on the electrospun PVDF/NP-ZnO nanofibers for application in environmental energy harvesting. *J. Mater. Res. Technol.* **2019**, *8*, 1608–1615. [CrossRef]
20. Ruan, L.; Yao, X.; Chang, Y.; Zhou, L.; Qin, G.; Zhang, X. Properties and applications of the β phase poly(vinylidene fluoride). *Polymers* **2018**, *10*, 228. [CrossRef]
21. Salea, A.; Chaipo, S.; Permana, A.A.; Jehlaeh, K.; Putson, C. The microstructure of negative electrocaloric Polyvinylidene fluoride-hexafluoropropylene copolymer on graphene loading for eco-friendly cooling technology. *J. Clean. Prod.* **2020**, *251*, 119730. [CrossRef]

22. Cataldi, P. Graphene Nanoplatelets-Based Advanced Materials and Recent Progress in Sustainable Applications. *Appl. Sci.* **2018**, *8*, 1438. [CrossRef]

23. Yang, D.; Xu, H.; Yu, W.; Wang, J.; Gong, X. Dielectric properties and thermal conductivity of graphene nanoplatelet filled poly(vinylidene fluoride) (PVDF)/poly(methyl methacrylate) (PMMA) blend. *J. Mater. Sci. Mater. Electron.* **2017**, *28*, 13006–13012. [CrossRef]

24. Yang, L.; Li, X.; Allahyarov, E.; Taylor, P.L.; Zhang, Q.M.; Zhu, L. Novel polymer ferroelectric behavior via crystal isomorphism and the nanoconfinement effect. *Polymer (Guildf).* **2013**, *54*, 1709–1728. [CrossRef]

25. Plecenik, T.; Tofail, S.A.M.; Gregor, M.; Zahoran, M.; Truchly, M. Direct creation of microdomains with positive and negative surface potential on hydroxyapatite coatings. *Appl. Phys. Lett.* **2012**, *98*, 113701. [CrossRef]

26. Gregor, M.; Plecenik, T.; Tofail, S.A.M.; Zahoran, M.; Truchly, M.; Vargova, M.; Laffir, F.; Plesch, G.; Kus, P.; Plecenik, A. Hydrophobicity of electron beam modified surface of hydroxyapatite films. *Appl. Surf. Sci.* **2015**, *337*, 249–253. [CrossRef]

27. Thakur, P.; Kool, A.; Bagchi, B.; Das, S.; Nandy, P. Effect of in situ synthesized Fe2O3 and Co3O4 nanoparticles on electroactive β-phase crystallization and dielectric properties of poly(vinylidene fluoride) thin films. *Phys. Chem. Chem. Phys.* **2015**, *17*, 1368–1378. [CrossRef]

28. Zhu, Y.; Jiang, P.; Zhang, Z.; Huang, X. Dielectric phenomena and electrical energy storage of poly(vinylidene fluoride) based high- k polymers. *Chin. Chem. Lett.* **2017**, *28*, 2027–2035. [CrossRef]

29. Ribeiro, C.; Costa, C.M.; Correia, D.M.; Nunes-Pereira, J.; Oliveira, J.; Martins, P.; Goncalves, R.; Cardoso, V.F.; Lanceros-Mendez, S. Electroactive poly (vinylidene fluoride)-based structures for advanced applications. *Nat. Publ. Gr.* **2018**, *13*, 681–704. [CrossRef]

30. Martins, P.; Lopes, A.C.; Lanceros-Mendez, S. Electroactive phases of poly(vinylidene fluoride): Determination, processing and applications. *Prog. Polym. Sci.* **2014**, *39*, 683–706. [CrossRef]

31. Chenyang, X.; Zhao, M. Ionic liquid modified poly(vinylidene fluoride): Crystalline structures, miscibility, and physical properties. *Polym. Chem.* **2013**, *4*, 5726–5734.

32. Jenkins, A.D.; Kratochvíl, P.; Stepto, R.F.T.; Suter, U.W. Glossary of basic terms in polymer science (IUPAC Recommendations 1996). *Pure Appl. Chem.* **1996**, *68*, 2287–2311. [CrossRef]

33. Gérard, J. Structural dependence of cations and anions to building the polar phase of PVDF. *Eur. Polym. J.* **2018**, *107*, 236–248.

34. Sousa, R.E.; Nunes-Pereira, J.; Ferreira, J.C.C.; Costa, C.M.; Machado, A.V.; Silva, M.M.; Lanceros-Mendez, S. Microstructural variations of poly(vinylidene fluoride co-hexa fluoropropylene) and their influence on the thermal, dielectric and piezoelectric properties. *Polym. Test.* **2014**, *40*, 245–255. [CrossRef]

35. Magalhaes, M.; Duraes, R.; Silva, N. The Role of Solvent Evaporation in the Microstructure of Electroactive β-Poly(Vinylidene Fluoride) Membranes Obtained by Isothermal Crystallization. *Soft Mater.* **2011**, *9*, 1–14. [CrossRef]

36. Kitabata, M.; Taddese, T.; Okazaki, S. Molecular Dynamics Study on Wettability of Poly(vinylidene fluoride) Crystalline and Amorphous Surfaces. *Langmuir* **2018**, *34*, 12214–12223. [CrossRef] [PubMed]

37. Wang, X.; Xiao, C.; Liu, H.; Huang, Q.; Hao, J.; Fu, H. Poly(vinylidene Fluoride-Hexafluoropropylene) Porous Membrane with Controllable Structure and Applications in Efficient Oil/Water Separation. *Materials* **2018**, *11*, 443. [CrossRef] [PubMed]

38. Aronov, D.; Rosenman, G. Surface energy modification by electron beam. *Surf. Sci.* **2007**, *601*, 5042–5049. [CrossRef]

39. Daneshkhah, A.; Shrestha, S.; Siegel, A.; Varahramyan, K.; Agarwal, M. Cross-selectivity enhancement of poly(vinylidene fluoride-hexafluoropropylene)-based sensor arrays for detecting acetone and ethanol. *Sensors* **2017**, *17*, 595. [CrossRef]

40. Khalifa, M.; Mahendran, A.; Anandhan, S. Probing the synergism of halloysite nanotubes and electrospinning on crystallinity, polymorphism and piezoelectric performance of poly(vinylidene fluoride). *RSC Adv.* **2016**, *6*, 114052–114060. [CrossRef]

41. He, F.A.; Lin, K.; Shi, D.; Wu, H.; Huang, H.; Chen, J.; Chen, F.; Lam, K. Preparation of organosilicate/PVDF composites with enhanced piezoelectricity and pyroelectricity by stretching. *Compos. Sci. Technol.* **2016**, *137*, 138–147. [CrossRef]

42. George, B.K. PVDF-ionic liquid modified clay nanocomposites: Phase changes and shish-kebab structure. *Polymer (Guildf).* **2017**, *115*, 70–76.

43. Tan, S.; Hu, X.; Ding, S.; Zhang, Z.; Li, H.; Yang, L. Significantly improving dielectric and energy storage properties via uniaxially stretching crosslinked P(VDF-co-TrFE) films. *J. Mater. Chem. A.* **2013**, *1*, 10353–10361. [CrossRef]

44. Guan, F.; Yuan, Z.; Shu, E.W.; Zhu, L. Fast discharge speed in poly(vinylidene fluoride) graft copolymer dielectric films achieved by confined ferroelectricity. *Appl. Phys. Lett.* **2009**, *94*, 10–13. [CrossRef]

45. Thakur, P.; Kool, A.; Bagchi, B.; Das, S.; Nandy, P. Enhancement of β phase crystallization and dielectric behavior of kaolinite/halloysite modified poly (vinylidene fluoride) thin films. *Appl. Clay Sci.* **2014**, *99*, 149–159. [CrossRef]

46. Shrivastav, B.D.; Barde, R.; Mishra, A.; Phadake, S. Frequency and Temperature Dependence of Dielectric Properties of Fish Scales Tissues. *Res. J. Phys. Sci.* **2013**, *1*, 24–29.

47. Laxmayyaguddi, Y.; Mydur, N.; Pawar, A.S.; Hebri, V.; Vandana, M.; Sanjeev, G.; Hundekal, D. Modified Thermal, Dielectric, and Electrical Conductivity of PVDF-HFP/LiClO4 Polymer Electrolyte Films by 8 MeV Electron Beam Irradiation. *ACS Omega.* **2018**, *3*, 14188–14200. [CrossRef]

48. Moharana, S.; Mishra, M.K.; Chopkar, M.; Mahaling, R.N. Enhanced dielectric properties of surface hydroxylated bismuth ferrite–Poly(vinylidene fluoride-co-hexafluoropropylene) composites for energy storage devices. *J. Sci. Adv. Mater. Devices* **2016**, *1*, 461–467. [CrossRef]

49. Nawaka, K.; Putson, C. Enhanced electric field induced strain in electrostrictive polyurethane composites fibers with polyaniline(emeraldine salt) spider-web network. *Compos. Sci. Technol.* **2020**, *198*, 108293. [CrossRef]

50. Soulestin, T.; Ladmiral, V.; Dos Santos, F.D.; Améduri, B. Vinylidene fluoride- and trifluoroethylene-containing fluorinated electroactive copolymers. How does chemistry impact properties? *Prog. Polym. Sci.* **2017**, *72*, 16–60. [CrossRef]

Proceedings I (Published)

Improvement of electrocaloric properties of P(VDF-HFP)/GNPs composites for refrigerator cooling

A A Permana, W Ngamdee and C Putson

Journal of Physics: Conference Series

Improvement of electrocaloric properties of P(VDF-HFP)/GNPs composites for refrigerator cooling

View the article online for updates and enhancements.

Improvement of electrocaloric properties of P(VDF-HFP)/GNPs composites for refrigerator cooling

A A Permana, W Ngamdee and C Putson*

Department of Physics, Faculty of Science, Prince of Songkla University, Hat Yai, Songkhla, 90112, Thailand

*E-mail: chatchai.p@psu.ac.th

Abstract. Electrocaloric effect originally comes from the cross-coupling between temperature and polarization of dielectric materials. Poly (vinylidene fluoride)/P(VDF) and its copolymers exhibit high displacement and dielectric properties among all ferroelectric polymers with additional advantages like lightweight, flexible and low cost compared with other dielectric materials. Moreover, poly (vinylidene fluoride hexafluoroprophylene)/P(VDF-HFP) copolymers shows highest breakdown strength. P(VDF-HFP) copolymers was used as the main matrix with graphene nanoplatelets (GNPs) casting materials as nanofillers. The P/GNPs composites thin films were prepared by solution casting method with the final thickness of 30 +/- 5 μm using N,N-dimethylformamide (DMF) as solvents. The GNPs content was varied of 0, 1, 2, 3, 4 and 5% by weight. The dielectric and electrical properties were measured by LCR meter with various frequency of 1 to 100 kHz. The structure and crystallinity were observed by XRD and DSC. The polarization as a function of external electric field was investigated by P-E loop instrument in 40 MV/m with varying temperature from room temperature to 140 ºC. Furthermore, electrocaloric effect was measured by indirect method by calculating adiabatic temperature change (ΔT) with help of Maxwell relation. The experimental results show that dielectric constant of P/GNPs composites was increased by increasing the GNPs content but dielectric loss is kept constant with low loading, far away from the percolation threshold. Moreover, the ΔT of the P/GNPs composites is higher than the pure P(VDF-HFP) copolymers that leads to higher electrocaloric effect. The Increasement of the ΔT of P/GNPs composites will be discussed based on their microstructure, phase transition and crystallinity. As conclusion, adding GNPs nanofillers to P(VDF-HFP) matrix can improve dielectric constant as well as electrocaloric properties which has capability for refrigeration cooling system.

1. Introduction

Compared with another materials that possess pyroelectric, piezoelectric, and ferroelectric, P(VDF) and its copolymers like P(VDF-HFP) are the best one that possess all electroactive properties [1]. P(VDF)-based materials have three molecular conformation modes, TGTG′, TTTT, and $T_3GT_3G′$ with five crystalline phase, α, β, γ, δ, and ε. Among them, β-phase possesses the strongest pyroelectricity as well as piezoelectricity that very useful for real application. It is caused by its disimetris structure that creates highest dipole density compared with another phases [2]. To get higher β-phase of the semicrystalliine polymers, graphene nanoplatelets (GNPs) were used as filler. GNPs is carbon-based material that contain positive ions that can facilitate β-phase transformation when interacting with negative ions from fluorine atoms of P(VDF-HFP). Hence, the higher polarization will be obtained. Besides that, (GNPs) particles show a good performance in dispersion since no significant

agglomerates were observed at micron scale [3]. This study focuses on how to enhance the electrical properties as well as electrocaloric effect for refrigerator cooling.

2. Materials and methods

2.1. Materials and film preparation method
P(VDF-HFP) powder, Solef 11010/1001, was purchased from Solvay Solexis, Belgium. Graphene nanoplatelets (GNPs) powder 306633-25G, was purchased from Sigma Aldrich, USA. N,N-dimethylformamide (DMF, $\geq$ 99% purity), was purchased from RCI Labscan, Thailand.

Pure poly(vivylidene fluoride-hexafluoroprophylene), P(VDF-HFP), and poly(vivylidene fluoride-hexafluoroprophylene)/Graphene nanoplatelets, P/GNPs composites thin films were prepared by solution casting method with the final thickness of 30 $\pm$ 5 μm. For P/GNPs composites, GNPs were added to the P(VDF-HFP) copolymers at different loadings (1, 2, 3, 4 and 5 wt% based on the weight of copolymers). Firstly, GNPs was dispersed in DMF by using sonicateur for 20 min. Then, P(VDF-HFP) were added into the suspension of GNPs in DMF. The mixtures were stirred by using magnetic stirrer for 16 h and rested for 1 h. Then, the solutions were casted onto the glass plate and dried in the oven for 12 h at 80 °C.

2.2. Characterizations and measurements
The dielectric properties and AC conductivity were measured by LCR meter (IM 3533 HIOKI) at frequency range 1 Hz - 100 kHz at room temperature by applying 1 V AC of voltage. The capacitance (C), conductance (G) and dielectric loss value were obtained.

To determine the crystalline phase, X-ray diffraction (XRD) from Empyrean, PANalytical, Netherlands was operated at 40 kV and 30 mA using wavelength of 0.154 nm (CuKα). Samples were scanned in the Cu tube with the scan range (2θ) of 5 - 90° at a speed of 0.04° sec^{-1}.

Differential scanning calorimetric (DSC) was used to determine melting point and crystallization. The analyses were finished on 1-3 mg samples using DSC7 from Perkin Elmer (USA) from 20 °C to 200 °C at a heating rate of 10 °C min^{-1} in nitrogen atmosphere. The melting temperature (T_m) is gained from the maximum endothermic peak. Degree of crystallinity (X_c) was calculated from DSC results.

To obtain the polarization-electric field hysteresis loops, high voltage supplier with low current, Trek model 601E was carried out. A 40 MV m^{-1} electric field with frequency of 10 Hz was applied to the samples. The temperature was varied from 21 °C to 140 °C. The electrocaloric effect was measured by indirect method. The adiabatic temperature change (ΔT) was calculated by using Maxwell relation:

$$\Delta T = -\frac{T}{C} \int_{E_1}^{E_2} \left(\frac{\partial P_i}{\partial T}\right)_{X,E} dE_j \qquad (1)$$

where T, C, P and E are temperature, heat capacity (1600), polarization and electric field [4].

3. Results and discussion
Figure 1 shows frequency dependence of dielectric constant (ε_r) and dielectric loss ($\varepsilon^{''}_r$) for pure P(VDF-HFP) and P/GNPs composites with various GNPs contents at room temperature. ε_r at low frequency (1 Hz) increases significantly when GNPs were added. At that condition, GNPs conducting nanofillers take a role as microcapacitor electrodes that very close each other and arrange serial or parallel but still in isolated system [3]. As frequency increased, the net polarization of the materials drops due to the ceasing of each polarization mechanism. The lack of structural components that can couple to the external electric field in the repeat unit causes the maximum dipole reorientation cannot be reached [5]. Consequently, the dielectric constant drops when the frequency increases. Figure 1 also shows that the dielectric loss ($\varepsilon^{''}_r$) of the obtained composites is not significant and still low content below the percolation threshold.
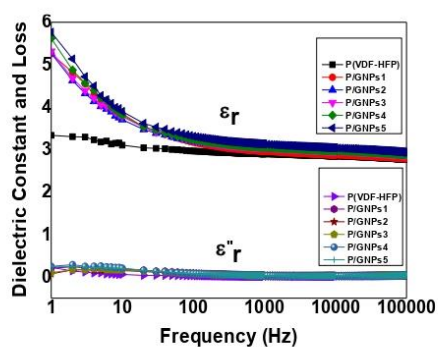
Figure 1. Dielectric constant and dielectric loss of pure P(VDF-HFP) and P/GNPs composites as a function of electric field frequency.
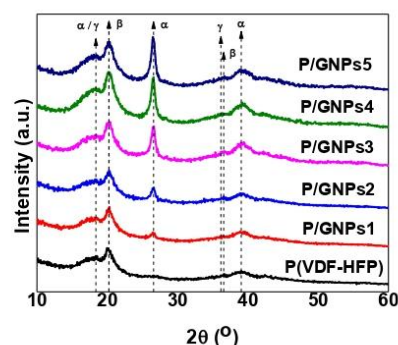

Figure 2. XRD patterns of pure P(VDF-HFP) and P/GNPs composites.

Figure 2 shows the XRD patterns of pure P(VDF-HFP) and P/GNPs composites for different phases. Peaks at 18.5°, 26.5° and 39.0° that correspond to (020), (002) and (211) are the characteristic of α-phase. The peak at 26.5° is identified as GNPs (002) plane. Peaks at 18.5° and 36.2° that correspond to (020) and (200) crystal planes of PVDF are the characteristic of γ-phase [6]. Nevertheless, the γ-crystal planes (020) assigned at peak 18.5° can overlap with (020) α-crystal planes. On the other hands, peaks at 20.2° and 36.6° that correspond to (200) and (101) crystal planes of PVDF are the characteristic of β-phase [3,6-7]. Pure P(VDF-HFP) shows diffraction peaks at 18.5° and 20.2° that refers to γ- and β-phase with intensity of 525 and 653 respectively. The intensity of these peaks drastically increases by the increasing of GNPs content from 1 wt% (P/GNPs1) until 4 wt% (P/GNPs4), and then slightly decreases for 5 wt% (P/GNPs5 composites). It showed by the γ- and β-phase peaks get sharper than that of pure P(VDF-HFP). Hence, P/GNPs4 possesses the highest intensity of 825 and 1146 respectively. Besides that, adding GNPs fillers also leads to create new peaks at 36.2° and 36.6° that also refers to γ- and β-phase respectively.

Figure 3 shows the polarization-electric field loop (P-E loop) of pure P(VDF-HFP) and P/GNPs composites with various filler content at room temperature (25 °C). Adding GNPs content effects to the bigger loop as well as higher remnant polarization. P-E loop data then were calculated to get the adiabatic temperature change (delta T). It is well known that high electrocaloric effect refers to high adiabatic temperature change [4]. The adiabatic temperature change results showed by figure 4. The highest delta T belong to P/GNPs composites of -72.34 °C that is much higher than that of pure P(VDF-HFP) of -52.95 °C. Besides high delta T, many studies also focus on lowering Curie temperature (T_c) that leads to reduce the energy barrier that resist the polar β-phase to be released before the polymer chain segments could freely to rotate [8]. The P/GNPs4 composites possess the lowest T_c of 86.28 °C among the others condition. P/GNPs4 generally also shows the best condition for electrocaloric effect. It can be seen from the biggest ratio of delta T/T_c with value of 0.79, much bigger than pure P(VDF-HFP) of 0.45.
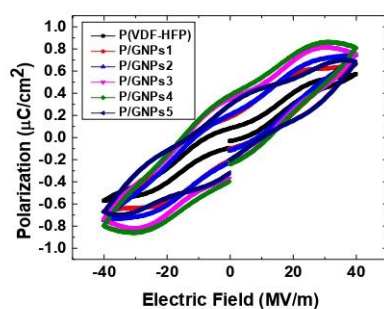
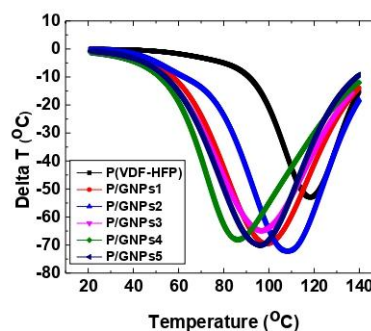**Figure 3.** P-E loop of pure P(VDF-HFP) and P/GNPs composites at 25 ℃.

Figure 4. Delta T versus temperature of pure P(VDF-HFP) and P/GNPs.

DSC results summarize the melting enthalpy (ΔH_m), melting temperatures (T_m), and degree of crystallinity (X_c). T_m of the composites shows the enhancement as well. The highest value gained by P/GNPs4 of 162.67 ℃. It has been reported that T_m relate to the crystalline phase [9]. The T_m enhancement of P/GNPs composites might be caused by the transformation of α- to dominant γ-phase and small amount of β-phase. It indicates that adding small amount of GNPs filler to the P(VDF-HFP) can induce the transformation of nonpolar to polar phase. Furthermore, the degree of crystallinity (X_c) of P/GNPs composites tend to increase from 26.52 of pure P(VDF-HFP) to the highest 38.34% of P/GNPs2. The role of the fillers in influencing the crystallization process depends on the dispersion state and the quantity of the fillers [10].

4. Conclusions

Adding GNPs nanofillers to P(VDF-HFP) significantly increases the dielectric constant especially in low frequency. As mentioned, GNPs act as a nucleation agent. So, adding small amount of GNPs fillers to the P(VDF-HFP) matrix can induce the transformation of nonpolar α-phase to the polar γ- and β-phase. Besides that, P/GNPs composites possess better electroaloric properties for refrigerator cooling. It showed by the ratio of adiabatic temperature change and Curie temperature. Among all conditions, P/GNPs4 shows the best properties for electrocaloric effect.

Acknowledgments

References

[1]   Martins P, Lopes A C and L-Mendez S 2014 *Prog. Polym. Sci.* **39** 683
[2]   He F A *et al* 2016 *Compos. Sci. Technol.* **137** 138
[3]   Yang D, Xu H, Yu W, Wang J and Gong X 2017 *J. Mater. Sci. Mater. Electron.* **28** 13006
[4]   Correia T and Zhang Q 2014 *Engineering Materials Electrocaloric Materials* (Berlin: Springer-Verlag)
[5]   Shrivastav B D, Barde R, Mishra A and Phadake S 2013 *Res. J. Phys. Sci.* **1** 24
[6]   Gérard J 2018 *Eur. Polym. J.* **107** 236
[7]   Khalifa M, Mahendran A and Anandhan S 2016 *RSC Adv.* **6** 114052
[8]   Zhu Y, Jiang P and Zhang Z 2017 *Chinese Chem. Lett.* **28** 2027
[9]   Ince-gunduz B S *et al* 2010 *Polymer (Guildf.)* **51** 1485
[10]   Yu L and Cebe P 2009 *Polymer (Guildf.)* **50** 2133

Proceedings II (Published)

Discharge Energy Efficiency Improvement of P(VDF-HFP) Copolymers Thin Films by Stretching and Electron Beam Irradiation

A A Permana, C Putson

2020 The 5th International Conference on Manufacturing, Material and Metallurgical Engineering

IOP Conference Series: Materials Science and Engineering

Discharge Energy Efficiency Improvement of P(VDF-HFP) Copolymers Thin Films by Stretching and Electron Beam Irradiation

View the article online for updates and enhancements.

Discharge Energy Efficiency Improvement of P(VDF-HFP) Copolymers Thin Films by Stretching and Electron Beam Irradiation

A A Permana, C Putson

Department of Physics, Faculty of Science, Prince of Songkla University, Hat Yai, Songkhla, 90110, Thailand

chatchai.p@psu.ac.th

Abstract. Toward improving the applications for energy-based technology, dielectric polymers is getting attention due to its relatively high dielectric constant, dielectric breakdown and flexibility, with easily preparation, lightweight and low cost. Dielectric contribution and polarization responses lead to different shape and size of hysteresis loop. This work presents the techniques on reducing domain size for slimmer loop, indicating lower energy loss. As-casted P(VDF-HFP), stretched P(VDF-HFP) and electron irradiated-stretched P(VDF-HFP) thin films were prepared by solution casting method. The irradiation was prepared by emitting electron beam. The dielectric and AC conductivity properties were investigated by LCR meter, while polarization-electric field loops were observed by P-E loop instrument. The results show that stretching and electron beam irradiation significantly increase the dielectric constant of P(VDF-HFP). Their ability on modifying the domain size leads to reduce P-E loop of P(VDF-HFP), followed by reducing energy loss but improving storage energy density and discharge energy efficiency.

1. Introduction

The outstanding materials for current applications in renewable energy-based electronics [1], [2] and power electronics [3] cannot be separated from its high dielectric constant [4] as well as low dielectric loss. One of the applications of dielectric polymers related to energy-based electronics is capacitor [5]. Since invented in 1990, dielectric polymers film capacitor with higher capacitance stability, owning high-voltage characteristics and possessing extremely low losses [6], has been improved due to its advantages over electrolytic and ceramic capacitor. In power and energy-based applications, low dielectric loss and high dielectric constant could lead to a higher energy efficiency and better performance as well.

Beyond its advantages that can be fabricated into thin film and large size device, P(VDF)-based semi-crystalline polymers [7] are the best materials that containing all electroactive characteristics among other ferroelectric, piezoelectric and pyroelectric materials [8]. With addition of hexafluoropropylene (HFP) into the main chain of P(VDF), P(VDF-HFP) copolymers is rich on stability, chemically resistance, non-toxicity and ability on tailoring the size and shape as well as recycling capability [9], [10].

Based on ferroelectricity of P(VDF)-based polymers including P(VDF-HFP) copolymers, a normal ferroelectric dielectric materials polarization response on applied external electric field will exhibit a

broad hysteresis loop [11]. That phenomenon leads to a high energy loss and low storage energy density. As the consequence, the discharge energy efficiency is also drop. This work focuses on increasing storage energy density and energy efficiency with lowering energy loss at the same time.

2. Materials and methods

2.1. Materials and method
P(VDF-HFP) Solef 11010/1001 copolymers powder was supplied by Solvay Solexis, Belgium. DMF N,N-dimethylformamide with ≥ 99% purity was supplied by RCI Labscan, Thailand.

First condition, poly(vivylidene fluoride-hexafluoroprophylene) thin films, named as-casted P(VDF-HFP) were kindly prepared by solution casting. The P(VDF-HFP) powder was stirred with DMF solvent in room temperature using magnetic stirrer for 16 hour. The solution then been filled out and casted on the glass plate using blade with the thickness of 30 ± 5 μ m. The samples then been dried for 12 hour at 80 °C in the oven. The second condition, named stretched P(VDF-HFP) was prepared by stretching P(VDF-HFP) films from 120 ± 5 μ m to 30 ± 5 μ m by stretching machine at 70 °C. Lastly, the stretched film then been emitted by 15 kV electron beam using conventional scanning electron microscopy (SEM) HITACHI TM3030Plus from Germany for 5 minutes. This condition named electron beam irradiated-stretched P(VDF-HFP) or EI stretched P(VDF-HFP).

2.2. Characterizations and measurements
LCR meter IM 3533 HIOKI was carried out for measuring dielectric constant and dielectric loss as well as AC conductivity. It was conducted on 1 V of AC voltage with varying the range of frequency from 1 Hz to 100 kHz at room temperature. The Dielectric constant and AC conductivity can be generated by calculating the data of the capacitance (C) and conductance (G) that gained from the measurements. Meanwhile, the value of dielectric loss can be gained directly from the measurements.

The hysteresis loops of polarization and electric field were measured by P-E loop instrument Trek type 601E. Conducted in temperature range from 21 °C to 140 °C, a 40 MV m^{-1} of external electric field with 10 Hz of frequency were applied to the thin films. Those P-E hysteresis loops were compared between each condition by calculating the area inside the loop (ferroelectric energy loss) and the area outside of the loop (ferroelectric energy density). Furthermore, the discharge energy efficiency can be obtained for each condition. Mathematically, it can be expressed as:

$$\eta = \frac{U_e}{U_e + U_l} \tag{1}$$

where η, U_e, and U_l refers to energy efficiency, energy density and energy loss, respectively [12].

3. Results and discussion

3.1. LCR meter results
The dielectric constant of as-casted P(VDF-HFP), stretched P(VDF-FP) and EI stretched P(VDF-HFP) are presented by figure 1. Figure 1 clearly shows that as-casted P(VDF-HFP) possesses the lowest value of dielectric constant. As reported by other works, as-casted P(VDF-HFP) is dominated by α-phase that is the most stable crystalline phase due to its symmetric structures [13]. On the other hands, the dielectric constant is increase significantly after mechanical stretching in every frequency. There is no doubt that mechanical stretching is one of the most effective ways to increase dielectric constant of the materials. It is due to the ability of mechanical stretching on facilitating the transformation of non-polar α-phase to the most useful β-phase [11]–[14]. Furthermore, mechanical stretching is also responsible to rearrange the crystal grains orientation and increase its uniformity [15]. Those mechanism will leads to the more order β-phase dipole TTTT conformation of P(VDF-HFP).
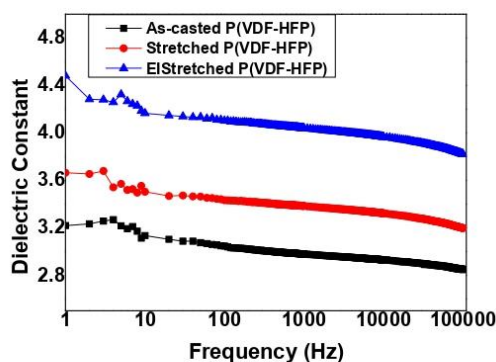
Figure 1. Dielectric constant of as-casted, stretched and EI
stretched P(VDF-HFP) as a function of electric field frequency.

The dielectric constant improvement of P(VDF-HFP) caused by electron beam irradiation on stretched P(VDF-HFP) is about two times compared than that of the only stretched thin films in all frequencies. This shows that both mechanical stretching and electron beam irradiation are effective to modify the structure of the thin film. As the results, the dielectric constant are increase significantly compare with as-casted condition. For example, dielectric constant of as-casted, stretched and EI stretched at 1 Hz frequency are 3.22, 3.66 and 4.48 respectively.

Dielectric loss is relatively referred to AC conductivity. Normally, the improvement of dielectric constant will be followed by the increasement of dielectric loss and AC conductivity also. That is a challenge that usually found in every dielectric material.
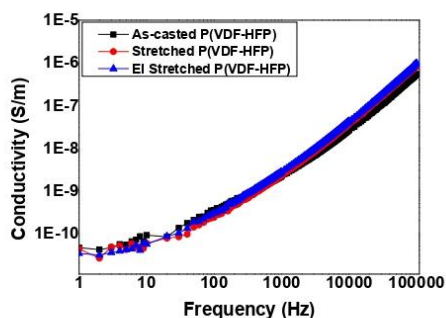

Figure 2. AC conductivity of as-casted, stretched and EI stretched P(VDF-HFP) as a function of electric field frequency.
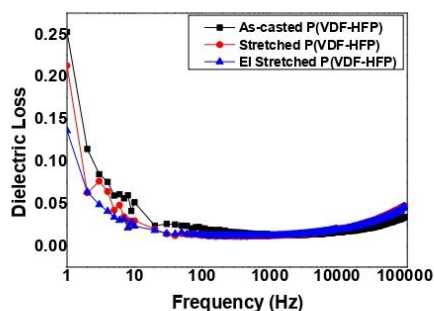
Figure 3. Dielectric loss of as-casted, stretched and EI stretched P(VDF-HFP) as a function of electric field frequency.

Nevertheless, figure 2 and 3 show that AC conductivity and dielectric loss of P(VDF-HFP) are not drastically change after stretching and electron beam irradiation. Somehow, at low frequency the numbers are even gradually drops. Some previous works reported that stretching [11], [15] is responsible to the improvement of dielectric constant due to its ability to convert non-polar α-phase to polar β-phase. At the same time, stretching also effects to destroy the big ferroelectric domain of P(VDF-HFP). Hence, the crystalline size/ferroelectric domain after stretching tends to be smaller as

reported by Li and Wang in 2016 [11]. As a final result, mechanical stretching could control the dielectric loss or even decrease its number, while increasing the dielectric constant at the same time.

Similar with the effect of stretching on AC conductivity and dielectric loss, electron beam irradiation is also responsible to stabilize those two parameters. It is well known that electron beam irradiation is becoming an alternative way to boost dielectric constant and keep control or even drop the AC conductivity and dielectric loss. Its ability is associated with its role when cutting the long chain to be shorter [16]. Furthermore, generating smaller crystalline size, electron beam irradiation would be very useful on generating smaller P-E loop that refers to smaller energy loss.

3.2. P-E loop measurements

Figure 4 shows P-E loop at room temperature (28 $^{\circ}$C) with the external electric field of 40 MV/m. It shows clearly that stretched and electron beam irradiated stretched P(VDF-HFP) possess higher maximum polarization (P_{max}). P_{max} is increase from 0.56 for as-casted film to 0.64 and 0.65 μ C/cm^2 for stretched and EI stretched films, respectively. At the same time, the remnant polarizations (P_r) of those two conditions are smaller than that of as-casted P(VDF-HFP). P_r is decrease from 0.09 for as-casted film to 0.04 and 0.02 μ C/cm^2 for stretched and EI stretched films, respectively.
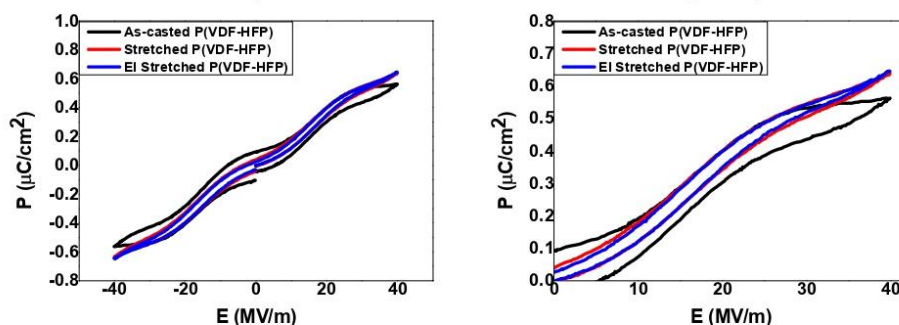

Figure 4. P-E loop of as-casted, stretched and EI stretched P(VDF-HFP).

The bigger loop of as-casted films refers to large size of the ferroelectric domain that consist of big number of dipoles, causing higher remnant polarization [12], [17]. The dropping of P_r that caused by stretching and electron irradiation effects to the polarization responses on external electric field, exhibiting the slimmer loops. In another word, stretching and electron beam irradiation are effectively reduce the area inside the loop of the P(VDF-HFP) thin films, confirming the previous work [15].

3.3. Energy efficiency

Based on P-E loop for each condition, the storage energy density, energy loss as well as energy efficiency value have been obtained. The results were shown by figure 5. It is clear that stretching and electron beam irradiation are effective to boost the storage energy density of P(VDF-HFP) thin films. At the same time, both treatments also drop the energy loss, drastically. The combination of these two parameters effects to the energy efficiency itself, as shown by figure 6. Hence, the discharge energy efficiency tends to exhibit much better value. The results of P-E loop measurements are also confirmed by dielectric constant result. In 2012, Zhu was reported that storage energy density can be improved by improving dielectric constant and electrical breakdown strength [12], [18].
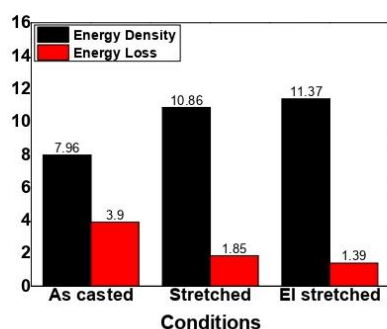
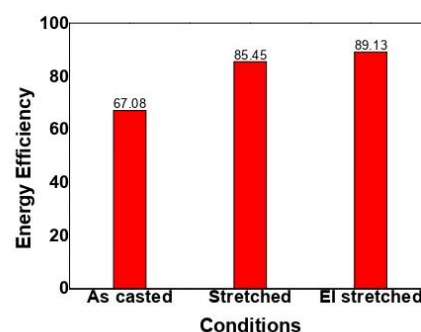**Figure 5.** Energy density and loss of as-casted, stretched and EI stretched P(VDF-HFP).

Figure 6. Energy efficiency of as-casted, stretched and EI stretched P(VDF-HFP).

4. Conclusion

Stretching and electron beam irradiation effectively improve the dielectric constant of P(VDF-HFP) copolymers thin films. The improvement was observed at all range of frequency. It corresponds to the ability of both mechanical stretching as well as electron beam irradiation on changing the crystalline phase from nonpolar α-phase to the polar β-phase. It also effect on changing the polarization-electric field loop (P-E loop) of the P(VDF-HFP). The improvement of maximum polarization and drops of remnant polarization cause the hysteresis loop getting slimmer. It represents that energy loss is decrease while storage energy density and discharge energy efficiency are increase at the same time. Hence, these properties are good to be applied on energy-based electronics.

References

[1]   Satake A, Jike J and Mitani Y 2019 *Int. J. Elec. & Elecn. Eng. & Telcomm.* 8 146
[2]   Lim Y S, Chok E T, Chua K H and Liew S 2018 *Int. J. Elec. & Elecn. Eng. & Telcomm.* 7 38
[3]   Abdukhakimov A, Bhardwaj S, and Kim D 2019 *Int. J. Elec. & Elecn. Eng. & Telcomm.* 8 233
[4]   Jung H 2019 Int. J. Elec. & Elecn. Eng. & Telcomm. 8 334
[5]   Qiao Y, Yin X, Zhu T, Li H and Tang C 2018 *Prog. Polym. Sci.* 80 153
[6]   Baer E and Zhu L 2017 *Macromolecules.* 50 2239
[7]   Liu J, Lu X and Wu C 2013 *Membranes.* 3 389
[8]   Martins P, Lopes A C and L-Mendez S 2014 *Prog. Polym. Sci.* 39 683
[9]   Roy S, Thakur P, Hoque N, Bagchi B and Das S 2016 *RSC Adv.* 6 21881
[10] Thakur V K and Gupta R K 2016 *Chem. Rev.* 116 4260
[11] Li Q and Wang Q 2016 *Macromol. Chem. Phys.* 217 1228
[12] Zhu Y, Jiang P, Zhang Z and Huang X 2017 *Chinese Chem. Lett.* 28 2027
[13] He F A *et al* 2016 *Compos. Sci. Technol.* 137 138
[14] Tiwari V K *et al* 2013 *Macromolecules.* 46 5595
[15] Tan S, Hu X, Ding S, Zhang Z, Li H and Yang L 2013 *J. Mater. Chem. A.* 1 10353
[16] Zhu Y, Jiang P, Zhang Z and Huang X 2017 *Chinese Chem. Lett.* 28 2027
[17] Cheng Z Y, Olson D, Xu H, Xia F, Hundal J S and Zhang Q M 2002 *Macromolucules.* 35 664
[18] Zhu L and Wang Q 2012 *Macromolecules.* 45 2937

VITAE

Name   : Mr. Ardian Agus Permana

Student ID   : 6110220043

Educational Attainment

Degree	Institution	Year of Graduation
Bachelor of Physics Education	Universitas Islam Negeri Sunan Kalijaga, Yogyakarta, Indonesia	2016

Scholarship Award

Thailand Education Hub-ASEAN Countries (TEH-AC)

List of Publications and Proceedings

Salea, A., Chaipo, S., **Permana, A. A.**, Jehlaeh, K., and Putson, C. (2020). The microstructure of negative electrocaloric Polyvinylidene fluoride-hexafluoropropylene copolymer on graphene loading for eco-friendly cooling technology. *Journal of Cleaner Production*. (Published)

Permana, A. A., Chirasatitsin, S., and Putson, C. (2020). Electron beam irradiation for boosting storage energy density of tuned poly(vinylidene fluoride-hexafluoropropylene)/graphene nanoplatelet polymer composites. *Crystals*. (Published)

Permana, A. A., Ngamdee, W., and Putson, C. (2019). Improvement of electrocaloric

properties of P(VDF-HFP)/GNPs composites for refrigerator cooling. *Journal of Physics: Conference Series (JPCS)*. (Published)

Permana, A. A., and Putson, C. (2020). Discharge Energy Efficiency Improvement of P(VDF-HFP) Copolymers Thin Films by Stretching and Electron Beam Irradiation. *IOP Conference Series: Materials Science and Engineering*. (Published)

Award

2020 The 5th International Conference on Manufacturing, Material and Metallurgical Engineering as Best Oral Presentation, Osaka International Convention Center, Osaka, Japan.